Università degli Studi di Pisa

Department of Aerospace Engineering
Ph.D. in Aerospace Engineering
Cycle XX

Doctoral Thesis

Electric Propulsion Interplanetary Missions using Libration Points

Development of Analytic approaches and Mission Design

Supervisor
Prof. Mariano Andrenucci

Candidate
Cosmo Casaregola

Director of the Doctoral School
Prof. Maria Vittoria Salvetti

December 2008

The most beautiful thing we can experience is the mysterious. It is the source of all true art and science.

Albert Einstein

Elena: "Oh, we're going home. We have just spent three months calibrating the new antennae at Tchalinko... And what about you?" Dr. Floyd: "I'm just on my way up to Clavius".

Stanley Kubrick - 2001: A Space Odyssey.

Abstract

In this dissertation, the advantageous combination of Dynamical Systems Theory of three-body models with Electric Propulsion to design novel spacecraft interplanetary missions in multi-body regimes has been investigated. Particular attention has been focused on interplanetary transfers towards outer planets that are intrinsically associated with long transfer times and high ΔV budgets, especially if a final planetary capture is desired.

A reference mission using Electric Propulsion in the three-body model has been selected in which, after the interplanetary phase, a planetary tour of the Uranian system orbiting consecutively Oberon, Titania, Umbriel, Ariel and Miranda has been designed. Application of low-thrust propulsion with its advantages with respect to propellant requirements has been used to interconnect ballistic trajectories on invariant manifolds associated with multiple three body systems. This has implied the necessity to investigate both in the field of the Dynamical Systems Theory applied to the Circular Restricted Three-Body problem and in the field of optimal control theory as optimization schemes have been necessary to design low-thrust arcs subjected to boundary constraints. Both the interplanetary trajectory and the planetary tour have been computed in different three-body environments, where the start of the interplanetary phase has been assisted by a high energy launch to limit the transfer time.

Based on the reference mission, a preliminary spacecraft configuration has been developed in which Radioisotope Thermoelectric Generators have been considered to provide the necessary power source.

Sommario

Il presente lavoro di tesi è volto all'indagine dei potenziali benefici che possono derivare dal disegno di traiettorie interplanetarie a bassa spinta nell'ambito di un modello a tre corpi. Da un lato l'uso della Propulsione Elettrica primaria permette una maggiore efficienza propulsiva che si traduce in una riduzione della massa di propellente necessario per compiere la missione, dall'altro la dinamica caotica del modello a tre corpi garantisce una riduzione del "costo" energetico di trasferimento rispetto all'approccio kepleriano. Nel presente studio, particolare interesse è posto nel disegno di trasferimenti interplanetari verso pianeti esterni, sia per le difficoltà che sono intrinsecamente contenute nel raggiungimento di tali obiettivi, sia per i tanti aspetti ancora ignoti che circondano questi pianeti causa l'assenza in passato di missioni ad essi dedicate.

In questo contesto è stata individuata una missione di riferimento che prevede un trasferimento Terra-Urano con conseguente tour delle sue lune principali. Sia la fase interplanetaria che quella planetaria di Urano sono state calcolate in differenti ambienti a tre corpi. In particolare, la fase interplanetaria è stata concepita con un lancio ad alta energia così da ridurre il tempo di trasferimento. Dopo la fase interplanetaria, è stato disegnato un tour che transita dalle lune più esterne a quelle più interne passando rispettivamente per Oberon, Titania, Umbriel, Ariel e Miranda fino alla cattura finale intorno ad Urano. Durante l'intera missione, la propulsione a bassa spinta è stata impiegata per connettere tratti balistici appartenenti a 'manifolds' invarianti associati a sistemi a tre corpi multipli. E' facile dunque intuire come tali problematiche hanno reso necessaria una ricerca approfondita sia nel campo della Teoria dei Sistemi Dinamici applicata al modello a tre corpi, sia nel campo della teoria del controllo ottimale applicata all'astrodinamica.

Infine, sulla base della missione di riferimento prescelta, è stata sviluppata una configurazione preliminare di una sonda spaziale in cui è previsto l'utilizzo di generatori termoelettrici a radioisotopi per la generazione di potenza.

Acknowledgements

Firstly, I would like to acknowledge Prof. Mariano Andrenucci who gave me the opportunity to begin this adventure in the fascinating world of Electric Propulsion and its application to astrodynamics. His guidance and motivation have been an integral part in helping me to pursue my goals. Thank you also for all the helpful discussions that helped me to open my eyes on different perspectives and ways to face a new problem, thank you for all comments and suggestions both on academic and professional matters. I will never forget all that.

Furthermore, I extend my special thanks and appreciation to two special collaborators: Koen Geurts, who started with me side by side this long and hard walk, who shared with me concerns and all the joy and the emotions for our first successful results of our research and who has been first a good friend and then a colleague. Unfortuntely, in the last three years he learnt better the dialect language of Pisa than the Italian! Pierpaolo Pergola, the missing piece for the perfect trio of the ”MAD” (Mission Analysis and Design) Team, for his tireless ”optimization” work and for his constant support. Thank you guys, it was my pleasure to work side by side with you.

I would also like to thank Leonardo Biagioni who never hesitated to support and guide me during the challenging research and professional experiences I was committed. Thank you for all the professional opportunities you entrust with me.

Finally, and most importantly, I would like to thank those closest to me. My parents Anna Maria and Pasquale, my sisters Federica and Chiara for their constant support of my endeavors, Gianluca and Attilio who support me and...my sisters and, last but not least, Linda for standing by my side with her relentless encouragement. This thesis is dedicated to you all.

Contents

List of Figures

List of Tables

List of Acronyms

ACS *Attitude Control Subsystem*

ASRG *Advanced Stirling Radioisotope Generator*

AU *Astronomical Unit*

CR3BP *Circular Restricted Three-Body Problem*

DST *Dynamical Systems Theory*

EMI *Electro-Magnetic Interference*

EP *Electric Propulsion*

GPHS *General Purpose Heat Source*

HG *High Gain*

LG *Low Gain*

MLI *MultiLayer Insulation*

NASA *National Aeronautics and Space Administration*

NLP *Non-Linear Programming*

PCDU *Power Conditioning and Distribuition Unit*

PCR3BP *Planar Circular Restricted Three-Body Problem*

PPU *Power Processing Unit*

RTG *Radioisotope Thermoelectric Generator*

S/C *Spacecraft*

SOI	*Sphere of Influence*
TPBVP	*Two Point Boundary Value Problem*
TWTA	*Traveling Wave Tube Amplifier*
VHE	*Hyperbolic Excess Velocity*

Chapter 1

Introduction

1.1 The Challenge of Space Exploration

Space exploration and human migration into space are still in their infancy as they started about fifty years ago. Many steps were done but many others need to be taken in this new ocean.

Nevertheless, sustainable space exploration is a challenge that needs a global vision and coordination for both robotic and human missions. In fact, both from an economic and scientific point of view, strategies and efforts of all space agencies must be shared in order to achieve mission goals more effectively and safely.

The Moon and Mars represent without any doubt the prime targets for human space exploration. The former has an enormous scientific significance and can represent an essential stepping stone to study Earth and the universe and to prepare humans and machines for exploration of Mars and beyond. The latter, with an atmosphere and water, may hold key secrets to the evolution of life in our solar system. Besides, because of its similarity to Earth, Mars is the place in the solar system where human life could most likely be sustained in the future.

Recent activities involve developing a robust and flexible capability to visit several potential destinations. A Lunar Gateway Station near Earth-Moon libration point LL_1 has been proposed as a 21st century hub for science and a jumping off point for deep space missions, eventually to land humans on Mars.

Looking beyond, exploration of asteroids and comets has high scientific interest as these celestial bodies contain important information on solar system history, new kind of telescopes into deep space are planned to be launched whose goal would be to find Earth-like planets, new probes to solar system planets and their moons are planned as they are extremely important scientifically and, even if these targets are not realistic for human exploration in the coming decades, they will become more accessible as space exploration technologies improve.

In this picture, trajectory design is part of this fascinating exploration program as space missions which reach these destinations are complex and challenging to design, requiring new and unusual kinds of orbits to meet their goals, orbits that cannot be found by classical approaches to the problem.

1.2 New Trends in Mission Design: Low-Energy Trajectories

Classical approaches to spacecraft trajectory design based on the integrability of the Kepler's problem have been quite successful and accurate preliminary results have been provided. Moreover, the concept of the sphere of influence as approximation of the region in which a body experiences the gravity field of one attractor, allows the patched-conics method to define the whole trajectory as a link of solutions of the two-body problem.

This first guess solution is often very close to the real trajectory experienced by the spacecraft during the operative life. For instance, Hohmann transfers for the Apollo Moon landings and swing-bys of outer planets for Voyager were designed using this approach and results are well known.

However, in terms of propellant mass consumption, these missions were costly as large burns were required to perform their trajectory. The minimization of propellant mass consumption (or in other words of the energy needed to perform the transfer) is a key factor for the feasibility of each mission.

Furthemore, the two-body problem fails in designing certain missions that spend long time in regions where two or more gravitational fields are comparable (for example when orbiting in the vicinity of the sphere of influence borderline).

Fortunately, a new class of *low energy trajectories* have recently been discovered and employed which make possible missions which classical approaches could not. Besides, the theoretical growth of the dynamical systems theory and of its application mainly motivated by the recent progress in the development of numerical techniques for dynamical problems and by the availability of more powerful computational facilities, yields the possibility to generate different types of transfer trajectories.

These trajectories, also called *non-Keplerian* orbits, are defined in a $n - body$ model ($n \geq 3$). It has been proven that, when non-Keplerian orbits are considered in the preliminary trajectory design, the ΔV necessary to carry out the transfer is reduced.

This is possible because such trajectories are modelled by making use of gravity as much as possible, using the natural dynamics arising from the presence of a third body (or more bodies). In this way, by simply exploiting the simultaneous gravitational fields of two or more attarctors, the ΔV needed to perform the transfer is reduced.

In order to effectively exploit these passage-ways, the global transport mechanism in the restricted three-body problem will be discussed, involving the stable and unstable invariant manifolds associated to two libration points, equilibrium locations in a rotating two-body gravity field situated along a line joining the two attracting bodies.

Apart from a reduction of the transfer cost, preliminary design of low-energy trajectories provides a more accurate solution. In fact, in a $n - body$ model ($n \geq 3$), a spacecraft experiences the n gravitational forces acting simultaneously on it and therefore a more accurate modelization of the reality is obtained.

The case of the Earth-Moon transfers is the one mostly investigated as the ΔV reduction of a lunar transfer and the consequent possible increase of payload mass fraction are of great importance from the strategic point of view in the future space activities.

In particular, the concept of *Weak Stability Boundaries* introduced by Belbruno needs to be mentioned as it first conceived the possibility of Earth-Moon transfers with no hyperbolic excess velocity at Moon arrival.

Moreover, low-energy trajectory design allowed and will allow space agencies to envision missions involving long duration observations and/or constellations of spacecraft using little amount of propellant. In the past, many missions (ISEE-3, WIND, SOHO, ACE, WMAP, GENESIS) were designed under these assumptions and flew on periodic orbits around collinear lagrangian points.

1.3 Thesis Motivations and Goals

In the past, several studies applied low-energy tranfer solutions to design complex missions and successfully coupled three-body environments to design low-energy ballistic trajectories with consequent significant savings in propellant mass and high scientific outcome.

However, few past studies are known to the author in which low-thrust trajectories are defined in a n-body model. Belbruno first dealt with this combination in the frame of the Lunar GAS mission,[5] then other studies investigated low-thrust trajectories for periodic orbit around libration points.[6][7][8]

It is well known from Tsiolkowski equation that propellant mass fraction can be reduced if a higher thruster specific impulse is available and/or a lower ΔV is necessary to perform the overall orbit transfer.
Electric Propulsion is a low-thrust, high efficiency propulsion technology that can rely on specific impulses ten times higher than conventional propulsion. This is the reason why space transportation systems based on it are an important building block of all recent architectures for space exploration.

Therefore, taking in mind advantages deriving from both low-energy transfers and from this high efficiency propulsion technology, the primary objective of this research is to investigate and outline the potential benefits deriving from coupling the trajectory design of non-Keplerian orbits in a Circular Restricted Three-Body model (with the consequent reduction of the ΔV transfer) with the use of the Electric Propulsion.

This implies the necessity to investigate both in the field of the Dynamical Systems Theory applied to the Circular Restricted Three-Body problem and in the field of optimal control theory as optimization schemes are necessary to design low-thrust arcs subjected to boundary constraints.

In this research, particular attention is focused on mission design to outer solar system planets that are intrinsically associated with long transfer times and high ΔV budgets, particularly if a final planetary capture is desired. In detail, a tour of the Uranian system orbiting consecutively its main moons and the required interplanetary trajectory are studied.

1.4 Contents

The theoretical background related to the Circular Restricted Three-Body Problem (CR3BP) has been summarized in Chapter 2 where the definition of the system of reference and of the equations of motion are discussed as far as considerations on the energy integral and the regions of possible motions related to it.

Chapter 3 is dedicated to the explanation of the orbit structure and of the motion near the collinear libration points. In detail, starting from the linearized dynamics around collinear libration points, construction of periodic orbits and the determination of invariant manifolds associated both to collinear points and periodic orbits is outlined. In many practical mission design problems under the assumptions of CR3BP, it represents the starting point for a preliminary trajectory design.

In Chapter 4, optimization techniques are presented. In particular, this chapter does not want to be a survey of all numerical methods available in trajectory design since it would be a huge task, but only a focused overview of the optimization techniques used in this work for the achieved results.

In Chapter 5 and Chapter 6, the computations and the results obtained for interplanetary low-thrust transfers using libration points are presented. Both chapters pay particular attention to missions to outer planets.
In detail, in Chapter 5 interplanetary transfers to Uranus both in the three-body and two-body model are shown in order to obtain comparable results. In the two-body model, two different transfer strategies were investigated.
On the other hand, Chapter 6 is dedicated to the design of a reference mission, in particular a tour of the Uranian system (Uranus plus its main moons) and the required interplanetary trajectory in the CR3BP model are presented. Furthermore, the preliminary spacecraft design is also shown.

Finally, in Chapter 7, conclusions, open problems and suggestions for further improvements about this thesis are discussed.

Chapter 2

The Circular Restricted Three-body Model

All of the celestial bodies, in accordance with Newton's law of universal gravitation, are attracted to each other. Therefore, the motion of a spacecraft in the solar system or in the overall universe is governed by an infinite network of attractions to all celestial bodies and a rigorous analysis of all the instantaneous contributes experienced by the spacecraft would be impossible. Fortunately, if we consider the motion of a body dominated by only one central body at a time (the *2-body problem*), the error we are making is small and results are very close to the reality. In fact, the 2-body problem is an integrable system and therefore has explicit solutions to the equations of motion which correspond to three types of orbit (ellipse, parabola and hyperbola) where the central body must be at a focus of the conic.

In particular, under specific assumptions (mass of the second body negligible with respect to the attracting body → *Restricted 2-body problem*, inertial system of reference, spherical symmetry and uniform density of the two bodies, only gravitational forces acting on the two-bodies), the 2-body problem is crucial to astrodynamics as it represents the starting point for more complex study.

However, even if the standard two-body relations underlie much of the general work in astrodynamics, sometimes, when higher accuracy is required, we need to model the real world by including other bodies. When three or more bodies are gravitationally interacting a wide variety of orbital regimes becomes available. Open trajectories, close encounters, collisions, resonances and all intermediate and transition patterns from one case to another. In other words *chaos.*

In an inertial reference system (X,Y,Z), celestial bodies obey Newton's laws of motion and his law of universal gravitation. If we assume that N point masses are moving uniquely under their gravitational attraction and

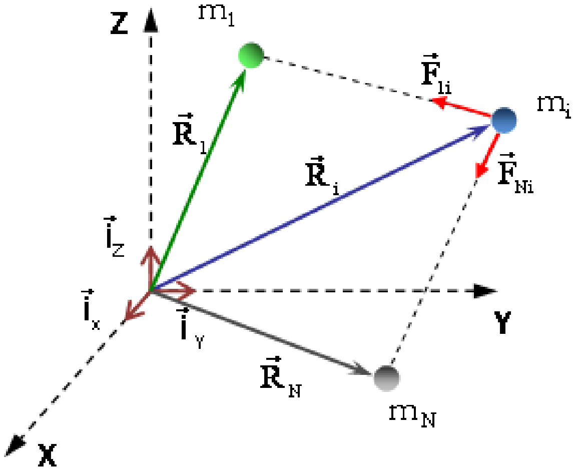

Figure 2.1: Gravitational forces acting on the i-th body in the classical N-body problem.

that there are no other celestial bodies (masses) outside the system, these assumptions define the classical *N-body problem* (see Fig. 2.1) whose non-linear differential equations of motion are

$$m_i \ddot{\vec{\mathbf{R}}}_i = -Gm_i \sum_{\substack{j=1 \\ j \neq i}}^{N} \frac{m_j}{R_{ij}^3} (\vec{\mathbf{R}}_i - \vec{\mathbf{R}}_j) \qquad i = 1, \ldots, N \tag{2.1}$$

where G is the *universal gravitation constant*, R_{ij} is the Euclidean distance between two bodies of mass m_i and m_j

$$R_{ij} = \sqrt{(X_i - X_j)^2 + (Y_i - Y_j)^2 + (Z_i - Z_j)^2} \tag{2.2}$$

and $\vec{\mathbf{R}}_i$ ($\vec{\mathbf{R}}_j$) is the position vector of the i-th (j-th) body defined in the cartesian inertial reference system as

$$\vec{\mathbf{R}}_i = X_i \mathbf{i}_x + Y_i \mathbf{i}_y + Z_i \mathbf{i}_z \tag{2.3}$$

Eq. (2.1) is simply Newton's second law of motion where the left-hand side is the force acting on the i-th point mass and the right-hand side is the sum of the gravitational forces acting on it. The set of $3N$ second-order differential equations describes the dynamics of all N point masses that influence each other through the gravitational forces so that each single mass moves under the vector field generated by the other $N-1$ masses. Unfortunately, as H. Bruns demonstrated in 1887, for $N > 2$ this set of differential equations of motion has only 10 first integrals, thus no analytical solution is possible to solve the $6N$ variables ($3N$ for the position components and $3N$ for the velocity components). However, the non-existence of a general solution to the N-body problem for $N > 2$ does not prevent the motion of a system being accurately described in some specific cases.

2.1 The Circular Restricted 3-Body Problem

The *general 3-body problem* is one of the oldest problems in dynamical systems designed to determine the behavior of three interacting masses. As said before, no one has solved it in closed form, but much work has been done to simplify the problem.[9] In particular, one special analytical solution has been known since the time of Euler and Lagrange: *the Circular Restricted 3-body Problem* (CR3BP). Nevertheless, in spite of simplifying assumptions, the resulting motion can be chaotic.

In the CR3BP we consider a case where one of the bodies (the third body with mass m) is so much less massive than the other two bodies (the primary masses or primaries) so that primaries behavior is unaffected by third body gravitational potential:

$$m_1 > m_2 >> m \tag{2.4}$$

As we can easily realize, this scenario is good for modeling the trajectories of a spacecraft in the gravitational potential of two massive bodies (sun-planet or planet-moon system).

Since third body mass is negligible with respect to the other two bodies, the total mass of the system is

$$M = m_1 + m_2 \tag{2.5}$$

and the mass ratio is defined as

$$\mu = \frac{m_2}{M} \tag{2.6}$$

Thus it is

$$m_2 = \mu M \tag{2.7}$$

$$m_1 = (1-\mu)M \tag{2.8}$$

2.2 CR3BP Equations of Motion

System of Reference Before formulating the equations of motion for the CR3BP, it is necessary to choose an appropriate Cartesian system of reference. With reference to Eq. (2.1) where $N = 3$, the equation of motion of the third body in an inertial (or sidereal) system of reference would read

$$\ddot{\vec{\mathbf{R}}}_3 = -Gm_1 \frac{(\vec{\mathbf{R}}_3 - \vec{\mathbf{R}}_1)}{R_{13}^3} - Gm_2 \frac{(\vec{\mathbf{R}}_3 - \vec{\mathbf{R}}_2)}{R_{23}^3} \tag{2.9}$$

Moreover, assuming the primaries to move in circular orbits around their common centre of mass and assuming a new inertial frame with the origin in the barycenter of the two primaries, Eq. (2.9) reads

$$\ddot{\vec{\mathbf{R}}} = -Gm_1 \frac{(\vec{\mathbf{R}} - \vec{\mathbf{R}}_1)}{R_1^3} - Gm_2 \frac{(\vec{\mathbf{R}} - \vec{\mathbf{R}}_2)}{R_2^3} \tag{2.10}$$

where $\vec{\mathbf{R}} = \{X, Y, Z\}^T$ denotes the spacecraft's position, $\vec{\mathbf{R}}_1$ and $\vec{\mathbf{R}}_2$ the distance of the spacecraft from the primaries.

However, Eq. (2.10) is time-dependent and to get the system autonomous it must be rewritten in a system of reference where the primaries are at rest. Thus a *synodic* or *rotating* frame (x, y, z) is defined rotating uniformly with the primaries with angular velocity $\vec{\omega} = \{0, 0, n\}^T$ equal to the mean motion of either mass and with its origin on their barycenter. It coincides with the inertial frame (X, Y, Z) at $t = 0$. The x-axis lies along the primaries line from m_1 to m_2, the y-axis is perpendicular and on the plane of motion and the z-axis completes a right-handed coordinate system (see Fig. 2.2).

Besides, it is convenient to make the system nondimensional by the following choice of units:

1. The unit of mass $M = m_1 + m_2$
2. The unit of length L = distance between the centers of the primaries
3. The unit of time $T = 2\pi$ (orbital period of m_1 and m_2 about their centre of mass)

With these assumptions the universal gravitation constant becomes $G = 1$ and the common mean motion of the primaries, n, is also unity. In addition, in the synodic system of reference, the larger mass m_1 is located at $(-\mu, 0, 0)$ and m_2 in $(1 - \mu, 0, 0)$. This is also true for the inertial frame only when $t = 0$.

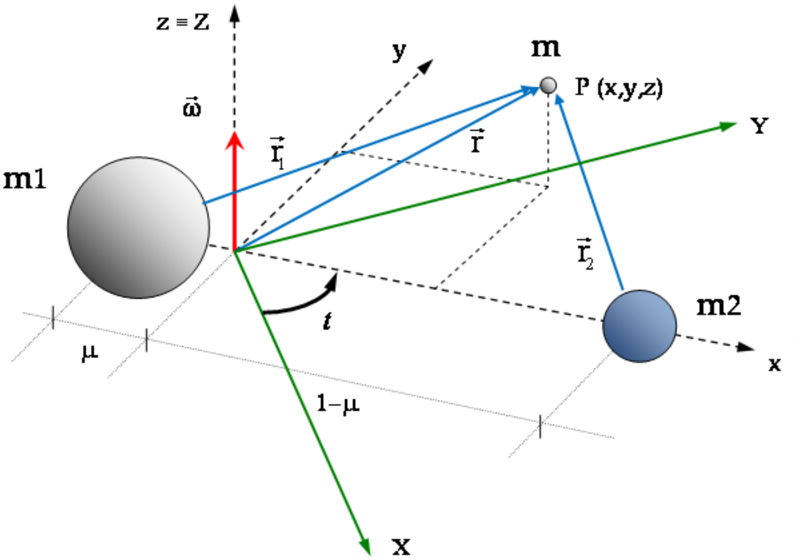

Figure 2.2: CR3BP System of Reference

In normalized units, we shall transform the coordinates of the m-body from the inertial coordinates $\{X, Y, Z\}$ to the rotating frame coordinates $\{x, y, z\}$ using a transformation matrix A_t:[1]

$$\begin{pmatrix} X \\ Y \\ Z \end{pmatrix} = A_t \cdot \begin{pmatrix} x \\ y \\ z \end{pmatrix} \tag{2.11}$$

where

$$A_t = \begin{pmatrix} cos\ t & -sin\ t & 0 \\ sin\ t & cos\ t & 0 \\ 0 & 0 & 1 \end{pmatrix} \tag{2.12}$$

In order to obtain velocity components, we can differentiate Eq. (2.11):

$$\begin{aligned} \begin{pmatrix} \dot{X} \\ \dot{Y} \\ \dot{Z} \end{pmatrix} &= \dot{A}_t \cdot \begin{pmatrix} x \\ y \\ z \end{pmatrix} + A_t \cdot \begin{pmatrix} \dot{x} \\ \dot{y} \\ \dot{z} \end{pmatrix} \\ &= A_t \cdot \begin{pmatrix} \dot{x} - y \\ \dot{y} + x \\ \dot{z} \end{pmatrix} \end{aligned} \tag{2.13}$$

Lagrange and Hamiltonian Approach Letting q_1, q_2, .., q_n denote a set of generalized configuration coordinates for a conservative physical system with n degrees of freedom, the equations of motion of the system are

$$\frac{d}{dt}\left(\frac{\partial L}{\partial \dot{q}_j}\right) = \frac{\partial L}{\partial q_j} \qquad j = 1, 2, \ldots, n \tag{2.14}$$

where L is the *Lagrangian* of the system, i.e., the difference between the kinetic and the potential energies, expressed in terms of the generalized coordinates and their time derivatives. These equations are known as *Euler-Lagrange* equations because, although Lagrange was the first to formulate them specifically as the equations of motion, they were previously derived by Euler as the conditions under which a point passes from one specified place and time to another in such a way that the integral of a given function L with respect to time is stationary.
In the inertial frame Eq. (2.14) can be written as

$$L(X,Y,Z,\dot{X},\dot{Y},\dot{Z},t) = \frac{1}{2}\left(\dot{X}^2 + \dot{Y}^2 + \dot{Z}^2\right) - U(X,Y,Z,t) \tag{2.15}$$

where

$$U(X,Y,Z,t) = -\frac{1-\mu}{R_1} - \frac{\mu}{R_2} - \frac{1}{2}\mu\,(1-\mu) \tag{2.16}$$

is the gravitational potential experienced by the third body due to m_1 and m_2 (the last term on the right-hand side is added by convention to offer a more symmetric form) and

$$\begin{aligned} R_1^2 &= (X + \mu cos\ t)^2 + (Y + \mu sin\ t)^2 + Z^2 \\ R_2^2 &= [X - (1-\mu) cos\ t]^2 + [Y - (1-\mu) sin\ t]^2 + Z^2 \end{aligned} \tag{2.17}$$

Thanks to the power of Euler-Lagrange equations that are invariant under general coordinate transformations, the Lagrangian can be written down also in the rotating frame in order to become *time-independent*(recall transformations expressed in Eqs. 2.11 and 2.13):

$$L(x,y,z,\dot{x},\dot{y},\dot{z}) = \frac{1}{2}\left[(\dot{x}-y)^2 + (\dot{y}+x)^2 + \dot{z}^2\right] - U\,(x,y,z) \tag{2.18}$$

where

$$U(x,y,z) = -\frac{1-\mu}{r_1} - \frac{\mu}{r_2} - \frac{1}{2}\mu\,(1-\mu) \tag{2.19}$$

with

$$\begin{aligned} r_1^2 &= (x+\mu)^2 + y^2 + z^2 \\ r_2^2 &= [x-(1-\mu)]^2 + y^2 + z^2 \end{aligned} \tag{2.20}$$

Thus, using Eqs. 2.14, the equations of motion in the CR3BP with a lagrangian approach are:

$$\begin{aligned}\frac{d}{dt}\left(\dot{x}-y\right)&=\dot{y}+x-U_x\\ \frac{d}{dt}\left(\dot{y}+x\right)&=-\left(\dot{x}-y\right)-U_y\\ \frac{d}{dt}\dot{z}&=-U_z\end{aligned}$$

and after simplification

$$\begin{aligned}\ddot{x}-2\dot{y}&=-\bar{U}_x\\ \ddot{y}+2\dot{x}&=-\bar{U}_y\\ \ddot{z}&=-\bar{U}_z\end{aligned}\tag{2.21}$$

where

$$\begin{aligned}\bar{U}(x,y,z)&=-\frac{1}{2}\left(x^2+y^2\right)+U(x,y,z)\\ &=-\frac{1}{2}\left(x^2+y^2\right)-\frac{(1-\mu)}{r_1}-\frac{\mu}{r_2}-\frac{1}{2}\mu\left(1-\mu\right)\end{aligned}\tag{2.22}$$

is the *effective potential*

The correspondence between the conservation of energy and the Lagrangian equations of motion suggests that there might be a convenient variational formulation of mechanics in terms of the total energy E = T + U (Kinetic Energy + Potential Energy) as opposed to the Lagrangian L = T - U. Notice that the partial derivative of L with respect to $\dot{q}$ is the *momentum* of the particle. In general, given the Lagrangian, we can define the generalized momenta as (Legendre transformation):

$$p_i=\frac{\partial L}{\partial \dot{q}_i}\tag{2.23}$$

and the total energy of the system in terms of these conjugate parameters is the so called *Hamiltonian function H*

$$H\left(q_i,p_i\right)=\sum_{i=1}^{n}p_i\dot{q}_i-L\left(q_i,p_i\right)\tag{2.24}$$

that in *autonomous*, *conservative* systems of n degrees of freedom is conserved.

Therefore the equations in Hamiltonian form read:

$$\dot{q}_i=\frac{\partial H}{\partial p_i};\qquad \dot{p}_i=-\frac{\partial H}{\partial q_i}\tag{2.25}$$

According to Eqs. 2.23 and 2.24, the Hamiltonian function of the CR3BP reads

$$\begin{aligned} H\left(x,y,z,p_x,p_y,p_z\right) &= p_x\dot{x} + p_y\dot{y} + p_z\dot{z} - L \\ &= \frac{1}{2}\left[\left(p_x+y\right)^2 + \left(p_y-x\right)^2 + p_z^2\right] + \bar{U}(x,y,z) \end{aligned} \tag{2.26}$$

Therefore, from Eqs. 2.25, Hamilton equations are given by

$$\begin{aligned} \dot{x} &= \frac{\partial H}{\partial p_x} = p_x + y \\ \dot{y} &= \frac{\partial H}{\partial p_y} = p_y - x \\ \dot{z} &= \frac{\partial H}{\partial p_z} = p_z \\ \dot{p}_x &= -\frac{\partial H}{\partial x} = p_y - x - \bar{U}_x \\ \dot{p}_y &= -\frac{\partial H}{\partial y} = -p_x - y - \bar{U}_y \\ \dot{p}_z &= -\frac{\partial H}{\partial z} = -\bar{U}_z \end{aligned} \tag{2.27}$$

It is worth noting that both the Lagrangian and the Hamiltonian formulation of CR3BP equations of motion in the synodic system of reference gives a six dimensional *autonomous* system, respectively in $(x, y, z, \dot{x}, \dot{y}, \dot{z})$ and in (x, y, z, p_x, p_y, p_z).

Energy Integral and Jacobi Constant The energy associated with the particle's motion in the rotating frame can be expressed as

$$E(x,y,z,\dot{x},\dot{y},\dot{z}) = \frac{1}{2}\left(\dot{x}^2 + \dot{y}^2 + \dot{z}^2\right) + \bar{U}(x,y,z) \tag{2.28}$$

Moreover, if we derive the first term on the right-hand side and, using relations obtained in Eqs. 2.21, we have

$$\begin{aligned} \frac{1}{2}\frac{d}{dt}\left(\dot{x}^2 + \dot{y}^2 + \dot{z}^2\right) &= \dot{x}\ddot{x} + \dot{y}\ddot{y} + \dot{z}\ddot{z} \\ &= \dot{x}\left(2\dot{y} - \bar{U}_x\right) + \dot{y}\left(-2\dot{x} - \bar{U}_y\right) + \dot{z}\left(-\bar{U}_z\right) \\ &= -\left(\dot{x}\bar{U}_x + \dot{y}\bar{U}_y + \dot{z}\bar{U}_z\right) = \frac{d}{dt}\left(-\bar{U}\right) \end{aligned}$$

Thus

$$\frac{d}{dt}\left(\dot{x}^2 + \dot{y}^2 + \dot{z}^2\right) = 2\frac{d}{dt}\left(-\bar{U}\right) \Rightarrow \frac{d}{dt}\left[-\left(\dot{x}^2 + \dot{y}^2 + \dot{z}^2\right) - 2\bar{U}\right] = 0 \tag{2.29}$$

It turns out that

$$C\left(x, y, z, \dot{x}, \dot{y}, \dot{z}\right) = -\left(\dot{x}^2 + \dot{y}^2 + \dot{z}^2\right) - 2\bar{U} = -2E \tag{2.30}$$

The constant or conserved quantity $C = -2E$ is the so called *energy integral* or *Jacobi integral* or *Jacobi constant*

2.3 Realms of Possible Motion in the CR3BP

Lagrangian libration points Given two massive bodies in circular orbits around their common centre of mass, it can be shown that there are five positions of equilibrium in space, the *Lagrangian libration points*, where a third body of comparatively negligible mass would maintain its position relative to the two massive bodies. In other words, in the rotating system of reference introduced before, the gravitational fields of the primaries combined with their centrifugal force are in balance at the Lagrangian points and the spacecraft would stay there if placed with zero velocity. For a static equilibrium is necessary to find the position vector $\mathbf{x} = (x, y, z)$ so that accelerations and velocities are zero in the system of equations of motion derived before (Eqs 2.21).

Lagrangian points are labeled with L_i with $i = 1, .., 5$; three of them L_1, L_2 and L_3 are *collinear* with the primaries and are locally *unstable* (saddle points) while L_4 and L_5 are *triangular* forming equilater triangles with the primaries. In the next paragraph the computation of the location of these stationary points will be shown.

Energy surface, Zero Velocity surfaces and Hill's Region Any set of $(x, y, z, \dot{x}, \dot{y}, \dot{z})$ satisfying the Jacobi constant will represent a possible motion for a given energy level. With reference to Eq. (2.30), some preliminary considerations can be done. The term $\left(\dot{x}^2 + \dot{y}^2 + \dot{z}^2\right)$ is the square of third body velocity; if we imagine to fix an energy level (in other words the value of C) and to fix an initial position of the third body (x_0, y_0, z_0), the magnitude of velocity is thus fixed. Alternatively, if we impose the velocity to be zero at a given energy level, a set of third body positions will be automatically determined. In fact, the Jacobi integral represents a five-dimensional manifold for the states of the spacecraft (third body) within the six-dimensional phase space. Once the energy integral is set equal to a costant k (the value of μ is fixed once we choose the primaries), the motion is then reduced to the hypersurface or energy surface M:

$$M(\mu, k) = \left\{(x, y, z, \dot{x}, \dot{y}, \dot{z}) \in \Re^6 | C\left(x, y, z, \dot{x}, \dot{y}, \dot{z}\right) = k\right\} \tag{2.31}$$

Moreover, the Jacobi integral can be used to establish some allowed and forbidden regions for the motion of the spacecraft once an initial condition

$\mathbf{x}_0 = (x_0, y_0, z_0, \dot{x}_0, \dot{y}_0, \dot{z}_0)$ is given. These regions are bounded by the *zero velocity surfaces* or *Hill's surfaces* on which the kinetic energy is zero.

In order to obtain 3-D and 2-D plots (but without loss of generality), let us consider a spacecraft bounded to move on the plane described by the motion of the primaries. The prblem to be faced is the so called *Planar Circular Restricted 3-Body Problem* (PCR3BP) in which we set $z = \dot{z} = 0$.

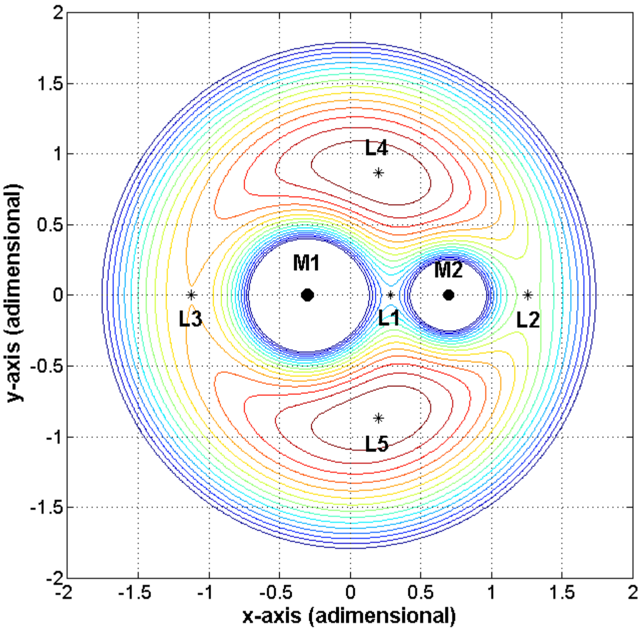

Figure 2.3: Zero velocities curves (or Hill's regions) in the rotating system for various values of energy and for $\mu = 0.3$

Now equations of motion read

$$\begin{aligned} \ddot{x} - 2\dot{y} &= -\bar{U}_x \\ \ddot{y} + 2\dot{x} &= -\bar{U}_y \end{aligned} \tag{2.32}$$

where

$$\bar{U}(x, y) = -\frac{1}{2}\left(x^2 + y^2\right) + U(x, y) \tag{2.33}$$

with

$$U(x,y) = -\frac{1-\mu}{r_1} - \frac{\mu}{r_2} - \frac{1}{2}\mu\,(1-\mu) \tag{2.34}$$

$$\begin{aligned} r_1^2 &= (x+\mu)^2 + y^2 \\ r_2^2 &= [x-(1-\mu)]^2 + y^2 \end{aligned} \tag{2.35}$$

Besides, the Jacobi constant becomes

$$C\,(x,y,\dot{x},\dot{y}) = -\left(\dot{x}^2+\dot{y}^2\right) - 2\bar{U} = -2E$$

In this case, the energy hypersurface of Eq. (2.31) becomes a three-dimensional manifold in the four-dimensional space. The projection of this surface onto position space represents the regions of possible motions or *Hill's region* for a third body of fixed energy k (Fig. 2.3). Moreover, as in these regions the spacecraft can move, the term $\left(\dot{x}^2+\dot{y}^2\right)$ must be positive. It turns out that, according to Jacobi constant, in these realms must be $\bar{U}(x,y) \leq k$. This concept is mathematically expressed as

$$S\,(\mu,k) = \left\{(x,y)\,|\bar{U}(x,y) \leq k\right\}$$

The boundary of this surface is called the *zero velocity curve* and represents the locus of points in which the kinetic energy is zero, i.e. $\bar{U}(x,y) = k$. Therefore, for a given μ, there are five basic configurations for the Hill's regions corresponding to five intervals of energy value k. Thus, for increasing values of the energy, Hill's regions open first at L_1, then at L_2 and so on (see Fig. 2.5). The critical values of energy which separate these five cases are the values of k_i, $i = 1,..5$ (where $k4 = k5$) corresponding to the lagrangian points L_i, $i = 1,..,5$ (Fig. 2.4).

Regions of Possible Motion in the CR3BP According to the considerations done in the previous paragraph and with reference to Fig. 2.5, there are three main regions of possible motion called *realms* and five possible cases. In particular:

- **Case 1: E<k1**. When the third body (spacecraft) has an energy below the value $k1$, it can only move in the small surrounding regions of the two primaries m_1 and m_2 called respectively *interior realm* and m_2 *realm* without crossing them as a forbidden region is between the two realms.

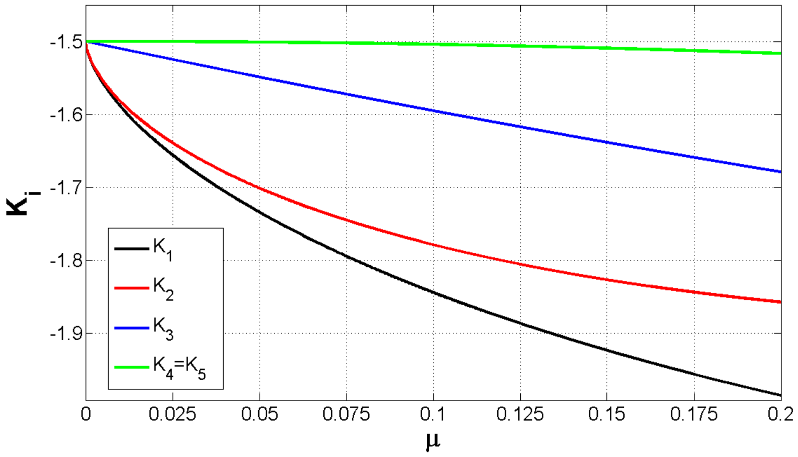

Figure 2.4: Energy values of k_i, $i = 1, ..5$ corresponding to the five lagrangian points L_i vs. the mass ratio μ

- **Case 2: k1<E<k2**. As the energy level is higher than $k1$, a neck around L_1 opens up between the two regions around m_1 and m_2 allowing the spacecraft to move between the two. Since the energy level is lower than $k2$, the *exterior realm* which lies outside both m_1 and m_2 is still forbidden.

- **Case 3: k2<E<k3**. When the energy level becomes higher than $k2$ value, a second neck around L_2 opens up permitting the third body to move also in the exterior realm.

- **Case 4: k3<E<k4=k5**. In this case the spacecraft can move from the vicinity of m_1 to the exterior realm passing not necessarely from L_2 but directly from L_3.

- **Case 5: E>k4=k5**. When the energy level is higher than $k4 = k5$, no forbidden regions longer exist and the third body is free to move in the entire plane.

2.4 Location of the Libration Points

As the libration points are equilibrium points, it is possible to compute their location in the synodic system of reference starting, for simplicity, from the planar equations of motion (Eqs. 2.32) in which we set the velocities and accelerations to zero, i.e. $\dot{x} = \ddot{x} = \dot{y} = \ddot{y} = 0$. Thus, it sufficient to solve $\bar{U}_x = 0$ and $\bar{U}_y = 0$, therefore:

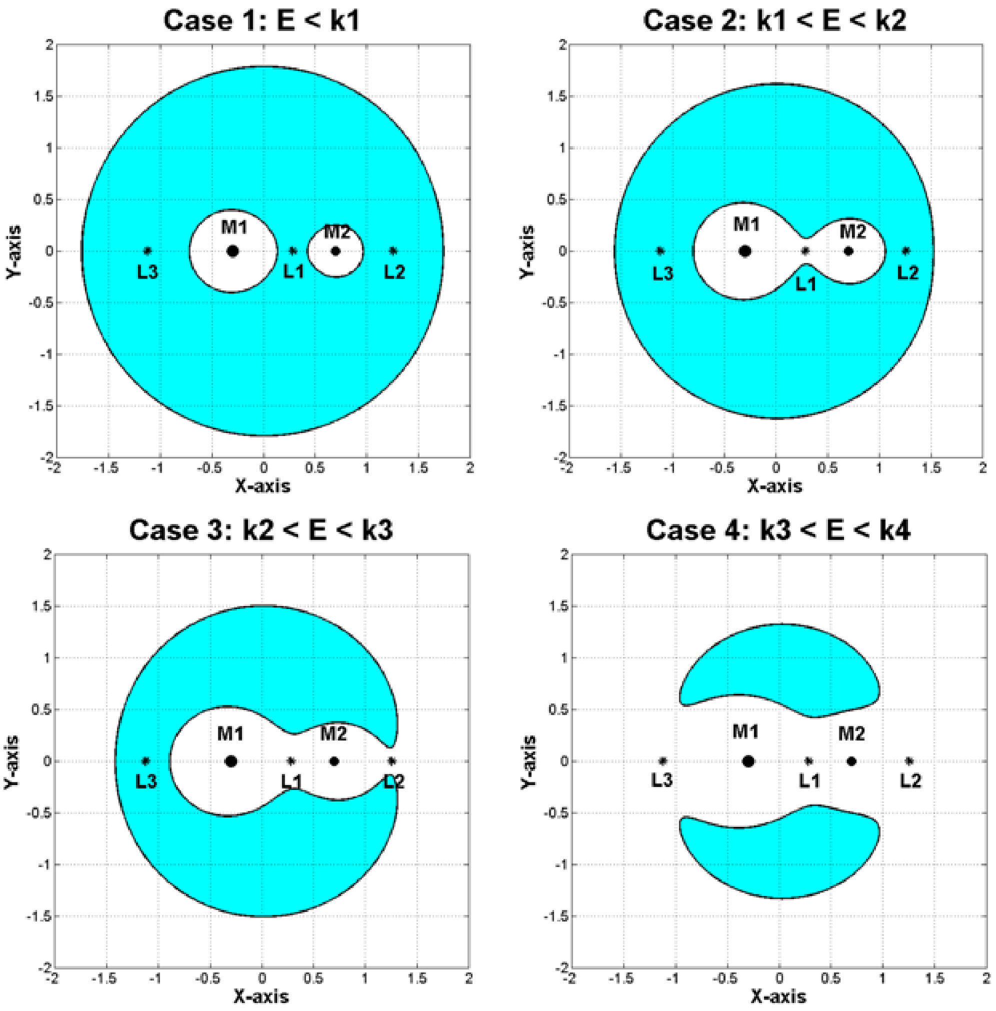

Figure 2.5: Zero velocities curves for four values of the energy. The curves bound the zone accessible by the spacecraft, in white, and the part inaccessible (colored)

$$\bar{U}_x = 0 = x - \frac{(x+\mu)(1-\mu)}{\left(\sqrt{(x+\mu)^2+y^2}\right)^3} - \frac{\mu(x-1+\mu)}{\left(\sqrt{(x-1+\mu)^2+y^2}\right)^3} \tag{2.38}$$

$$\bar{U}_y = 0 = y - \frac{2y\cdot(1-\mu)}{\left(\sqrt{(x+\mu)^2+y^2}\right)^3} - \frac{2y\cdot\mu}{\left(\sqrt{(x-1+\mu)^2+y^2}\right)^3} \tag{2.39}$$

In particular, in order to find the three collinear Lagrange points on the x-axis L_1, L_2 and L_3, we write $y = 0$ in Eq. (2.38) obtaining

$$x - \frac{(x+\mu)(1-\mu)}{|x+\mu|^3} - \frac{\mu(x-1+\mu)}{|x-1+\mu|^3} = 0 \tag{2.40}$$

where the left hand side is zero if and only if the numerator is zero. Then a fifth order polynomial must be solved numerically.

Doing that, we have to consider the three cases $x < -\mu$, $-\mu < x < (1-\mu)$ and $x > (1-\mu)$ that correspond respectively to the libration points L_3, L_1 between the two primaries and L_2. The distance from L_i, $i = 1, 2$ to the smaller primary m_2 is given by the unique real positive solution γ_i of the following equation

$$\gamma^5 \mp (3-\mu)\gamma^4 + (3-2\mu)\gamma^3 - \mu\gamma^2 \pm 2\mu\gamma - \mu = 0 \tag{2.41}$$

where the upper sign is for L_1 and the lower for L_2. With reference to Szebely,[9] the series expansion found for such solutions are

$$\gamma_1 = r_h\left(1 - \frac{1}{3}r_h - \frac{1}{9}r_h^2 + \dots\right) \tag{2.42}$$

$$\gamma_2 = r_h\left(1 + \frac{1}{3}r_h - \frac{1}{9}r_h^2 + \dots\right) \tag{2.43}$$

where $r_h = \left(\frac{\mu}{3}\right)^{\frac{1}{3}}$ is the *Hill radius*, i.e. a 3-D sphere of influence in the position space in which the primary m_2 is dominant on the third body's motion. Therefore, we obtain the abscissas of L_1 and L_2 from

$$x(L_1) = 1 - \mu - \gamma_1$$
$$x(L_2) = 1 - \mu + \gamma_2$$

A similar equation can be found for γ_3, the distance between L_3 to the larger primary from the fifth order polynomial[9]

$$\gamma^5 + (2+\mu)\gamma^4 + (1+2\mu)\gamma^3 - (1-\mu)\gamma^2 - 2(1-\mu)\gamma - (1-\mu) = 0 \tag{2.44}$$

obtaining

$$\gamma_3 = 1 - \nu\left(1 + \frac{23}{84}\nu^2 + \dots\right) \tag{2.45}$$

where $\nu = \frac{7}{12}\mu$ and thus the L_3 abscissa

$$x(L_3) = -\mu - \gamma_3$$

Concerning the two equilateral points L_4 and L_5, they can be easily found from geometric considerations, obtaining

$$\begin{aligned} x(L_4) &= x(L_5) = 0.5 - \mu \\ y(L_4) &= +\frac{\sqrt{3}}{2} \\ y(L_5) &= -\frac{\sqrt{3}}{2} \end{aligned}$$

Moreover, taking into account that

$$\frac{d^2\bar{U}(x,0)}{dx^2} = -1 - \frac{1-\mu}{|x+\mu|^3} - \frac{\mu}{|x-1+\mu|^3} \tag{2.47}$$

is always negative, it can be easily realized that the three collinear equilibrium points are unstable.

Chapter 3

Dynamical Systems Theory applied to CR3BP

The Dynamical Systems Theory is a geometric approach developed by Poincarè to solve differential equations.[10][11][12] Together with the *Weak Stability Boundary* transfers studied by Belbruno,[5][13][14] it represents the second branch of low-energy orbit transfer design methods.
Application of dynamical systems theory in the CR3BP yields the possibility to generate different types of transfer trajectories between libration points of different three-body systems in order to produce a first guess solution for a "patched" CR3BP design process.
In the previous chapter a framework for understanding the three-body system, its equations of motion and its constant of motion (the energy) which divides the phase space of the particle motion into five cases was developed.
In the following sections, a general discussion on the spacecraft (the third body) dynamics in the neighbourhood of collinear libration points (in particular L_1 and L_2) is held. This will help to understand the local orbit structure on the phase space.
Then computation of periodic orbits around L_1 and L_2 and of the invariant manifolds associated is discussed as it is fundamental for the comprehension of the global orbit structure and it represents the starting point for the preliminary mission design process under the assumptions of the CR3BP. In the end, construction of orbits and of prescribed itineraries is treated.

3.1 Motion near the Collinear points

As the spacecraft dynamics around L_3 is too slow and associated to higher energy levels and L_4 and L_5 libration points are linear stable for the time

span of the mission design and therefore less interesting for our applications, the preliminary trajectory design in the CR3BP involving the L_1 and L_2 lagrangian points is without any doubt the most interesting. In particular, Case 2 and Case 3 of Fig. 2.5 will be investigated more in depth as they allow the third body to move between the primaries and in their exterior realm.
Moreover, it is very interesting to study the dynamics in the neighborhood of L_1 and L_2. In this context, it will be necessary to consider a suitable fixed energy E (as in the Case 2 and Case 3) and then, in the neighborhood of the two collinear lagarangian points whose position space projection is in the neck region around L_1 or L_2, to find the linearized equations. In fact, thanks to the theorem of Moser[15] that generalizes the theorem of Lyapunov, all the qualitative results obtained from the linearized equations apply to the full nonlinear system.
Therefore, starting from equations of motion 2.21 written in a L_i $(i = 1, 2)$ centered and rescaled frame and expanding the nonlinear terms, in a lagrangian approach the resulting linearized equations of motion are[16]

$$\begin{aligned} \ddot{x} - 2\dot{y} - ax &= 0 \\ \ddot{y} + 2\dot{x} + by &= 0 \\ \ddot{z} + cz &= 0 \end{aligned} \tag{3.1}$$

or analogously

$$\begin{aligned} \dot{x} &= v_x \\ \dot{y} &= v_y \\ \dot{z} &= v_z \\ \dot{v}_x &= 2v_y + ax \\ \dot{v}_y &= -2v_x - by \\ \dot{v}_z &= -cz \end{aligned} \tag{3.2}$$

where $a = 1 + 2c$, $b = c - 1$ and c is a costant depending on μ

$$c = \frac{\mu}{(1 - \mu - x_e)^3} + \frac{1 - \mu}{(\mu + x_e)^3} \tag{3.3}$$

with x_e the x-coordinate of L_i, $i = 1, 2$. The energy function thus becomes

$$E_l = \frac{1}{2}\left(\dot{x}^2 + \dot{y}^2 + \dot{z}^2 - ax^2 + by^2 + cz^2\right) \tag{3.4}$$

The system (3.1) or (3.2)can be solved analytically and the eigenvalues of this linear system have the form $\pm\lambda$, $\pm i\omega$ and $\pm i\nu$ where λ, ω and ν are positive constants with $\omega \neq \nu$:

$$\begin{aligned} \lambda &= \sqrt{\frac{c-2+\sqrt{9c^2-8c}}{2}} \\ \omega &= \sqrt{\frac{2-c+\sqrt{9c^2-8c}}{2}} \\ \nu &= \sqrt{c} \end{aligned} \tag{3.5}$$

Phase Space and Flow in the Equilibrium Region To better understand the orbit structure on the phase space, we can make a linear change of coordinates with the eigenvectors as the axes of the new system. Using the corresponding new coordinates (q_1, p_1, q_2, p_2, q_3, p_3), the differential equations of system (3.2) assume the simple form,[1][17]

$$\begin{aligned} \dot{q_1} &= \lambda q_1 & \dot{p_1} &= -\lambda p_1 \\ \dot{q_2} &= \omega p_2 & \dot{p_2} &= -\omega q_2 \\ \dot{q_3} &= \nu p_3 & \dot{p_3} &= -\nu q_3 \end{aligned} \tag{3.6}$$

and the energy function (3.4) becomes

$$E_l = \lambda q_1 p_1 + \frac{\omega}{2}\left(q_2^2+p_2^2\right) + \frac{\nu}{2}\left(q_3^2+p_3^2\right) \tag{3.7}$$

Solutions of Eqs. (3.6) can be conveniently written as

$$\begin{aligned} q_1(t) = q_1^0 e^{\lambda t} \qquad & p_1(t) = p_1^0 e^{-\lambda t} \\ q_2(t) + ip_2(t) &= (q_2^0 + ip_2^0)e^{-i\omega t} \\ q_3(t) + ip_3(t) &= (q_3^0 + ip_3^0)e^{-i\nu t} \end{aligned} \tag{3.8}$$

where the constants q_1^0, p_1^0, q_2^0, p_2^0, q_3^0 and p_3^0 are the initial conditions.
If we set $E_l = \epsilon$ and $|p_1 - q_1| \leq c$ with ϵ and c positive, we determine a region R homeomorphic to the product of 4-sphere and an interval ($S^4 \times I$). For each fixed value of $p_1 - q_1$ in the interval $[-c, c]$, the equation $E_l = \epsilon$ determines a 4-sphere

$$\frac{\lambda}{4}\left(p_1+q_1\right)^2 + \frac{\omega}{2}\left(q_2^2+p_2^2\right) = \epsilon + \frac{\lambda}{4}\left(p_1-q_1\right)^2 \tag{3.9}$$

The bounding 4-sphere of the region for which $p_1 - q_1 = -c$ will be called $n1$, and that where $p_1 - q_1 = c$, n2.

We can consider the projections of the flow on the $(p_1 - q_1)$ plane (that is tilted by 45° with respect to the coordinate axes to correspond to the flow direction) and on the $(p_2 - q_2) \times (p_3 - q_3)$ space respectively. The solutions obtained show that in the neighborhood of L_1 and L_2 the CR3BP dynamics behave like the product *saddle* × *center* × *center* (Fig. 3.1).

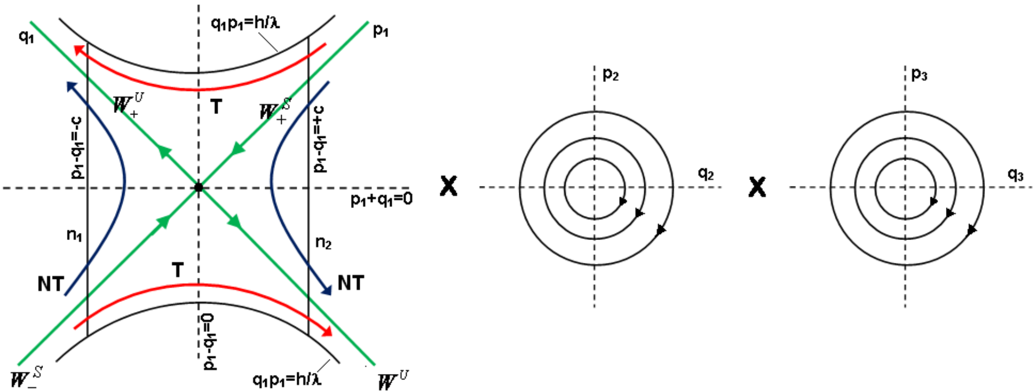

Saddle Projection

Planar Oscillations Projection

Vertical Oscillations Projection

Figure 3.1: The flow in the equilibrium region has the form *saddle* × *center* × *center*. On the left is shown the projection onto the $(p_1 - q_1)$ plane with axes tilted 45. Shown are the bounded orbits (black dot at the centre), the asymptotic orbits (labelled **W**), two red transit orbits (**T**) and two blue non-transit orbits (**NT**).

In the *saddle* projection, the picture of a standard unstable critical point is shown where a set bounded on two sides by the hyperbola $q_1 p_1 = \epsilon/\lambda$ (corresponding to $q_2^2 + p_2^2 = q_3^2 + p_3^2$) and on two other sides by the line segments $p_1 - q_1 = \pm c$ which correspond to the bounding 4-spheres.

The hyperbola $p_1 q_1$=constant are the locus of projections of the orbits on the $p_1 - q_1$ plane, as $q_1 p_1$ is an integral of motion, except in the case $p_1 q_1 = 0$. If $p_1 q_1 > 0$, the branches connect the bounding line segments $p_1 - q_1 = \pm c$, if $p_1 q_1 < 0$, the branches have both end points on the same segment and then on the same side.

We can distinguish nine classes of orbits grouped into four categories:

1. The point at the origin $(q = p = 0)$ correspond to a periodic orbit called **Lyapunov orbit**. In particular it corresponds to a 3-sphere S_h^3

of bounded orbits given by Eq. (3.9) with the new values of q_1 and p_1

$$\frac{\nu}{2}\left(q_2^2+P_2^2\right)+\frac{\omega}{2}\left(q_3^2+p_3^2\right)=\epsilon \tag{3.10}$$

2. The four green segments with arrows pointing toward or away from the origin on the axes $q_1 p_1 = 0$ correspond to four cylinders of orbits asymptotic to the invariant S_h^3 sphere of Eq. (3.10) either for increasing time ($p_1 = 0$) and for decreasing time ($q_1 = 0$). They are called **asymptotic** orbits and they form the stable and unstable manifolds. The *stable manifolds* $W_{\pm}^{s}(S_h^3)$ are given by

   $$\frac{\nu}{2}\left(q_2^2+p_2^2\right)+\frac{\omega}{2}\left(q_3^2+p_3^2\right)=\epsilon, \qquad q_1=0 \tag{3.11}$$

   For convention, $W_{+}^{s}(S_h^3)$ is the branch going from right to left with $p_1 > 0$, while $W_{-}^{s}(S_h^3)$ is the branch going from left to right with $p_1 < 0$. On the contrary, the *unstable manifolds* $W_{\pm}^{u}(S_h^3)$ are given by

   $$\frac{\nu}{2}\left(q_2^2+p_2^2\right)+\frac{\omega}{2}\left(q_3^2+p_3^2\right)=\epsilon, \qquad p_1=0 \tag{3.12}$$

   where $W_{+}^{u}(S_h^3)$ is the branch going from right to left with $q_1 > 0$, while $W_{-}^{u}(S_h^3)$ is the branch going from left to right with $q_1 < 0$

3. The hyperbolic projections determined by $q_1 p_1 = \mathit{constant} > 0$ correspond to two cylinders of orbits that cross the the bounding spheres in the same emisphere. As these orbits transit from one region to the other, they are called **transit** orbits

4. The hyperbolic projections determined by $q_1 p_1 = \mathit{constant} < 0$ correspond to two cylinders of orbits that does not cross the bounding spheres and run from one emisphere to the other on the same bounding sphere thus returning on the same side. For this reason they are called **non-transit** orbits. In case of $q_1 > 0$ the 4-sphere is $n_1(p_1 - q_1 = -c)$, in case of $q_1 < 0$ the 4-sphere is $n_2(p_1 - q_1 = +c)$.

Summarizing, what we must observe is that asymptotic orbits are pieces of stable and unstable manifold tubes of Lyapunov (periodic) orbits. These invariant manifolds act like separatrices between two distinct types of orbits: transit orbits, inside the cylindrical manifolds and able to pass from one manifold to the other (or analogously from one region to the other), and non-transit orbits that are outside the manifold and bounded to stay on the same region.

Trajectories in the Neck Region After a preliminary study of the orbit structure in the equilibrium region, a necessary investigation of the orbits' appearance in the position space will be carried out. According to that, let us take in mind Case 2 and Case 3 of Fig. 2.5 where a neck region is open around libration points L_1 and L_2.

The solution of the linear system (3.1) can be written as

$$\begin{aligned} x(t) &= A_1 e^{\lambda t} + A_2 e^{-\lambda t} + A_3 cos\ \omega t + A_4 sin\ \omega t \\ y(t) &= -k_1 A_1 e^{\lambda t} + k_1 A_2 e^{-\lambda t} - k_2 A_3 sin\ \omega t + k_2 A_4 cos\ \omega t \\ z(t) &= A_5\ cos\ \nu t + A_6\ sin\ \nu t \end{aligned} \tag{3.13}$$

where $A_i (i = 1, .., 6)$ are arbitrary constants determined by the initial conditions. The two constants k_1 and k_2 are

$$k_1 = \frac{2c + 1 - \lambda^2}{2\lambda}, \qquad k_2 = \frac{2c + 1 + \omega^2}{2\omega} \tag{3.14}$$

In a first approximation, as also seen in the previous paragraph, the motion in the vicinity of these equilibrium points is composed of some "hyperbolic" behaviour and of two oscillators (saddle × center × center). This means that the oscillations are not stable and that very small deviations will be amplified as time increases.

Besides, one of the oscillations takes place in the plane of motion of the primaries and the other orthogonal to this plane. These two periodic motions are known as the planar and vertical Lyapunov periodic orbits. The frequencies of the oscillations vary with the amplitudes (since the problem is not linear) and for a suitable amplitude, both frequencies become equal.

Rewriting the oscillatory part of system (3.13) as an amplitude plus a phase, thus setting $A_3 = A_x cos\varphi$, $A_4 = -A_x sin\varphi$, $A_5 = A_z cos\psi$ and $A_6 = -A_z sin\psi$, Eqs (3.13) become

$$\begin{aligned} x(t) &= A_1 e^{\lambda t} + A_2 e^{-\lambda t} + A_x cos\,(\omega t + \varphi) \\ y(t) &= -k_1 A_1 e^{\lambda t} + k_1 A_2 e^{-\lambda t} - k_2 A_x sin\,(\omega t + \varphi) \\ z(t) &= A_z\ cos\,(\nu t + \psi) \end{aligned} \tag{3.15}$$

whose solution is dependent on the four values A_1, A_2, A_x and A_z. Besides, while the former two are associated to the unstable (A_1) and stable (A_2) motion, the latter two regulate the periodic in-plane (A_x) and out-of-plane (A_z) orbits. Different combinations of their values will give us again (as seen in the previous paragraph) the same nine classes of orbits which can be grouped into the same four categories[18] (see also Fig. 3.2):

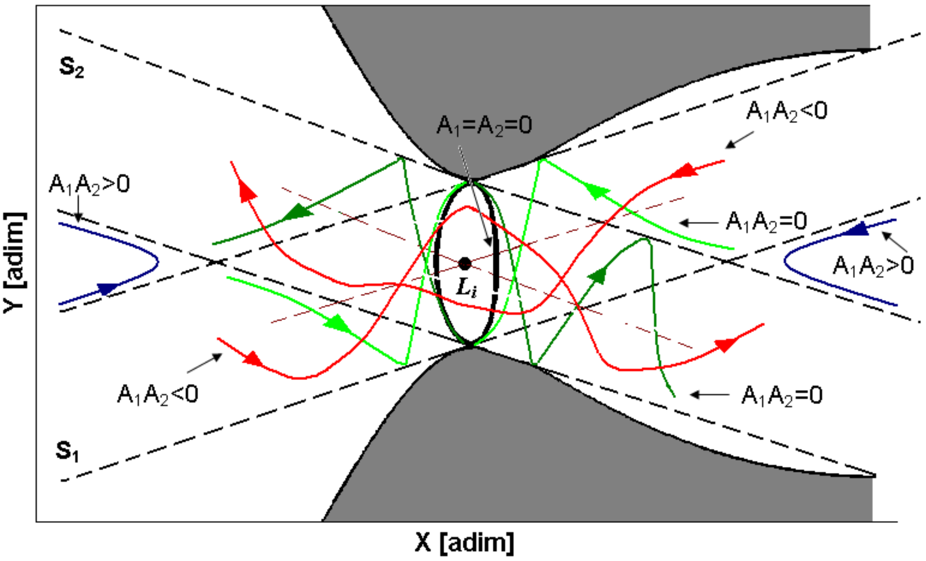

Figure 3.2: Artistic view of projections on the $(x - y)$ plane of trajectories near the L_i, $i = 1, 2$ neck region. Shown are the *periodic* orbit (black), the *asymptotic* orbits on the stable manifold (light green), the *asymptotic* orbits on the unstable manifold (dark green), the *transit* orbits (red) and *non-transit* orbits (blue)

.

1. $\mathbf{A}_x = \mathbf{A}_z = 0$: the saddle part can be isolated. According to the values of A_1 and A_2, different manifolds associated to the lagrangian point can be generated.
   For example, if $A_1 \neq 0$ and $A_2 = 0$ the **unstable manifold** is generated namely $W^u_{L_i}$, $i = 1, 2$. Vice versa, if $A_1 = 0$ and $A_2 \neq 0$ the **stable manifold** is generated namely $W^s_{L_i}$, $i = 1, 2$.

2. $\mathbf{A}_1 = \mathbf{A}_2 = 0$: we obtain planar (if $A_x \neq 0, A_z = 0$) and vertical (if $A_x = 0, A_z \neq 0$) **periodic** orbits (*Lyapunov* orbits) with different frequencies, ω and ν respectively. If at the same time $A_x \neq 0$, $A_z \neq 0$, and $\omega \neq \nu$, quasi-periodic linear *Lissajous* orbits are generated.
   Moreover, in the last case, if A_x and A_z are of sufficient magnitude so that the non-linear contributions to the system produce eigenfrequencies that are equal $(\omega = \nu)$, *Halo*-type periodic motion is obtained.[19]

3. $\mathbf{A}_1\mathbf{A}_2 = 0$: we have orbits that are asymptotic to the periodic orbit. That is why they are called **asymptotic** orbits. In this situation, the invariant manifolds associated to the periodic orbits arise. These are

denoted with $W^s_{L_i,p.o.}$ and $W^u_{L_i,p.o.}$, $i = 1, 2$ and if a spacecraft lies on the stable or unstable manifold, its asymptotic orbit winds onto or off the periodic orbit respectively. This feature is very important in mission design using libration points.

In particular, if $A_1 = 0$ their projection in the $(x - y)$ plane is into the strip S_1 centered around the eigenvector and bounded by the lines

$$y = \sigma x \pm 2\sqrt{\epsilon\left(\sigma^2 + \tau^2\right)/\kappa}$$

Similarly, if $A_2 = 0$, their projection in the $(x-y)$ plane is into the strip S_2 centered around the other eigenvector and bounded by the lines

$$y = -\sigma x \pm 2\sqrt{\epsilon\left(\sigma^2 + \tau^2\right)/\kappa}$$

4. $\mathbf{A}_1\mathbf{A}_2 < 0$: we obtain the so called **transit** orbits that are the only orbits able to cross the equilibrium region and also two different regions around the primaries.

   It is interesting to observe that transit orbits cross the equilibrium region passing from a stable manifold to an unstable manifold. This will lead to the necessity of further investigations in the following paragraphs.

5. $\mathbf{A}_1\mathbf{A}_2 > 0$: we obtain the so called **non-transit** orbits that are bounded around only one of the two primaries and cannot cross the equilibrium region.

3.2 Periodic Orbits and Invariant Manifolds around L_1 and L_2

In the previous section, starting from linearized CR3BP equations of motion in the neighbourhood of collinear libration points, orbit structure on the phase space and thus the trajectories in the neck regions around L_1 and L_2 have been analyzed.

In 1968, Farquhar[20] in his Ph.D. thesis coined the term ”Halo” while he was studying three-dimensional periodic orbits around Earth-Moon L_2 for the exploration of the far-side of the Moon. In general, the subject of periodic solutions in the CR3BP represents a key-point from the mission analysis and design point of view. In fact, in the past many space missions (*ISEE-3*, *WIND*, *SOHO*, *ACE*, *WMAP*, *GENESIS*) were performed in Halo or Lissajous periodic orbits around collinear lagrangian points; these kind of orbits were chosen as orbit maintenance with out-of-plane motion is fundamental for communication relay in order to assure a permanent direct link to ground stations or to avoid solar exclusion zone. That is why, in the preliminary mission design of such a missions, the choice of the out-of-plane ”semi-amplitude” A_z is important as through its value several mission constraints can be formulated.

Moreover, as said before, the invariant manifolds associated to the periodic orbits arise and allow the spacecraft to move from/to periodic orbits to complete the overall transfer. Therefore, for space applications, it is essential to be able to determine the invariant manifolds associated to the libration points or to their periodic orbits.

Computation of Periodic Orbits Recalling Eqs. (3.15) where $A_1 = A_2 = 0$, the three-dimensional motion is quasi-periodic as, in general, the two frequencies ω and ν are different. This is the case of Lissajous orbits where only a small excursion in the out-of-plane direction is allowed. To obtain bigger out-of-plane excursions, Halo orbits are needed in which both in-plane and out-of-plane frequencies are forced to be equal ($\omega = \nu$) by non-linear contributions. A constraint between A_x and A_z is therefore imposed.

First guess of Halo orbits are computed by means of a third-order analytical approximation by Richardson[19][21] in which perturbing potentials due to the primaries of the effective potential (Eq. 2.22) were expanded in power series.

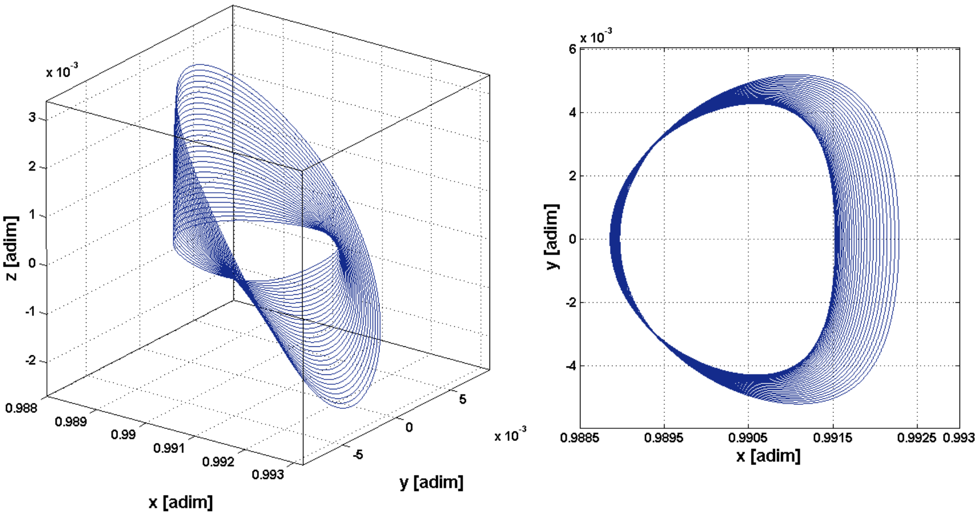

Figure 3.3: Family of Halo orbits obtained for several A_z out-of-plane amplitudes around L_1 of Sun-Earth system

.

However, if the A_x and A_z values obtained in the Richardson method are assigned as initial conditions in the linearized equations of motion and the full dynamic system is propagated, no periodic motion is obtained with the analytic approximation. Numerical schemes that correct the Richardson first-guess solution are necessary. In particular, the method of Thurman and Worfolk[22] has been applied for this scope.
Let $\mathbf{x_0}$ be a state vector located on the $(x - z)$ plane and obtained from the initial guess with only a component of the velocity in the y-direction ($v_0 \neq 0$)

$$\mathbf{x_0} = \{x_0, 0, z_0, 0, v_0, 0\}$$

Let $\mathbf{x_0}$ be the initial condition of the CR3BP equations of motion (Eqs. 2.21). If we stop the propagation after a semi-orbit $t = T_{1/2}$ (where T is the period of the periodic orbit), we obtain:

$$\Phi\left(\mathbf{x_0}, T_{1/2}\right) = \{\tilde{x}, 0, \tilde{z}, \tilde{u}, \tilde{v}, \tilde{w}\}$$

Therefore, if $\tilde{u} = \tilde{w} = 0$ then the initial guess is part of the periodic orbit, if not we need to improve it in order to obtain $\tilde{u} = \tilde{w} = 0$. So the initial condition is corrected through a first order expansion:

$$\Phi\left(\mathbf{x_0} + \Delta\mathbf{x}, T_{1/2} + \Delta t\right) = \Phi\left(\mathbf{x_0}, T_{1/2}\right) + \left[\frac{\partial \Phi\left(\mathbf{x_0}, T_{1/2}\right)}{\partial \mathbf{x}}\right] \cdot \Delta\mathbf{x} + \frac{\partial \Phi\left(\mathbf{x_0}, T_{1/2}\right)}{\partial t} \cdot \Delta t \tag{3.20}$$

where

$$\Delta\mathbf{x} = \{\Delta x, 0, \Delta z, 0, \Delta v, 0\}$$

and the periodicity is imposed by setting the flow equal to:

$$\Phi\left(\mathbf{x_0} + \Delta\mathbf{x}, T_{1/2} + \Delta t\right) = \{x^*, 0, z^*, 0, v^*, 0\}$$

that is still unknown. The second term on the right-hand side of Eq. (3.20) represents the *transition matrix* $M = \partial\Phi/\partial\mathbf{x}$ and it is also called the *monodromy matrix* for periodic orbits. Eq. (3.20) can be rewritten as

$$M \left\{\begin{array}{c} \Delta x \\ 0 \\ \Delta z \\ 0 \\ \Delta v \\ 0 \end{array}\right\} + \mathbf{f}(\Phi)\,\Delta t = \left\{\begin{array}{c} x^* \\ 0 \\ z^* \\ 0 \\ v^* \\ 0 \end{array}\right\} - \left\{\begin{array}{c} \tilde{x} \\ 0 \\ \tilde{z} \\ \tilde{u} \\ \tilde{v} \\ \tilde{w} \end{array}\right\} \tag{3.23}$$

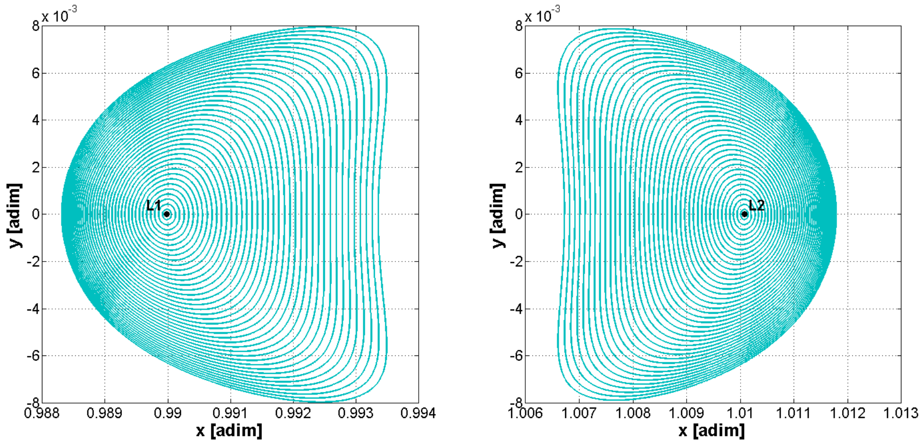

Figure 3.4: Family of Lyapunov orbits obtained for several A_x amplitudes around L_1 and L_2 of Sun-Earth system

.

where $\mathbf{f}(\Phi) = \partial\Phi/\partial t$. Considering only the second, fourth and sixth rows, we have three equations in the four unknowns $\Delta x, \Delta z, \Delta v$ and Δt.

Thus, setting $\Delta z = 0$, equations can be solved numerically by means of an iterative scheme where the initial condition is updated at each iteration

$$\mathbf{x_0}^{i+1} = \mathbf{x_0}^{i} + \Delta\mathbf{x} \tag{3.24}$$

till the flow, propagating under CR3BP equations, reaches the condition $\tilde{u} = \tilde{w} = 0$.

The monodromy matrix is computed by integrating the system:

$$\begin{aligned} \dot{\mathbf{x}} &= \mathbf{f}(\mathbf{x}), & \mathbf{x}(0) &= \mathbf{x_0} \\ \dot{M} &= \left[\frac{\partial \mathbf{f}}{\partial \mathbf{x}}\right] M, & M(0) &= \mathbf{I} \end{aligned} \tag{3.25}$$

where $\mathbf{I}$ is the 6×6 unity matrix. Results for a family of Halo orbits around the L_1 point in the Sun-Earth system are shown in Fig. 3.3.

The same considerations apply to the construction of Lyapunov orbits that are planar periodic orbit with $A_z = 0$. Therefore, third and sixth rows of Eq. (3.23) do not exist and finally we obtain two equations in three unknowns Δx, Δv and Δt. Fixing $\Delta x = 0$ and solving for the other two unknowns, we can find a family of periodic solutions parametrized by the intersection with the x-axis (Fig. 3.4).

Construction of Lissajous quasi-periodic orbits is slightly different as they are tridimensional orbits. In this case the definition of both A_x (or A_y) and

A_z is necessary. An example of Lissajous orbit in the L_1 Sun-Earth system with specified A_y and A_z amplitudes is shown in Fig. 3.5.

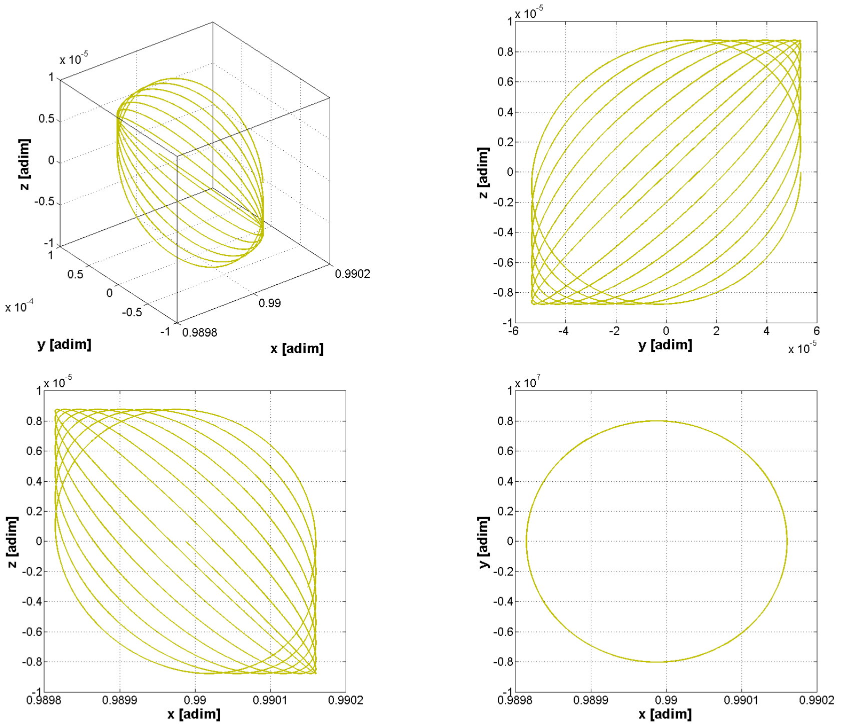

Figure 3.5: Lissajous orbit around L_1 Sun-Earth system with A_x=1937560.3 [km], A_y=600000 [km] and A_z=100000 [km] amplitudes

.

Determination of the Invariant manifolds associated to collinear libration points A manifold is a mathematical term for surfaces of arbitrary dimension. In dynamical system theory, an *invariant* manifold is a special manifold made out of orbits. Therefore, if we take a point on this surface, it belongs to a specific orbit and then it will remain on such a structure under the influence of CR3BP equations of motion. That is why the term 'invariant'.[23][24]

In other words, an invariant manifold is a m-dimensional surface formed by a collection of orbits that start and remain on it throughout their dynamical evolution. Besides, as outlined in the paragraph concerning the trajectories in the neck regions, invariant manifolds can be divided into *stable* and *unstable* manifolds depending on if they approach to or if they depart from the libration point/periodic orbit around the libration point.

Explaining this concept mathematically, we have to start from the fact that the CR3BP is a vector field bound in $\Re^6$ where one and one only vector is bound to every point in the vector field. Therefore, the integration of any point p in the vector field with respect to time generates only one trajectory Γ. Moreover, let α- and ω- limits be the set of points in $\Re^6$ as Γ tends toward $-\infty$ and $+\infty$ respectively.

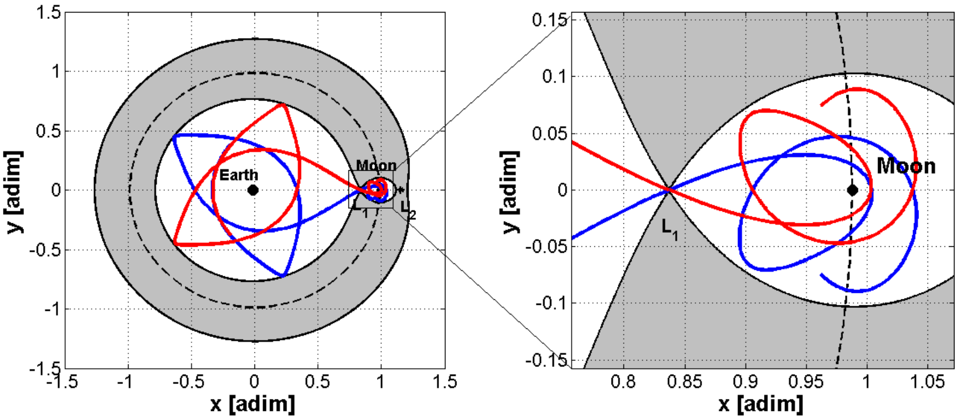

Figure 3.6: Stable (blue) and unstable (red) manifolds associated to L_1 of the Earth-Moon system with the forbidden region plotted.

We can say that a stable manifold is the set of all points whose trajectories have the same ω- limit set, while an unstable manifold is the set of all points whose trajectories have the same α- limit set.

As discussed in the previous sections, the orbit structure of collinear libration points behaves like the product *saddle* × *center* × *center*. The *saddle* part constitutes the necessary condition for the existence of the invariant manifold as it has eigenvectors with both positive and negative real part.

Thus, to obtain an invariant manifold of the Lagrange point, one put a particle at the Lagrange point and perturbes it by a small amount in both the positive and negative directions defined by the eigenvectors. To construct the stable/unstable manifold, it is necessary to propagate backward/forward in time.

Therefore, let d be the value of the perturbation, we have:

- For the stable manifold W^s_{Li} is necessary a backward integration of the selected initial condition $\mathbf{X_e}$ along the stable eigenvector $\mathbf{u_s}$:

$$\mathbf{X_0}^{W^s} = \mathbf{X_e} \pm d\mathbf{u_s}$$

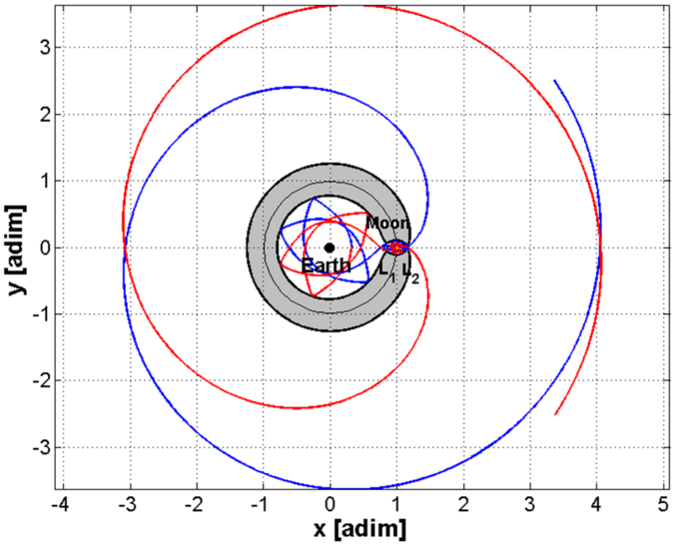

Figure 3.7: Stable (blue) and unstable (red) manifolds associated to L_2 of the Earth-Moon system with the forbidden region plotted.

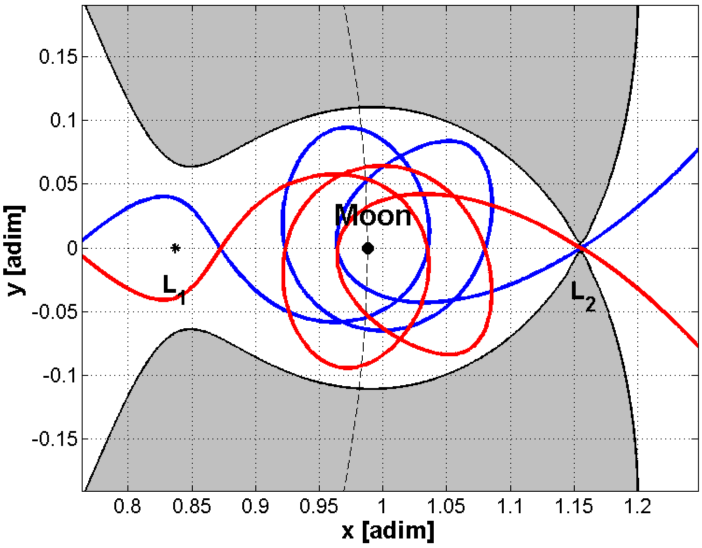

Figure 3.8: Stable (blue) and unstable (red) manifolds associated to L_2 of the Earth-Moon system with the forbidden region plotted (zoom).

- For the unstable manifold $W^u_{L_i}$ is necessary a forward integration of the selected initial condition $\mathbf{X_e}$ along the unstable eigenvector $\mathbf{u_u}$:

$$\mathbf{X_0}^{W^u} = \mathbf{X_e} \pm d\mathbf{u_u}$$

The sign "± " indicates two branches departing from/approaching to the initial point (see Fig. 3.6 and Fig. 3.8).

Determination of the Invariant manifolds associated to periodic orbits around collinear libration points To construct the invariant manifolds of a periodic orbit, first of all it is necessary to produce the monodromy matrix (recall Eq. (3.25)) whose eigenvalues provide information about the stability of the orbit. Once the monodromy matrix M has been obtained, the manifolds are computed by propagating the flow along the directions corresponding to eigenvalues of the monodromy matrix (the Floquet multipliers of that orbit).

In particular, if $\mathbf{X_0}$ is a point belonging to the periodic orbit, the monodromy matrix represents the first order appproximation for the mapping of a point $\mathbf{X}$, taken in a small neighbourhood through

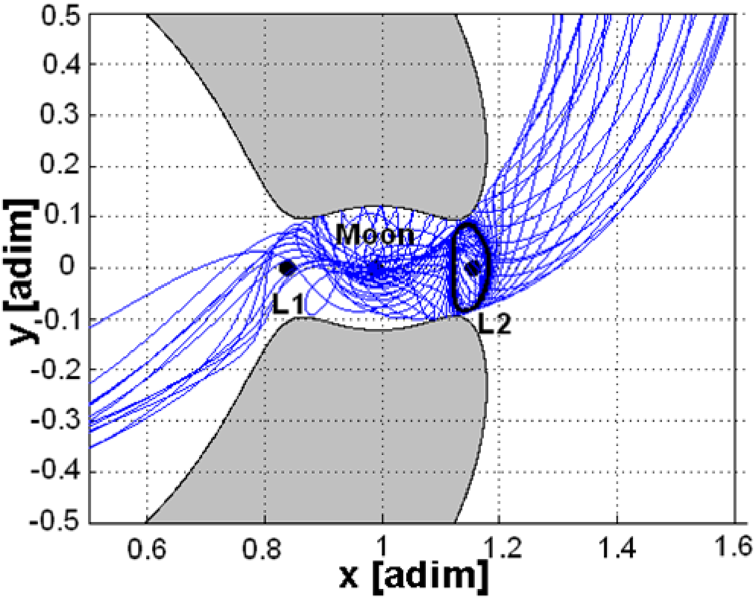

Figure 3.9: Stable manifolds associated to Halo orbit on L_2 of the Earth-Moon system with the forbidden region plotted.

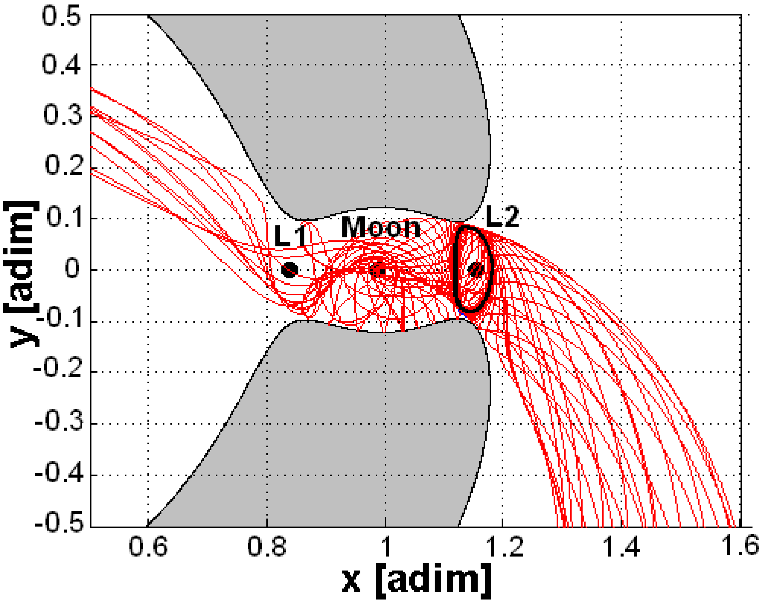

Figure 3.10: Unstable manifolds associated to Halo orbit on L_2 of the Earth-Moon system with the forbidden region plotted.

$$\mathbf{X} \rightarrow \mathbf{X_0} + M\left(\mathbf{X} - \mathbf{X_0}\right) \tag{3.28}$$

Thus, assuming the periodic orbit unstable, there will be one stable eigenvalue λ^s and an unstable eigenvalue λ^u that correspond to the stable and unstable eigenvector $\mathbf{v_s}$ and $\mathbf{v_u}$, respectively. Selected all the initial states $\mathbf{X_0}$ on the periodic orbit and assumed a perturbation value d, we have:

- For the stable manifold $W^s_{L_i,p.o.}$ associated to the periodic orbit is necessary a backward integration along the stable eigenvector $\mathbf{v_s}$:

$$\mathbf{X}^{W^s_{L_i,p.o.}} = \mathbf{X_0} \pm d\mathbf{v_s}$$

- For the unstable manifold $W^u_{Li,p.o.}$ associated to the periodic orbitis necessary a forward integration along the unstable eigenvector $\mathbf{v_u}$:

$$\mathbf{X}^{W^u_{L_i,p.o.}} = \mathbf{X_0} \pm d\mathbf{v_u}$$

It is worth noting that the magnitude of perturbation d should be small enough to avoid violating the linear estimate but not so small that the time of flight becomes too large due to the asymptotic nature of the manifold.

3.3 Connections of the local orbit structures

In the previous paragraphs, a detailed analysis about the linearized dynamics around collinear libration points has been carried out together with the comprehension of the orbit structure in both phase and position space. Then, computation of periodic orbits and of manifolds (associated to both libration points and to periodic orbits) has been analyzed as in many practical mission design problems under the assumptions of CR3BP, it represents the starting point for a preliminary analysis.
Therefore, if we consider different three-body systems, for each of them it is possible to design a set of manifolds (starting from periodic orbits or equilibrium points) that could intersect each other and allow the third body to move inside this ”dynamical channel” transferring from one system to the other.
In this picture, the understanding of the global orbit structure and of the necessary conditions to satisfy these transitions is fundamental.

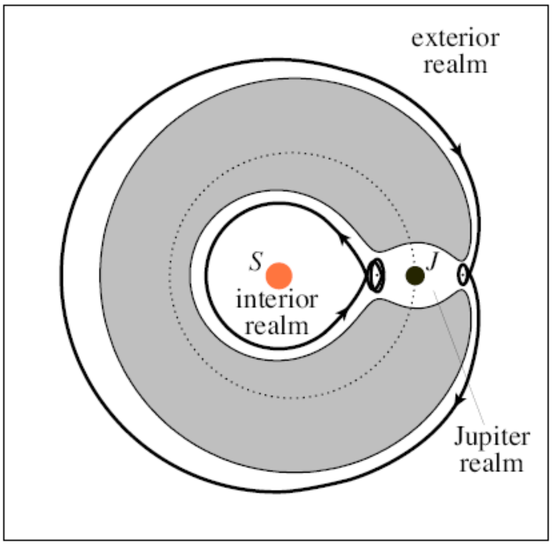

Figure 3.11: Example of homoclinic orbits in interior and exterior realms in the Sun-Jupiter system (from Ross[1]).

Homoclinic Connections *Homoclinic* orbits are orbits which are *double* asymptotic (i.e. both forward and backward asymptotic) to the unstable

periodic orbit (for example Lyapunov orbits). Therefore, the homoclinic orbit is both on the stable and unstable manifold of the same periodic orbit and, as consequence, a body moving on it will depart from the periodic orbit and will return to it (Fig. 3.11).
In 1969, McGehee[25] and Conley[18] demonstrated the existence of homoclinic orbits in both the interior and the exterior realm. McGehee also demonstrated that a body departing from a periodic orbit around L_1 and moving on a homoclinic orbit is bounded to move in the interior realm in the counterclockwise sense. On the other hand, a body departing from a periodic orbit around L_2 and moving on a homoclinic orbit is bounded to move in the exterior realm in the clockwise sense.
Later, Llibre, Martinez and Simò[26] spent their major efforts to demonstrate the transversality of homoclinic orbits under appropriate conditions.
As the homoclinic orbit can be seen as the intersection of the stable and of the unstable manifolds of the periodic orbit, the transversality of homoclinic orbits demonstrated by Llibre et al.[26] implies the transversality of the manifold intersection. This is of fundamental importance from the orbit structure point of view.
Before constructing a homoclinic orbit, it is necessary to find the intersection between the stable ($W^s_{L_i,p.o.}$) and the unstable ($W^u_{L_i,p.o.}$) manifolds by means of the so called "*Poincarè section*" (or *cut*) in the phase space.[26][2] When an orbit of the manifold reaches the desired location of the cut, the state variables are registered. For homoclinic orbits of L_1 (or L_2), the Poincarè cut is obtained by intersecating them with a plane located at $y = 0$ and $x < 0$ in the interior (or exterior) realm (see Fig. 3.12 and Fig. 3.13).

In Fig. 3.12 and Fig. 3.13, the first intersection $\Gamma_1^{u,S}$ and $\Gamma_1^{u,\chi}$ was used, where the superscripts S and χ indicate the realm. It is possible that orbits on the manifold, if integrated further, can intersect Poincare section several times without leaving the realm $\Re$ considered. In that case, the q-th intersection is then denoted with $\Gamma_q^{u,\Re}$ (or $\Gamma_p^{s,\Re}$ for stable manifold).

In general, a point in $y = 0$ belonging to $\Gamma_q^{u,\Re} \cap \Gamma_p^{s,\Re}$ (if not empty) will be called a $(q, p)-$homoclinic point and their existence for certain values of q and p is shown in McGehee.[25]
Consider again Fig. 3.12. By the symmetry of the CR3BP equations of motion:

$$s : (x, y, \dot{x}, \dot{y}, t) \rightarrow (x, -y, -\dot{x}, \dot{y}, -t) \tag{3.31}$$

Hence, once $\Gamma_1^{u,S}$ intersection is known, it turns out that $\Gamma_1^{s,S}$ will intersect the $x-$axis at the same point. These P points (see Fig. 3.12(b)) correspond to symmetric homoclinic orbits to the periodic orbit[2] and at each point P

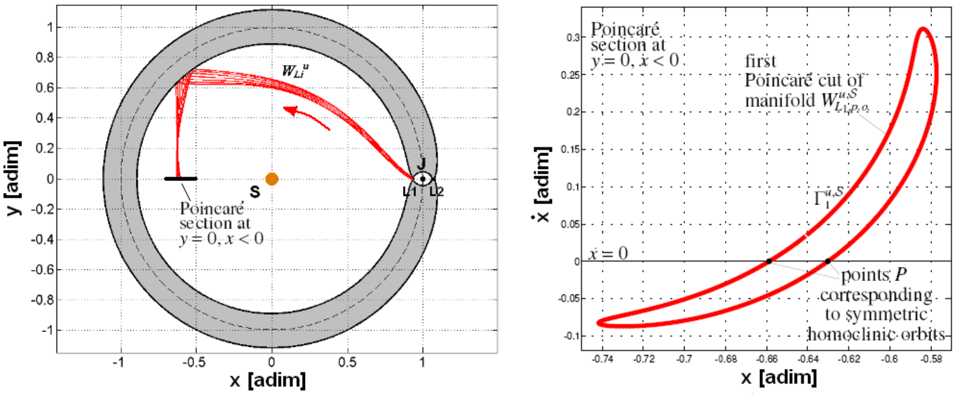

(a) (b)

Figure 3.12: (a) Projection in the position space of the interior branch of the unstable manifold $W^u_{L_1,p.o.}$ (b) First intersection (Poincarè cut) $\Gamma_1^{u,S}$ of the interior branch of $W^u_{L_1,p.o.}$ with the plane $y = 0, x < 0$ in the interior realm S (from Koon et al.[2]).

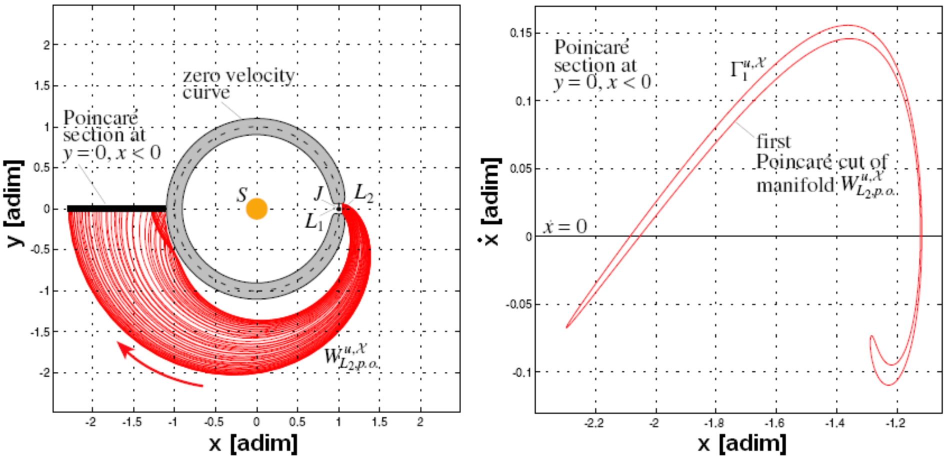

(a) (b)

Figure 3.13: (a) Projection in the position space of the exterior branch of the unstable manifold $W^u_{L_2,p.o.}$ (b) First intersection (Poincarè cut) $\Gamma_1^{u,\chi}$ of the exterior branch of $W^u_{L_1,p.o.}$ with the plane $y = 0, x < 0$ in the exterior realm χ (from Koon et al.[2]).

corresponds an orbit that tend to the same fixed orbit in positive and negative time. These orbits are called (symmetric) $(q, p)-$homoclinic orbits. Llibre et al.[26] demonstrated that the set of values of μ for which there is a symmetric

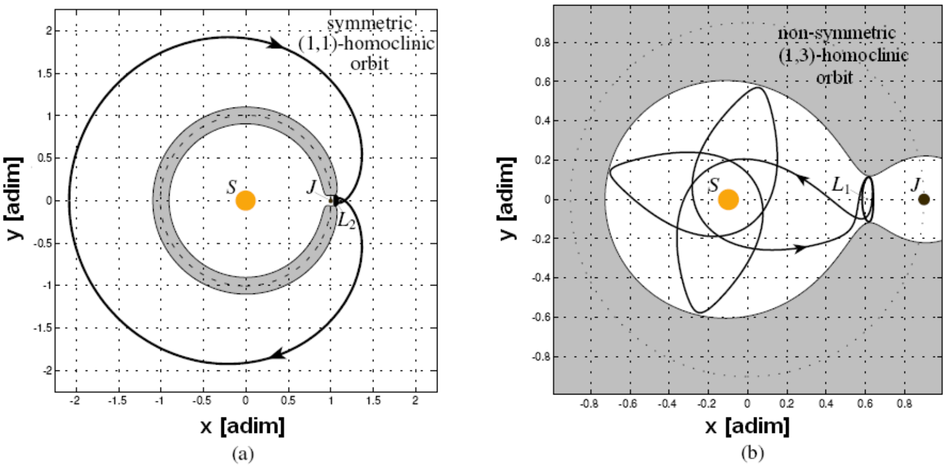

Figure 3.14: (a) Symmetric (1,1)-homoclinic orbit in the exterior region. (b) Non-symmetric (1,3)-homoclinic orbit in the interior region (from Ross[1]).

(1,1)-homoclinic orbit associated to L_1 is discrete.
In Fig. 3.14 examples of symmetric (1,1)-homoclinic (in the exterior realm) and non-symmetric (1,3)-homoclinic (in the interior realm) orbits are shown.

Heteroclinic Connections Another important family of orbits are the *heteroclinic* orbits that allow a connection between periodic orbits of L_1 and L_2. In fact, they are on the unstable manifold of one periodic orbit and on the stable manifold of the other one. Of course, essential assumption for such a connection is a suitable value of the energy associated to the third body motion (for example Case 3 or Case 4 of Fig. 2.5). Therefore, heteroclinic connections allow third body to cross the realm of the primary m_2.

To construct a heteroclinic connection, as did for homoclinic orbits, it is necessary to find intersection of the two manifolds on a suitable Poincarè section that cuts the flow with the plane $x = 1 - \mu$ (It was demonstrated that this plane maximizes the number of intersections under specific assumptions[2]). For example, as shown in Fig. 3.15, a heteroclinic orbit which goes from an L_1 Lyapunov orbit (for negative times) to an L_2 Lyapunov orbit (for positive times) is generated starting from the intersection of the two manifolds in the Poicarè cut at $x = 1 - \mu$. Once the values of y^* and $\dot{y}^*$ are identified, we can propagate backward and forward the initial point $(1 - \mu, y^*)$ with the initial velocity $(\dot{x}^*, \dot{y}^*)$ (we will see next paragraph how to compute $\dot{x}^*$) under CR3BP equations of motion. Then, the heteroclinic orbit is computed (see Fig. 3.16).

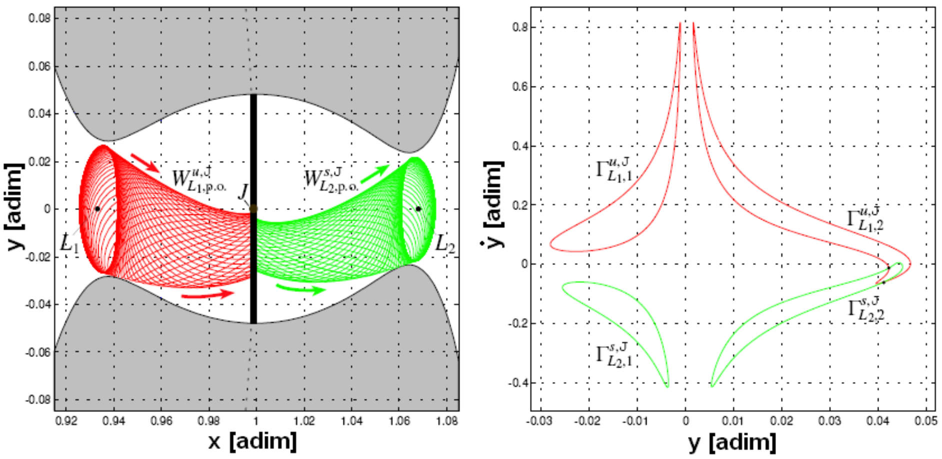

(a) (b)

Figure 3.15: (a) Projection of the unstable manifold $W^{u,J}_{L_1,p.o.}$ and of the stable manifold $W^{s,J}_{L_2,p.o.}$ in the position space of Jupiter realm. (b) The first two Poincarè cuts of the invariant manifolds with the plane $x = 1 - \mu$ (from Ross[1]).

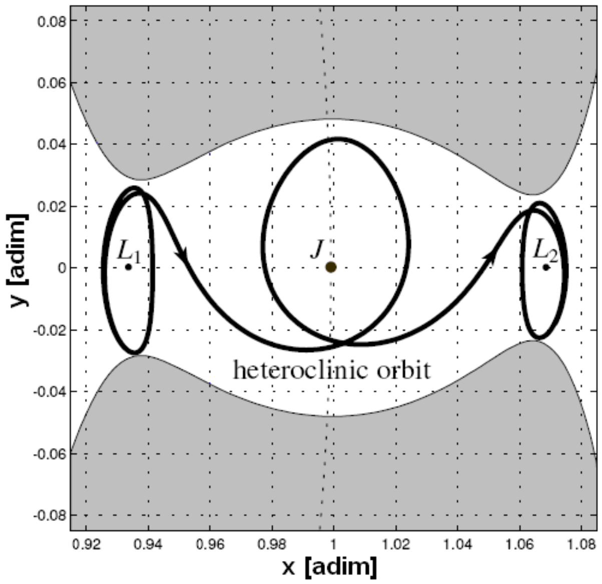

Figure 3.16: Transversal (2,2)-heteroclinic orbit generated starting from intersection point in Poincarè cut of $\Gamma^{u,J}_{L_1,2}$ and $\Gamma^{s,J}_{L_2,2}$ (from Ross[1]).

As already said for homoclinic orbits, intersections of manifold with the Poincarè section are labeled with $\Gamma^{u,J}_{L_1,q}$ and with $\Gamma^{s,J}_{L_2,p}$ where the superscripts indicate respectively if the manifold is stable or unstable and which realm is considered while the subscripts identify respectively the libration point of the periodic orbit of origin and the q-th (or p-th) intersection of $W^{u,J}_{L_1,p.o.}$ (or $W^{s,J}_{L_2,p.o.}$) with the Poincarè plane. It turns out out that the orbit obtained is a (q,p)-transversal heteroclinic orbit (the term *transversal* is because we only consider the cases in which manifolds intersect transversely). In the case of Fig. 3.15(b), the intersection considered to generate the heteroclinic orbit was the second for both the unstable and stable manifold. That is why the curves on the Poincarè section are labeled with $\Gamma^{u,J}_{L_1,2}$ and $\Gamma^{s,J}_{L_2,2}$ and the orbit obtained is a (2,2)-heteroclinic orbit.
According to Koon et al.,[2] the sum $q + p$ must be an even positive integer and the number or revolutions around the m_2 primary will be given by $(q + p - 1)/2$.

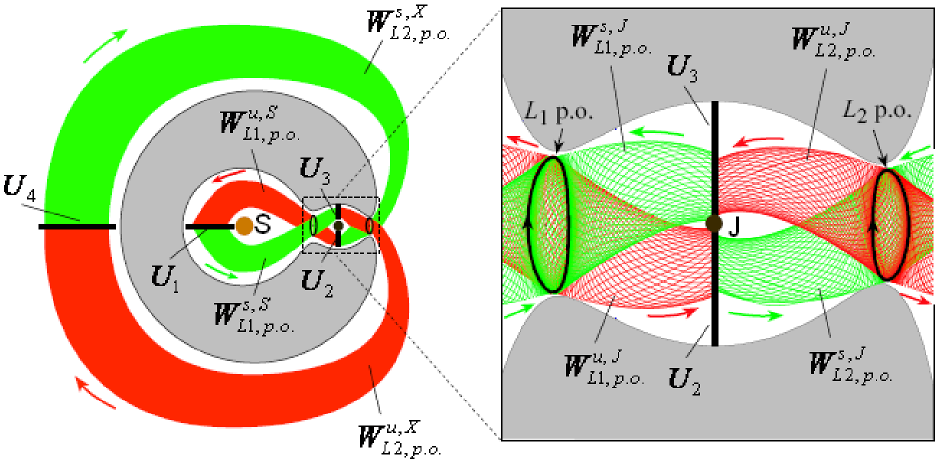

Figure 3.17: Location of the different Poincarè sections U_1, U_2, U_3, and U_4 with the magnification of Jupiter realm. (from Ross[1])

At this point, it is easy to figure out that suitable combinations of homoclinic and heteroclinic orbits of the same energy value can allow to design orbit transfers from interior to exterior realm (and vice versa) of a three-body system. That is what is called **homoclinic-heteroclinic chain** of orbits which connects asymptotically periodic orbits around L_1 and L_2.

In addition, it is worth noting that the essential contribution of the Poincarè sections in the dynamical systems theory applied to the CR3BP is to provide initial phase space conditions for orbits having prescribed itineraries.

We will see how in the next section. Besides, even if in principle the place in which the cut is made is arbitrary for the method and it does not affect the results,[27] according to Koon et al.[2] the preferred four Poincarè sections are shown in Fig. 3.17 with their corresponding stable and unstable manifolds. In detail, the U_1 and U_4 Poincarè sections are defined by the following two dimensional surfaces:

$U_1 = \{(x, \dot{x}) \mid y = 0,\ x < 0,\ \dot{y}\,(x, \dot{x}; e) < 0\}$, in the S realm

$U_4 = \{(x, \dot{x}) \mid y = 0,\ x < -1,\ \dot{y}\,(x, \dot{x}; e) > 0\}$, in the X realm

where $\dot{y}\,(x, \dot{x}; e)$ denotes that $\dot{y}$ is obtained from the energy equation. The U_2 and U_3 Poincarè sections are defined by the following:

$U_2 = \{(y, \dot{y}) \mid x = 1 - \mu,\ y < 0,\ \dot{x}\,(y, \dot{y}; e) > 0\}$, in the lower half of J realm

$U_3 = \{(y, \dot{y}) \mid x = 1 - \mu,\ y > 0,\ \dot{x}\,(y, \dot{y}; e) < 0\}$, in the upper half of J realm

where $\dot{x}$ is obtained from the energy equation.

3.4 Design of Prescribed itineraries

In this section, the construction of orbits with prescribed itineraries is described. For simplicity, the planar case is considered but the same considerations apply to the three-dimensional case. Once the three-body system has

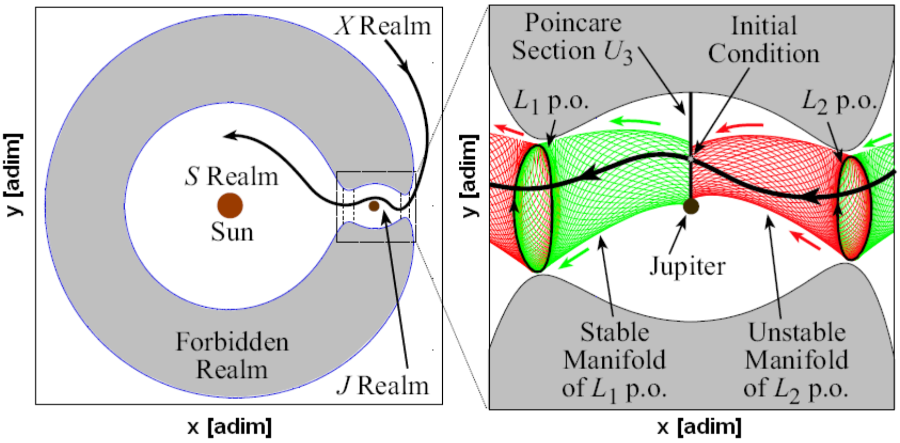

Figure 3.18: Schematic (X,J,S) trajectory and magnification of Jupiter realm. (from Ross[1])

been chosen (for example the Sun-Jupiter system), the appropriate level of energy must be selected. In fact, if we want to construct an orbit that allows the spacecraft to move between all the three realms of the system (Sun realm S, Jupiter realm J and exterior realm X), it is necessary to be in the case in which both the L_1 neck and the L_2 neck are open (Case 3 of Fig. 2.5).

Imagine to construct a trajectory with itinerary (X, J, S) that means a trajectory that starts from the exterior realm, crosses the Jupiter realm and then moves to the interior realm of the Sun (Fig. 3.18.

After the selection of the energy level, we must compute the periodic orbits for either L_1 and L_2 and the invariant manifolds associated to them as explained in Sec. 3.2.

At this point we have all the global structures to design our trajectory. In fact, connectivity between stable and unstable manifolds associated to periodic orbits of the libration points is the key-point to our design process.

The first thing to do is to find a suitable initial condition from which the orbit can propagate backward and forward under CR3BP equations of motion. As we are interested to a solution that comes from L_2 and moves toward L_1, the initial condition must be searched in the Poincarè cut of the invariant manifolds with the plane $x = 1 - \mu$ (U_3), in particular where the unstable Poincarè section $\Gamma^{u,J}_{L_2,q}$ intersects the stable Poincarè section $\Gamma^{s,J}_{L_1,p}$. In this

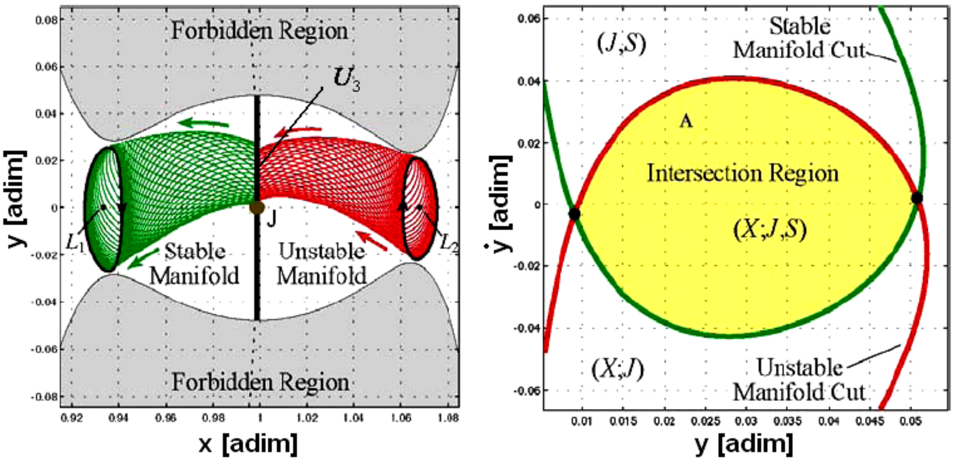

(a) (b)

Figure 3.19: (a) Invariant manifolds to be considered in the Jupiter realm to design the trajectory (X,J,S) (b) U_3 Poincarè section of the invariant manifold of L_1 (stable) and of L_2 (unstable) with the intersection zone in yellow (from Gomez et al.[3]).

way, the initial condition selected will propagate forward to L_1 periodic orbit and backward to L_2 periodic orbit creating a heteroclinic connection. It is worth noting that, without any additional mission constraint (minimum distance from the body m_2, number of revolutions around m_2, etc..), the set of initial conditions is composed by all geometrical points $(y^*, \dot{y}^*)$ included in the intersection region of the stable and unstable Poincarè sections (yellow region of Fig. 3.19(b)). Therefore, the initial condition we are searching is

$$\mathbf{s_0} = (x_0, y_0, \dot{x}_0, \dot{y}_0)^T \tag{3.32}$$

where $x_0 = 1 - \mu$, $y_0 = y^*$ and $\dot{y}_0 = \dot{y}^*$. The value of $\dot{x}_0$ comes from the energy equation (Eq. (2.28)) and therefore:

$$\dot{x}_0 = -\sqrt{-\dot{y}_0^2 - 2\bar{U}\left(x_0, y_0\right) + 2E\left(x_0, y_0, \dot{x}_0, \dot{y}_0\right)} \tag{3.33}$$

as the value of E is known from the first step of the procedure and the effective potential is given from Eq. (2.22). The negative sign of the square root is because we are considering the section U_3 in which the flow passes from right to left and thus for negative x-component of the velocity.

Chapter 4

Optimization Techniques

One of the most important tasks during the preliminary design of space missions is the analysis and optimization of suitable mission trajectories. In this chapter, the low-thrust trajectory optimization problem is formulated and characterized and then, by means of optimal control theory, solution is shown.
Concerning Electric Propulsion spacecrafts, once the preliminary set of mission constraints are defined (initial orbit/launcher, final orbit, mass, max thrust level, etc..), the optimization problem is finding the values of the variables (firing time, thrust angles, thrust level, etc..) that minimize (or maximize) the objective function (propellant mass consumption/payload mass, transfer time).

Optimal control problems for high-thrust systems are relatively straightforward as the duration of thrust arcs is usually short in comparison to the mission time. On the other hand, low-thrust propulsion systems operate for a significant part of the overall transfer and the low-thrust optimization problem is equivalent to the search for optimal control functions in an infinite dimensional function space.

Moreover, analytical solutions of the optimal control problem are available only for some special cases and specific numerical methods are necessary to obtain solutions. Basically, in literature, methods available for solving continuous trajectory optimization are classified into two categories:[28][29][30][31] the *indirect methods*, which are also referred to as *calculus of variation* or the *Maximum Principle of Pontryagin*, and the *direct methods* which transform the original optimal control problem into a nonlinear parameter optimization problem. The former are faster compared to direct methods but their convergence domain is very sensitive with respect to the initial conditions, the latter are numerically more robust and the quality of the initial guess is therefore not as crucial as for indirect methods.

4.1 The Optimal Control Problem Formulation and Low-Thrust Trajectory Optimization

A spacecraft trajectory is obtained integrating its equations of motion which are typically given by a set of first-order differential equations of the form

$$\dot{\mathbf{x}} = \mathbf{f}\left(\mathbf{x}, \mathbf{u}, t\right) \tag{4.1}$$

where $\mathbf{x} \in \Re^n$ is the state space (position and velocity), $\mathbf{u} = \mathbf{u}\left(t\right) \in \Re^m$ is the control function (for example magnitude and direction of thrust vector) and $t \in [t_0, t_f] \subset \Re$ is the time interval.
In trajectory optimization problems, the focus is to find the time history of the control vector $\mathbf{u} = \mathbf{u}\left(t\right)$ such that it minimizes (or maximizes) a scalar performance index. Moreover, in general both the state of the system and the control vector are subjected to a set of *path* constraints $\mathbf{g}$ and boundary constraints Ψ_0 and Ψ_f that must be satisfied at the solution. These constraints can be both equality or inequality constraints.

In the following, a general mathematical formulation of the optimal control problem is presented:

Find the control vector

$$\mathbf{u}^* = \mathbf{u}^*\left(t\right) \tag{4.2}$$

that minimizes the performance index

$$J = \phi\left(\mathbf{x}\left(t_f\right), t_f\right) + \int_{t_0}^{t_f} L\left(\mathbf{x}, \mathbf{u}, t\right) dt \tag{4.3}$$

subject to equations of motion

$$\dot{\mathbf{x}} = \mathbf{f}\left(\mathbf{x}, \mathbf{u}, t\right) \tag{4.4}$$

to path constraints for $t \in [t_0, t_f]$

$$\mathbf{g}\left(\mathbf{x}, \mathbf{u}, t\right) \geq 0 \tag{4.5}$$

and to boundary constraints

$$\Psi_0\left(\mathbf{x}_0, t_0\right) \geq 0 \qquad \Psi_f\left(\mathbf{x}_f, t_f\right) \geq 0 \tag{4.6}$$

where ϕ is the Mayer term that is in general a nonlinear function of the state of the system at t_f (i.e something that must be verified only at the final

state of the system) and L is the Lagrange term that, along the trajectory, is a function of both the state of the system and of the control vector (i.e. something that must be satisfied all along the trajectory).
In the optimal control problem, the equations of motion represent a set of dynamic constraints.

In trajectory design, minimization of the transfer time for a given payload/propellant mass, minimization of the propellant mass for a given transfer time and launch mass/payload mass can be typical mission objectives and the optimality of spacecraft trajectories can be measured with the *performance index* (or *cost function* or *objective function*) that can be mathematically expressed as for example:

$$J_{m_P} = \int_{t_0}^{t_f} \dot{m}_P dt = m_P(t_f) - m_P(t_0)$$

for minimum-propellant transfer problem or

$$J_T = \int_{t_0}^{t_f} dt = t_f - t_0 = T$$

for minimum-time transfer problem.

Practically, sometimes spacecraft trajectory has to be optimized with respect to conflicting mission objectives, e.g. minimize transfer time and propellant mass and this problem can be faced essentially in two different ways; the first way is to define only a single mission objective and treat the others as constraints, the second way is to define a new objective function as a combination of all mission objectives by means of weighting factors that can reflect coherently the scientific relationships of the mission objectives.

In a typical high-thrust optimal control problem, once the initial and final spacecraft position and velocities are assigned, once the transfer time is assigned, the optimization problem is reduced to find the minimum ΔV to perform the transfer (in other words minimization of the propellant mass).

On the other hand, as propulsion system operates for a significant portion of the overall transfer, a low thrust optimization problem must be modelled as a continuous system and therefore it is in general more challenging and numerically difficult as it is equivalent to the problem of finding the optimal control function $\mathbf{u}^* = \mathbf{u}^*(t)$ in an infinite-dimensional function space.
Besides, one of the major issues in such a problem is to find a first guess solution to start the optimization process.

4.2 Direct Methods

Direct trajectory optimization methods were developed in 1970s as consequence of the development of digital computers. In direct algorithms, the optimal control problem is transformed into a *NonLinear Programming (NLP) problem* which is solved either via a penalty function method or methods of augmented Lagrangian functions.
These methods have the power to be able to solve very complex problems without a strong effort in mathematical analysis as only the physical equations must be implemented by the user, but they require an efficient algorithm to solve constrained nonlinear programming problems with thousands of variables and nonlinear constraints.

Direct methods are essentially divided into two subclasses:

- Direct Shooting Methods
- Direct Collocation Methods

In both methods, time interval $[t_0, t_f]$ is discretized and both the control parameters (the unknowns of the optimization problem) and the path constraints of the nonlinear programming problem are evaluated at the grid points of the discretized problem.

The states are chosen to be continuously differentiable and the optimal control time history can be approximated by means of piecewise constant, linear or spline functions between the grid points. Obviously, higher-order polynomial approximations can be used to improve accuracy of the solution with a consequent significant increase of computation cost.
However, both the control approximation and the discretization of path constraints, are usually not critical in the framework of engineering problems and the error made by obtaining a sub-optimal solution due to the discretization is well below the modelling error. Nevertheless, if in direct methods solution is approximated and its accuracy increases as the number of control parameters increase (then a considerable increase in computational complexity and cost must be considered), on the other hand the major advantage of these methods is their numerical robustness that has no equivalent in indirect methods.

Besides, as result of the discretization process, another drawback of direct methods is the existence of multiple minima (or pseudo-minima) that satisfy all necessary conditions for the optimal solution but they are not so close to the actual minimum.

The Nonlinear Programming Problem An optimal control problem can be transformed into a *Nonlinear Programming Problem*, NLP for brevity, which represents a decisional problem concerning a scalar algebraic function and an algebraic vector of constraints. As opposite to the optimal control problem, no dynamics is involved into a NLP problem.

Suppose that the n variables $\mathbf{x}$ must be chosen to solve

$$\min_{x} F(\mathbf{x}) \tag{4.9}$$

subject to the m equality constraints

$$\mathbf{c}(\mathbf{x}) = 0 \tag{4.10}$$

where $m \leq n$. The Lagrangian of this problem can be written as

$$L(\mathbf{x}, \vec{\lambda}) = F(\mathbf{x}) - \vec{\lambda}\mathbf{c}(\mathbf{x}) \tag{4.11}$$

which is a scalar function of the n variables $\mathbf{x}$ and the m Lagrange multipliers $\vec{\lambda}$. The necessary conditions for a point $(\mathbf{x}^*, \vec{\lambda}^*)$ to be a constrained optimum require solving the following system:

$$\nabla_x L(\mathbf{x}, \vec{\lambda}) = \mathbf{g}(\mathbf{x}) - \mathbf{G}^T(\mathbf{x})\vec{\lambda} = 0 \tag{4.12}$$

$$\nabla_\lambda L(\mathbf{x}, \vec{\lambda}) = -\mathbf{c}(\mathbf{x}) = 0 \tag{4.13}$$

where $\mathbf{g} = \nabla_x F$ and $\mathbf{G}$ are the gradient of the objective function $F(\mathbf{x})$ and the Jacobian of the equality constraint vector $\mathbf{c}(\mathbf{x}) = 0$, respectively. The system 4.13 can be solved via a Newton's method to find the $(n+m)$ variables $(\mathbf{x}^*, \vec{\lambda}^*)$.
Given a generic initial guess $(\mathbf{x}, \vec{\lambda})$, its corrections $(\Delta\mathbf{x}, \Delta\vec{\lambda})$ to construct the new solutions $(\mathbf{x} + \Delta\mathbf{x}, \vec{\lambda} + \Delta\vec{\lambda})$ are given by solving the linear system

$$\begin{bmatrix} \mathbf{H}_L & -\mathbf{G}^T \\ \mathbf{G} & 0 \end{bmatrix} \left\{ \begin{array}{c} \Delta\mathbf{x} \\ \Delta\vec{\lambda} \end{array} \right\} = \left\{ \begin{array}{c} -\mathbf{g} \\ -\mathbf{c} \end{array} \right\} \tag{4.14}$$

also referred as Karush-Kuhn-Tucker system; the term $\mathbf{H}_L$ is the Hessian of Eq. 4.11 in x namely

$$\mathbf{H}_L = \nabla_x^2 F - \sum_{i=1}^{m} \lambda_i \nabla_x^2 c_i \tag{4.15}$$

It is important to observe that an equivalent way to define the search direction $\Delta\mathbf{x}$ is to minimize the quadratic form

$$\frac{1}{2}\Delta\mathbf{x}^T\mathbf{H}_L\Delta\mathbf{x}+\mathbf{g}^T\Delta\mathbf{x} \tag{4.16}$$

subject to the linear constraints

$$\mathbf{G}\Delta\mathbf{x}=-\mathbf{c} \tag{4.17}$$

This is the reason why this problem is also referred as a quadratic programming (QP) problem.

The NLP problem formulated above cn be also generalized when inequality constraints are imposed. The m constraints are of the form

$$\mathbf{c}(\mathbf{x})\geq 0 \tag{4.18}$$

Constraints that are strictly satisfied, i.e. $c_i(\mathbf{x})>0$, are called *inactive*, the remaining active set of constraints are on their bounds, i.e. $c_i(\mathbf{x})=0$. if the active set of constraints is known, th einactive constraints are ignored and the problem is simply solved using the method previously discussed for equality constraints.

Summarizing, the general NLP problem requires finding the n vectors to solve

$$\min_x F(\mathbf{x})$$

subject to the m constraints

$$\mathbf{c}_L\leq\mathbf{c}(\mathbf{x})\leq\mathbf{c}_U \tag{4.20}$$

and bounds

$$\mathbf{x}_L\leq\mathbf{x}\leq\mathbf{x}_U \tag{4.21}$$

In this formulation equality constraints can be imposed by setting $c_{j,L}=c_{j,U}$.

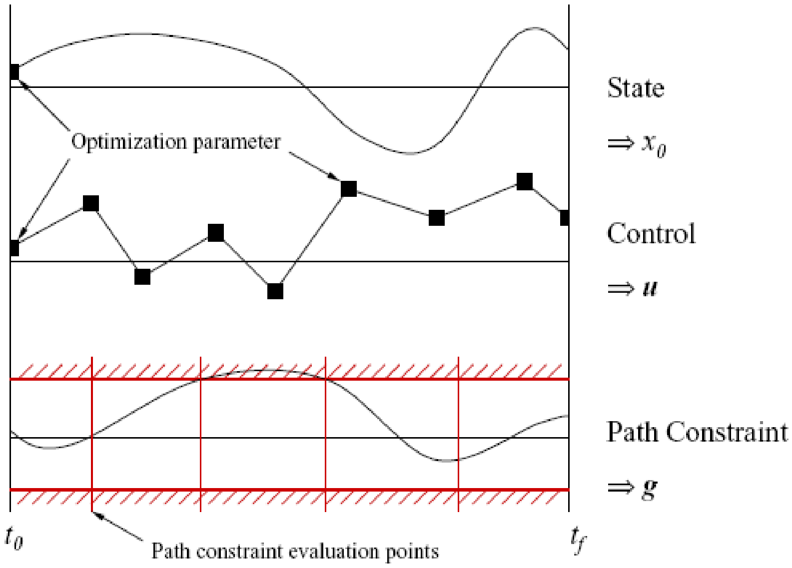

Figure 4.1: Discretization of a shooting phase.

Direct Shooting Methods Direct shooting methods are based on the integration of the trajectory during the optimization process. Such an integration is usually performed numerically with standard solvers for initial value problems.[32] [33]

As said previously, the control time histories are discretized using a parameter dependent control approximation. In addition to the controls, path constraints are discretized as well. In Fig. 4.1, a discretized shooting phase is shown including one state, one control and one path constraint. The initial state remains a scalar optimization parameter while the control becomes a vector of discrete optimization parameters. The path constraint is transformed into a vector of interior point constraints.

These methods are very popular for solving boundary value problems even if they are very sensitive to the terminal constraints with respect to changes in the initial conditions. In general, there are three possibilities to handle this difficulty. First, a better initial guess can be constructed. However, this is often very tedious or even impossible to do within a reasonable timeframe. The second method can be to let two trajectories start from both sides of the interval and let them to match at an intermediate point. The third possibility is to improve the stability of the optimization algorithm by introducing intermediate guesses for the states and restart the integrator at

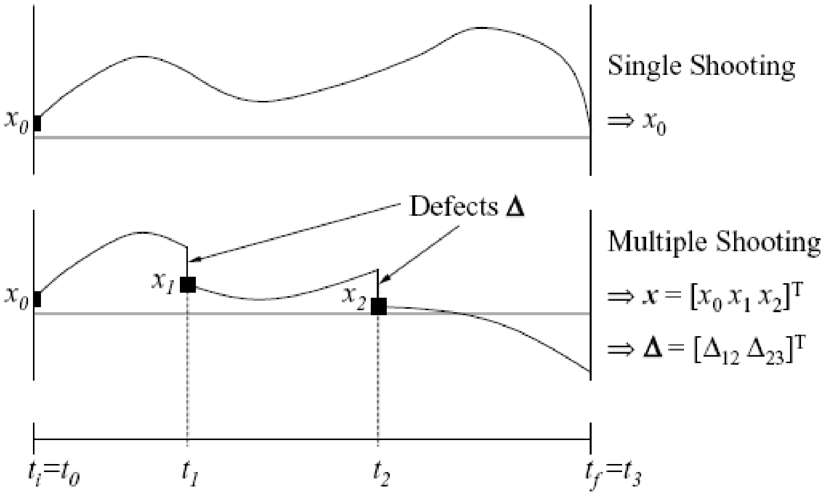

Figure 4.2: Application of multiple shooting to a phase with one state.

these multiple-shooting points (Fig. 4.2). Of course, such intermediate states must be optimizable parameters, and additional constraints must be introduced to the problem to ensure a continuous trajectory once the optimizer is converged.[34][35]

Direct Collocation Methods Direct collocation methods use Hermite-Simpson polynomials to approximate the state time histories. These methods were first proposed by Dickmanns and Well in 1974[36] and then extended by Hargraves and Paris in 1987.[37]

Since the state time histories are approximated by using polynomials within one interval, it is necessary to split the whole phase into several smaller collocation intervals.

In order to allow for discontinuities in the control between the collocation intervals, each of the boundary points includes two optimization parameters for each control: a left-hand and a right-hand control value (see Fig. 4.3). If a control function has to be continuous, an additional control continuity constraint is introduced to the problem. This approach increases the number of parameters and constraints, but it is found that this also improves the convergence behavior of the optimization method significantly.[38] In fact, major advantages of using these methods with respect to direct shooting ones are a larger convergence radius and a much better run-time performance.

It can be seen as an implicit integration of the dynamic system, while multiple shooting methods are using explicit integration formulas for such as

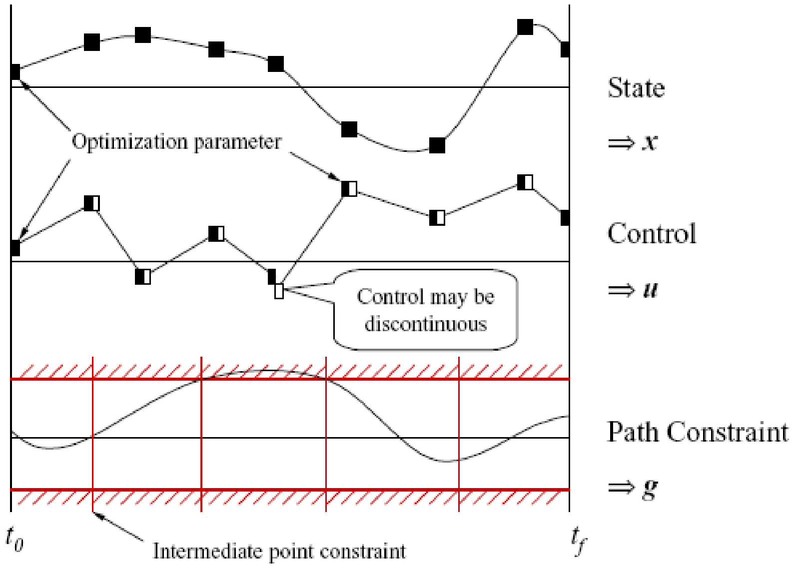

Figure 4.3: Discretization of a collocation phase

.

Runge-Kutta method. Besides, in direct collocation methods it is possible to place a path constraint evaluation point at the exact same locations where the dynamics are evaluated creating in this way a consistent node placement.

4.3 Indirect Methods

Indirect methods are based on the calculus of variation and Pontryagin's minimum principle.[28][39] Calculus of variation techniques were successfully applied for the first time by Sir Isaac Newton in 1686 and since then the theory was continuously developed. Euler and Lagrange formulated the first order necessary conditions in 1744 (the *Euler-Lagrange equations*) and then, almost a century later, Hamilton posed these conditions in a more clear form by means of a function (the *Hamilton function*).

The optimization problem is obtained via variation of an augmented performance index J that includes the equations of motion (the constraints of the dynamic optimal problem) and, when necessary, state and control variable constraints. The major drawback of indirect optimization methods is the requirement for a detailed mathematical analysis of each single problem. A slight change in the dynamics or in the boundary constraints can lead to a completely different solution structure. On the other hand, an in-depth inside into the problem is possible with such a method.

Imagine to compute the maximum of a function $f(\mathbf{z})$ subject to the equality constraint function $g(\mathbf{z}) = 0$:

$$\begin{cases} \max & f(\mathbf{z}) \\ g(\mathbf{z}) & = 0 \end{cases} \tag{4.22}$$

It is possible to define an augmented function $F(\mathbf{z})$ that includes both the function f and its constraint function g

$$F(\mathbf{z}) = f(\mathbf{z}) + \vec{\nu}^T g(\mathbf{z}) \tag{4.23}$$

where $\vec{\nu}$ is a coefficients vector called *Lagrange multiplier*.
It is demonstrated that $f(\mathbf{z})$ has a maximum subject to the contraint function g where $\partial F/\partial \mathbf{z} = 0$. Therefore, from the stationary solution of F the value of $\mathbf{z}$ is obtained and then, first the constraint function is evaluated and then the maximum value of f can be found.

Continuous Systems Optimal programming problems for continuous systems are problems in the calculus of variations. As said in par. 4.1, the optimal control problem is to find an optimal control input $\mathbf{u}^* \subset \Re^m$ for a set of generally nonlinear coupled first-order differential equations[40][41]

$$\dot{\mathbf{x}} = \mathbf{f}(\mathbf{x}, \mathbf{u}, t)\,, \qquad t \in [t_0, t_f] \tag{4.24}$$

subject to boundary conditions

$$\Psi\left(\mathbf{x}(t_0), \mathbf{x}(t_f), t_0, t_f\right) = \left(\psi_0\left(\mathbf{x}(t_0), t_0\right), \psi_f\left(\mathbf{x}(t_f), t_f\right)\right)^T = \mathbf{0} \tag{4.25}$$

and such that the associated cost function expressed in the Bolza-form (a Mayer term ϕ and a Lagrange term with the integrand L)

$$J = \phi\left(\mathbf{x}\left(t_f\right), t_f\right) + \int_{t_0}^{t_f} L\left(\mathbf{x}, \mathbf{u}, t\right) dt \tag{4.26}$$

is minimized.
In addition, state and control variables constraints must be also taken into account and they can be expressed in the optimal control problem in the form of inequality and equality constraints (e.g. the max thrust level, the specific impulse range in a low-thrust trajectory optimization problem). In the following, we will assume the absence of path and control variable constraints.

Let us define the augmented performace index

$$J = \phi\left(\mathbf{x}(t_f), t_f\right) + \vec{\nu}^T \cdot \psi\left(\mathbf{x}(t_f), t_f\right) + \int_{t_0}^{t_f} \left\{ L\left(\mathbf{x}, \mathbf{u}, t\right) + \vec{\lambda}^T \cdot \left[\mathbf{f}\left(\mathbf{x}, \mathbf{u}, t\right) - \dot{\mathbf{x}}\right] \right\} dt \tag{4.27}$$

in which $\vec{\nu}$ is the Lagrange multiplier vector for discrete constraints and $\vec{\lambda}$ is the Lagrange multiplier vector for continuous constraints also called *adjoint* or *costate* variables.

Let us also introduce the Hamiltonian function:

$$H = L\left(\mathbf{x}, \mathbf{u}, t\right) + \vec{\lambda}^T \cdot f\left(\mathbf{x}, \mathbf{u}, t\right) \tag{4.28}$$

Integrating by parts the augmented performance index and defining a new function $\Phi = \phi + \vec{\nu}^T \cdot \Psi$ we obtain:

$$J = \Phi + \vec{\lambda}^T(t_f) \cdot \mathbf{x}_f + \vec{\lambda}^T(t_0) \cdot \mathbf{x}_0 + \int_{t_0}^{t_f} \left[H_x + \dot{\vec{\lambda}}^T \cdot \mathbf{x}\left(t\right)\right] dt \tag{4.29}$$

An infinitesimal control variation $\delta\mathbf{u}$ will produce a state variation $\delta\mathbf{x}$ and then and index variation δJ, so:

$$\delta J = \left[\left(\Phi_x - \vec{\lambda}^T\right) \cdot \delta\mathbf{x}\right]_{t=t_f} + \left[\vec{\lambda}^T \cdot \delta\mathbf{x}\right]_{t=t_0} + \dot{\Phi} \cdot dt_f + \int_{t_0}^{t_f} \left[\left(H_x + \dot{\vec{\lambda}}^T\right) \cdot \delta\mathbf{x} + H_u \cdot \delta\mathbf{u}\right] dt \tag{4.30}$$

where

$$\dot{\Phi} = \left(\frac{\partial \Phi}{\partial t}\right)_{t=t_f} + \Phi_x \cdot \dot{\mathbf{x}} \tag{4.31}$$

For simpilicity, we can choose the multiplier functions $\vec{\lambda}(t)$ to cause the coefficients of $\delta\mathbf{x}$ to vanish. Thus we have:

$$\begin{cases} \dot{\vec{\lambda}}^T & = -H_x = -L_x - \vec{\lambda}^T \cdot f_x \\ \vec{\lambda}^T(t_f) & = \Phi_x(t_f) = \phi_x(t_f) + \vec{\nu}^T \cdot \Psi_x(t_f) \end{cases} \tag{4.32}$$

which are the so-called *Euler-Lagrange* equations and they define the set of differential equations for the adjoint vector $\vec{\lambda}$.
At this point, in order to obtain the minimum (maximum) value of J ($\delta J = 0$), the following first-order necessary conditions are obtained:[28]

$$H_u = 0 = L_u + \vec{\lambda}^T f_u \tag{4.33}$$

$$\dot{\Phi} = 0 \tag{4.34}$$

where Eq. (4.33) and the second derivative of the Hamiltonian with respect to the control variables (H_{uu}) rule the optimal control law. Equation (4.34) exists only for open time problems and represents the boundary conditions for the final adjoint variables and final Hamiltonian. It is also called the *transversality condition.*

Continuous Systems: terminal constraints at a fixed terminal time In this case, Eq (4.30) becomes

$$\delta J = \left[\vec{\lambda}^T \cdot \delta\mathbf{x}\right]_{t=t_0} + \int_{t_0}^{t_f} \left[H_u \cdot \delta\mathbf{u}\right] dt \tag{4.35}$$

where the functions H_u are called the *impulse response* functions as each component of $\partial H/\partial u$ represents the variation in J due to a unit impulse when $x(t_0)$ is kept constant.
Moreover, at the initial istant t_0, the integral term is zero and we have

$$\delta J = \left[\vec{\lambda}^T \cdot \delta\mathbf{x}\right]_{t=t_0} \Rightarrow \vec{\lambda}^T(t_0) = \left(\frac{\partial J}{\partial \mathbf{x}}\right)_{t=t_0} \tag{4.36}$$

therefore $\vec{\lambda}^T(t_0)$ is the gradient of J with respect to variations in the initial conditions while holding $\mathbf{u}(t)$ costant and satisfying the system dynamics.

In summary, in a continuous system with q terminal constraints

$$\psi[x(t_f), t_f] = 0 \tag{4.37}$$

at a fixed final time, where $\mathbf{x}(t)$ is a n-vector function, to find a control m-vector function $\mathbf{u}^*(t)$ that produces a stationary value of the performance index J, we must solve the following coupled $2n$ differential equations

$$\begin{cases} \dot{\mathbf{x}} & = \mathbf{f}(\mathbf{x}, \mathbf{u}, t) \\ \dot{\lambda} & = -H_x \end{cases} \tag{4.38}$$

and the $2n$ boundary conditions for these differential equations are split, some at $t = t_0$ and some at $t = t_f$:

$$\mathbf{x}(t_0) = \mathbf{x_0} \tag{4.39}$$

$$\vec{\lambda}(t_f) = \Phi_x(t_f) = \left(\frac{\partial \phi}{\partial \mathbf{x}} + \vec{\nu}^T \cdot \frac{\partial \psi}{\partial \mathbf{x}}\right)_{t=t_f} \tag{4.40}$$

This is a *Two-Points Boundary Value Problem (TPBVP)* with q parameters ν to be found in Eq (4.40) so that the q boundary conditions (4.37) are satisfied. The optimal control law $\mathbf{u}^*(t)$ is determined by minimizing the Hamiltonian function with respect to the control variables, that is the following m algebraic equations

$$H_u = 0$$

Continuous Systems: open final time An important application in trajectory design, is the *minimum time* problem which must have at least one terminal condition, since otherwise there is no indication of when to stop. In this kind of problems, the final time t_f is not specified, so it can be regarded as an additional control parameter. With respect to the previous case, this implies an additional condition to be imposed to the Hamiltonian function (see Eq. (4.34) of the general problem).
Practically, it is like solving several fixed time problems and then choosing the one that also satisfies the additional constraint on the Hamiltonian function.

Now we wish to find a control vector function $\mathbf{u}(t)$ for $t \in [t_0, t_f]$ and the final time t_f to minimize the performance index

$$J = \phi[\mathbf{x}(t_f), t_f] \tag{4.42}$$

subject to equations of motion

$$\dot{\mathbf{x}} = f\left(\mathbf{x}, \mathbf{u}, t\right) \tag{4.43}$$

and to boundary constraints

$$\psi[\mathbf{x}(t_f), t_f] = 0 \tag{4.44}$$

For minimum time problems, $\phi = t_f$.

In order to obtain a stationary solution of J for arbitrary $\delta u(t)$ and dt_f, necessary conditions are expressed from Eqs. (4.33) and (4.34). The additional equation $\dot{\Phi} = 0$ is called the *transversality condition* and it can be written in terms of the Hamiltonian $H = \vec{\lambda}^T \cdot f$ at the final time, since $\vec{\lambda}^T(t_f) = \Phi_x$ and $\dot{\mathbf{x}} = f$:

$$\dot{\Phi} = \left(\frac{\partial \Phi}{\partial t} + \frac{\partial \Phi}{\partial \mathbf{x}}\dot{\mathbf{x}}\right)_{t=t_f} = \Phi_{t_f} + \vec{\lambda}^T(t_f) \cdot f = \Phi_{t_f} + H = 0 \tag{4.45}$$

or else

$$\left[\frac{\partial \phi}{\partial t} + \vec{\nu}^T \cdot \frac{\partial \psi_f}{\partial t} + H\right]_{t=t_f} = 0 \tag{4.46}$$

According to this last equation, for minimum time problems where $\phi = t_f$, if $\psi_{t_f} = 0$, then the transversality equation becomes simply

$$1 + H(t_f) = 0 \tag{4.47}$$

Again, the minimum-time problem is obtained solving the TPBVP problem

expressed by the following equtaions:
the $2n$ differential equations

$$\begin{cases} \dot{\mathbf{x}} & = \mathbf{f}(\mathbf{x}, \mathbf{u}, t) \\ \dot{\lambda} & = -H_x \end{cases}$$

the $2n$ boundary conditions (split, some at $t = t_0$ and some at $t = t_f$):

$$\begin{aligned} &\mathbf{x}(t_0) = \mathbf{x_0} \\ &\vec{\lambda}(t_f) = \Phi_x(t_f) = \left(\frac{\partial \phi}{\partial \mathbf{x}} + \vec{\nu}^T \cdot \frac{\partial \psi}{\partial \mathbf{x}} \right)_{t=t_f} \end{aligned}$$

the necessary m optimality conditions for the control m-vector function $\mathbf{u}(t)$

$$H_u = 0$$

and one transversality condition

$$1 + H(t_f) = 0$$

The TPBVP As said previously, the system of adjoint variables is very sensitive to variations in the initial conditions, that is why the success of indirect methods heavily depends on the quality of the initial guess of the optimization parameters. Therefore, the first phase of every optimization algorithm is the generation of an initial acceptable set of optimization parameters and it is the most work-intensive and mathematically complex stage of the overall procedure.

There exists a wide variety of techniques to solve the general TPBVP, the most frequently used approach for trajectory optimization problems is based on shooting methods (see Sec. 4.2). A detailed analysis on the implementation of state and control variable constraints is outlined in Bryson and Ho,[28] Hartl et al.[42]

Chapter 5

Electric Propulsion Interplanetary Transfers using Libration Points

In this chapter, results obtained by the advantageous combination of Dynamical Systems Theory (DST) of the CR3BP with Electric Propulsion to design novel interplanetary missions are discussed.

In the past, several studies have applied these low energy solutions to design complex missions and have successfully coupled three-body environments to design low energy ballistic trajectories with consequent significant savings in propellant mass and high scientific outcome.

However, few past studies are known to the author in which low-thrust trajectories are defined in a n-body model. Belbruno first dealt with this combination in the frame of the Lunar GAS mission,[5] then other studies investigated low-thrust trajectories for periodic orbit around libration points.[6][7][8] In this chapter, both the interplanetary transfer preceding insertion into a planetary realm and the final planet's capture in the CR3BP with the use of Electric Propulsion are investigated.

Therefore, it is easy to figure out that this kind of problems require the necessity to investigate both in the DST-CR3BP field and in the optimal control theory field as optimization schemes are necessary in the design of low-thrust arcs subjected to both boundary and path constraints that allow transitions between manifolds.

In the current study, particular attention is focused on missions to outer planets that are intrinsically associated with long transfer times and high ΔV budgets, particularly if a final planetary capture is desired.

Firstly, mathematical procedures applied are described, in particular system dynamics under CR3BP assumption and the optimal trajectory design problem are presented.

Then, results of an Earth-Uranus transfer are shown in which a high energy launch is provided. The transfer is divided in to two phases: an interplanetary phase from Earth departure to the Sun-Uranus L_1 libration point in which the departure angle and and ΔV are computed as the ones that minimize transfer time and maximize spacecraft mass fraction (no coasting phase is foreseen).

Following, the second phase in the planetary realm is designed in which a ballistic and non impact orbit around Uranus is obtained. A planet's capture trajectory is also designed.

In the end, some results obtained in the 2-body model with alternative strategies are also shown in order to have compare results.

5.1 Mathematical Models

Mission design of spacecraft intended for outer planet exploration involves consideration of advanced technology options which can critically affect the mission feasibility, depending on their hypothesized characteristics. Especially when mission requirements impose a planetary captured operational orbit of a relatively heavy spacecraft, this asks for novel solutions to limit the total transfer time and required ΔV to acceptable values.

Previous studies, first by Noble[43]–[45] and later by Oleson[46], [47] combined the continuous availability of electric power deriving from RTGs with the application of Electric Propulsion (EP). Their studies showed the advantages of this combination with the capability of a direct transfer orbit insertion by a powerful launcher. The main constraint on this approach was the maximum admissible initial spacecraft mass, imposed by the launcher performance. An obvious penalty of the maximum initial mass constraint is the reduced payload fraction allocated for the scientific instrumentation.

In particular, the strategy suggested by Oleson assumes a powerful launcher able to place the spacecraft into a highly elliptical or hyperbolic transfer orbit and the EP system activated upon approaching the arrival planet to perform a deceleration and orbit circularization manoeuvre to accomplish planet's capture.

The description of the mathematical procedures applied is subdivided into two paragraphs, the first one describing the dynamics of the CR3BP and the second one describing the optimization theory used to compute the transfers.

System Dynamics According to theory introduced in chap. 2 and chap 3, the complete transfer was computed considering the dynamics of the CR3BP whose governing equations are (recall Eqs. (2.21)) :

$$\begin{cases} \ddot{x} - 2\dot{y} & = -\bar{U}_x \\ \ddot{y} + 2\dot{x} & = -\bar{U}_y \\ \ddot{z} & = -\bar{U}_z \end{cases}$$

where the subscripts denote the partial derivates and $\bar{U}$ is the *effective potential* (see Eq. (2.22)).

The x and y coordinates and their derivates are computed with respect to a non dimensional, synodic reference frame centered in the center of mass of the two main attractors and rotating with their relative angular velocity. The *mass parameter* (μ) of the system is the only parameter necessary for the characterization of the specific three body system. For the Sun - Uranus system here considered, $\mu = 4.3528 \cdot 10^{-5}$.

The distances between the two primaries and the third body are given by:

$$\begin{cases} r_1^2 & = & (x+\mu)^2 + y^2 + z^2 \\ r_2^2 & = & (x-1+\mu)^2 + y^2 + z^2 \end{cases} \tag{5.2}$$

where r_1 and r_2 are the Sun and Uranus-spacecraft distances, respectively.

An in-plane thrust has been included by means of an acceleration term a given by the thruster to the equations of motion, considering the max thrust modulus T and the instantaneous spacecraft mass m. In order to provide the ability to modulate the thrust value, a scaling parameter, $\tau \in [0, 1]$, was included as shown below:

$$\begin{cases} \ddot{x} - 2\dot{y} & = & -\bar{U}_x + a \cdot cos(\theta) \\ \ddot{y} + 2\dot{x} & = & -\bar{U}_y + a \cdot sin(\theta) \\ \ddot{z} & = & -\bar{U}_z \\ \dot{m} & = & -(T \cdot \tau)/(I_{sp} \cdot g_0) \end{cases} \tag{5.3}$$

where

$$a = \frac{T \cdot \tau}{m} \qquad T = \frac{2\eta P}{I_{sp} \cdot g_0} \tag{5.4}$$

Here, θ is the angle measured counterclockwise between the x-axis and the thrust direction, η is the thrust efficiency, P is the electrical power available for the electric thruster, I_{sp} is the thruster specific impulse and g_0 is the Earth gravitational acceleration.

The Optimal Trajectory Design Problem Equations of motion (5.3) obey a three-dimensional approach. However, for simplicity, the following discussion of the transfer optimization only deals with the planar case (PCR3BP). This simplification was made due to the small difference in inclination of the two primaries considered.
Nevertheless, in the next paragraphs, also the three-dimensional approach will be discussed.

The transfer from Earth to the Uranus libration point L_1 (in the following indicated as UL_1) was computed using two different, supplementary, optimization techniques. Initially a *gradient method* was applied to provide a relatively accurate initial guess for a subsequently used *forward shooting method*. The latter method requires a precise initial guess of the initial state, which is obtained by the former, more robust, optimization scheme.

The Gradient Method In the *gradient method*, the transfer problem that had to be solved was described as a problem in the calculus of variations. This enabled the employment of a numerical scheme providing a suitable solution that satisfies the boundary conditions, while minimizing the total transfer time (see the open final time problem in Sec. 4.3).

The transfer starts from a given initial state, defined by the position and velocity components corresponding with a location on the Earth's orbit. In addition, a departure ΔV was added to the Earth's circular velocity in order to simulate a high energy chemical launch.
Based on an initial guess, the numerical scheme varies the control parameters to move towards a stationary solution. The control parameters in this case are the thrust angle and thrust modulus, θ and τ, respectively, thus $u = [\theta, \tau]$.

Therefore, the objective function to be minimized is:

$$J = \phi[x(t_f), t_f] \Rightarrow \phi = t_f \tag{5.5}$$

subject to the constraints:

$$\left\{ \begin{array}{rcll} \dot{\mathbf{x}} & = & f(\mathbf{x}, \mathbf{u}, t) & \textit{System Dynamics} \\ \mathbf{x}(t_0) & = & \mathbf{x_0} & \textit{Initial Conditions} \\ 0 & = & \psi[\mathbf{x}(t_f), t_f] & \textit{Terminal Constraints} \end{array} \right. \tag{5.6}$$

The constraints were adjoined to the performance index by the Lagrange multiplier vectors $\vec{\nu}$ and $\vec{\lambda}(t)$, equating the modified performance index:

$$\bar{J} = \phi + \vec{\nu} \cdot \psi + \int_{t_0}^{t_f} \vec{\lambda}(t) \cdot [f(x(t), u(t), t) - \dot{x}]dt \tag{5.7}$$

The Hamiltonian of the system is defined as:

$$H(t) \triangleq \vec{\lambda}(t) \cdot [f(\mathbf{x}(t), \mathbf{u}(t), t)] \tag{5.8}$$

and the adjoints equations for the Lagrange multipliers are computed by the Euler-Lagrange equations (see Eqs. (4.32)) where now Φ is:

$$\Phi \triangleq \phi + \vec{\nu} \cdot \psi = t_f + \nu_1(x - x_f) + \nu_2(y - y_f) + \nu_3(u - u_f) + \nu_4(v - v_f) \tag{5.9}$$

Here, the boundary conditions $\mathbf{x}(t_f) = (x_f, y_f, u_f, v_f)$ correspond to the four position and velocity values that identify the first libration point, UL_1, required in our study.

Recalling now Eq. (4.30) for differential changes in the modified performance index and Eq. (4.31), the first-order necessary conditions for a stationary solution ($dJ = 0$), for an arbitrary $\delta\mathbf{u}(t)$ and dt_f are:

$$\left\{ \begin{array}{rcll} H_u(t) & = & 0 & t_0 \leq t \leq t_f \\ \dot{\Phi} & = & 0 & \textit{Transversality Condition} \end{array} \right. \tag{5.10}$$

The transversality condition can be also written in terms of the Hamiltonian at the final time:

$$\dot{\Phi} = \Phi_{t_f} + H(t_f) = 0 \tag{5.11}$$

which can be reduced even further for minimum time problems as Φ_{t_f} equates to unity. So the transversality conditions becomes:

$$1 + H(t_f) = 0 \tag{5.12}$$

The boundary value problem as described in the current form was solved by the numerical scheme that integrated the equations of motion and the adjoint equations in forward and backward direction, respectively.[40]

The Direct Shooting Algorithm The optimization technique based on gradient information, as previously discussed, was required to successfully implement a second, more accurate, optimization technique. This optimization technique based on a forward shooting process integrates the Euler-Lagrange equations (Eq. 4.32) forward to determine the boundary values and the final boundary condition errors. During the forward integration, the optimal control is determined considering $H_u = 0$ at each step.

The nature of the solution technique requires a very accurate initial estimate of the initial adjoint vector $\vec{\lambda}(t_0)$, the terminal Lagrange multipliers $\vec{\nu}$ and the final time t_f. These accurate initial guesses were obtained from a quasi-converged solution by the gradient method. Advantage of the employment of this second method was the very precise solution obtained, which is required as the final state is located in a region susceptible to chaotic motion.

In order to simplify the definition of the problem in this second case the ability to modulate the thrust was omitted. This reduces the problem to a true minimum time optimization where the thruster is continuously active and the control parameter is the thrust angle θ. This decision was motivated considering that a principal parameter assessing outer planetary mission feasibility is the total transfer time.

5.2 Earth-Uranus Transfer in the CR3BP: Results

The overall transfer design was subdivided into two parts: the interplanetary phase from Earth orbit to Sun-Uranus UL_1 and then from UL_1 ballistically into the planetary realm where a sensitivity analysis was performed.

In order to set up the transfer computation, some mission design parameters were assigned and, therefore, were not involved in the optimization process.

The value chosen are shown in Table 5.1. In detail, the initial spacecraft mass selected allow a powerful launcher to provide a high energy launch with consequent Earth escape on a higly elliptical or hyperbolic trajectory.

Thruster power level and specific impulse are obtained from previous studies[48] and are typical for RTG-EP missions while thrust efficiency of 0.5 is a typical value for many EP thrusters.

Departure Mass [kg]	1000
Specific Impulse [sec]	3200
Thruster Power [W]	1000
Thrust Efficiency [-]	0.5

Table 5.1: Fixed Parameters

Earth to UL_1 As first step, initial position and velocity for the interplanetary transfer were identified. This was done considering a circular orbit around the first primary (Sun) with an orbital radius of $1AU$ and where the position on this circle was described by the angle α, in counterclockwise direction from the x-axis.

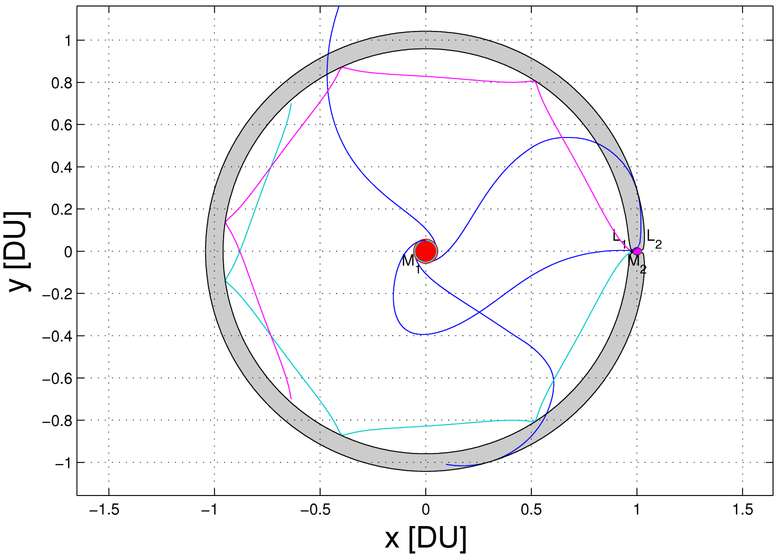

Figure 5.1: Earth - UL_1 transfers in the Sun-Uranus rotating frame for $\alpha = [0 - 90 - 180 - 270]$ degrees obtained with the Gradient Method (magenta and cyan lines represent the invariant manifolds associated to UL_1).

A first evaluation was based on the four angles $\alpha \in (0, 90, 180, 270)$ degrees for which the required ΔV and total transfer time were computed. The resulting transfers are seen in Fig. 5.1 and Fig. 5.2 for the two numerical methods applied. According to the resulting trajectory shapes, it is easy to realize that for $\alpha = 0^o$ and $\alpha = 90^o$ the transfer time is much longer than the other two solutions.

Based on these results a parametric refinement was performed concentrated on the angular region between 180 and 270 degrees with an initial $\Delta V \in [11.6, 13]$ km/s that is compatible with high energy launcher performance. These two parameter ranges defined a grid for which the solutions were computed, which resulted in the transfer time and final mass values for each grid point in the specified performance envelope. These two parameters are shown in Fig. 5.3 and Fig. 5.4 forming two surfaces above the defined grid.

It is immediately seen that the surfaces show a minimum and maximum for an angle of 230^o, which remains relatively equal for the different $\Delta V s$ considered. It is worth noting that both surfaces behave in opposite ways:

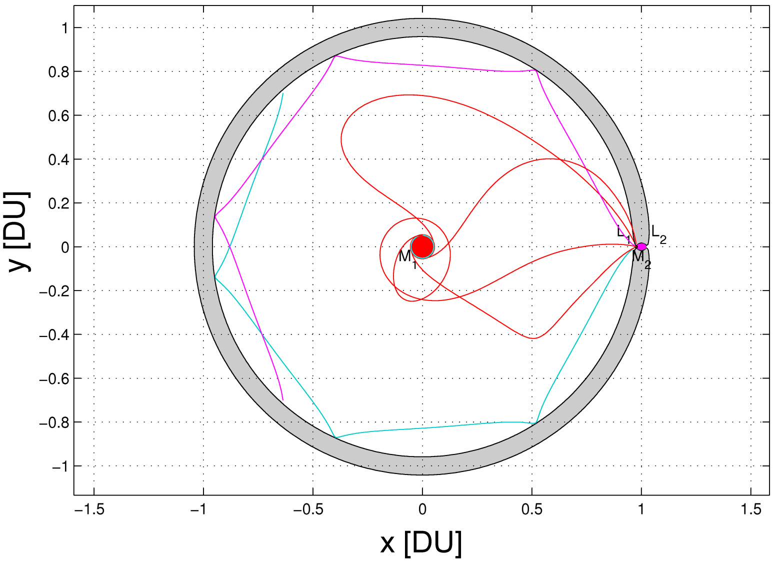

Figure 5.2: Earth - UL_1 transfers in the Sun-Uranus rotating frame for $\alpha = [0-90-180-270]$ degrees obtained with the Forward Shooting Method (magenta and cyan lines represent the invariant manifolds associated to UL_1).

continuous thrust gives a maximum propellant mass fraction for minimum time. According to the shooting method formulation and since no coasting phase is present, this result was expected.

Figure 5.5 shows a cross section of the two surfaces for the minimum ΔV, from which this minimum can be clearly observed. Identifying the angle minimizing the total transfer time is a process equivalent to the launch window determination required considering a conventional mission design approach.

Based on the above analysis, the parameters equating the global minimum for this transfer are $\alpha = 230^o$ and $\Delta V = 11.6$ km/s. Based on these two values the globally optimal transfer within the defined search space was computed and is shown in Fig. 5.6 and Fig. 5.7, both in a rotating and inertial frame of reference respectively.

The corresponding total transfer time is $T_{trans} = 10.13$ years and the propellant mass consumption is $m_{prop} = 337$ kg. Here the green line represents the initial guess used for the gradient method, the blue line the solution obtained by the gradient method and the red line the optimal solution by the forward shooting method.

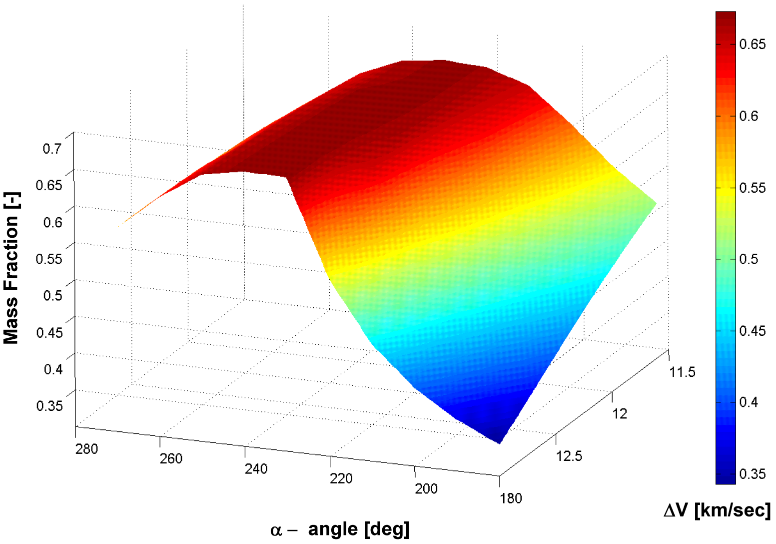

Figure 5.3: Earth orbit-UL_1 mass fraction surface with respect to the defined control grid in the Sun-Uranus rotating frame.

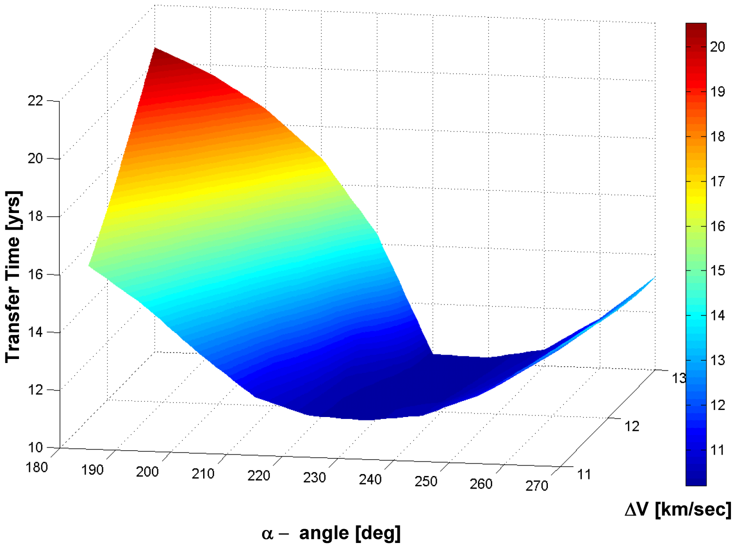

Figure 5.4: Earth orbit-UL_1 transfer time surface with respect to the defined control grid in the Sun-Uranus rotating frame.

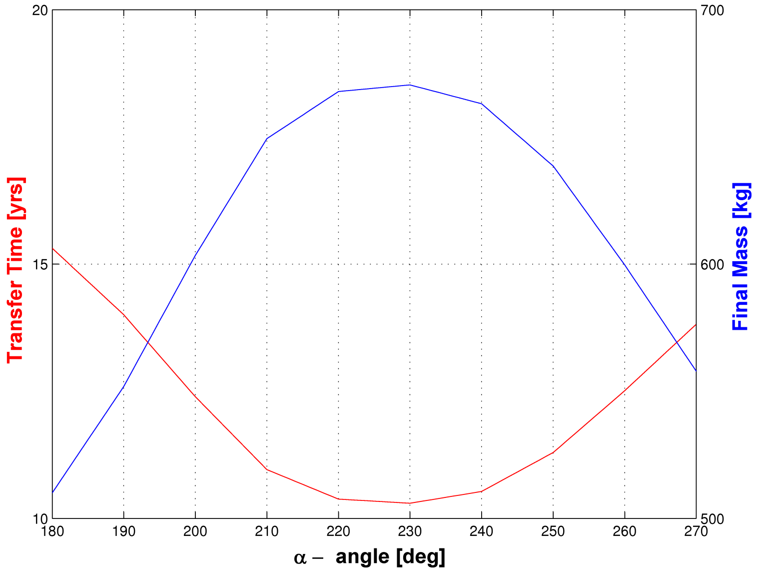

Figure 5.5: Trends of the transfer time and mass fraction with respect to the departure angle

The Planetary Realm Following the interplanetary transfer analysis transporting the spacecraft from Earth orbit to the first Uranus libration point, UL_1 under the CR3BP assumption, the planetary phase was investigated under the same assumptions and the evaluation of the characteristics of stable, ballistic and non impact orbits around Uranus was continued.

In the vicinity of the UL_1 libration point, the ballistic trajectories are subject to very slow dynamics where the velocities approach zero, with transfer times going to infinity. Therefore, several solutions were examined, considering both a periodic orbit around the libration point exploiting its associated unstable manifolds and arrival at the libration point with a velocity excess in the x-direction. Three periodic orbits were defined, governed by their out of plane amplitude (A_z) and computed using an analytical approximation based on Richardson's model[19][21] and a differential correction scheme[49] (see Sec. 3.2) to obtain a precise numerical solution. These orbits are characterized by their out of plane amplitude, thus a non-planar model, whereas the transfer was computed using a planar model. However, the point of entrance on the periodic orbit was always considered on the x-axis where the periodic orbit respects $A_z = 0$ and the only non-zero component of the velocity is in the y direction, which justified this transition to a non-planar model. The amplitudes considered were: $[5 \cdot 10^5,\ 1 \cdot 10^6,\ 2 \cdot 10^6]$ km. An example of the

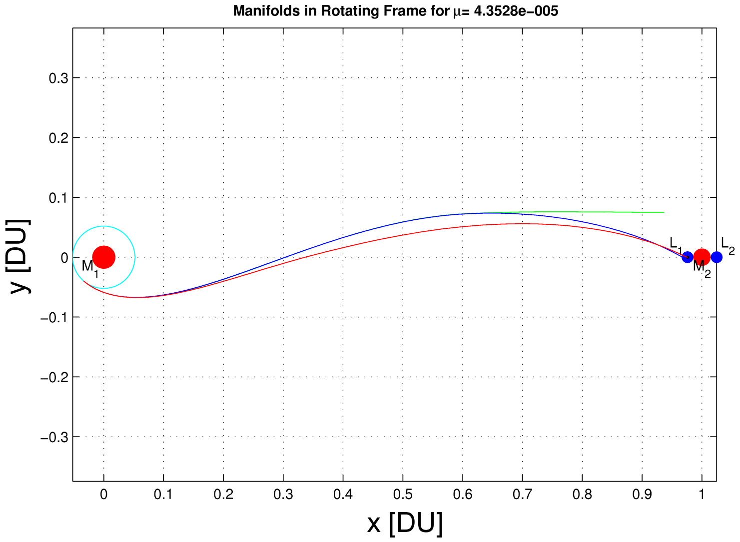

Figure 5.6: Optimum Earth - UL_1 transfer in the Sun-Uranus rotating frame (blue line = gradient method, red line = forward shooting method).

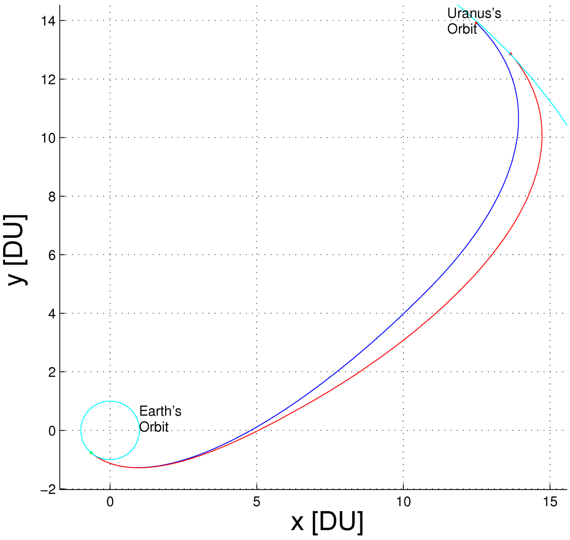

Figure 5.7: Optimum Earth - UL_1 transfer in the Sun-centered inertial frame (blue line = gradient method, red line = forward shooting method).

periodic orbit insertion with ballistic continuation, together with the three periodic orbits, is shown in Fig. 5.8.

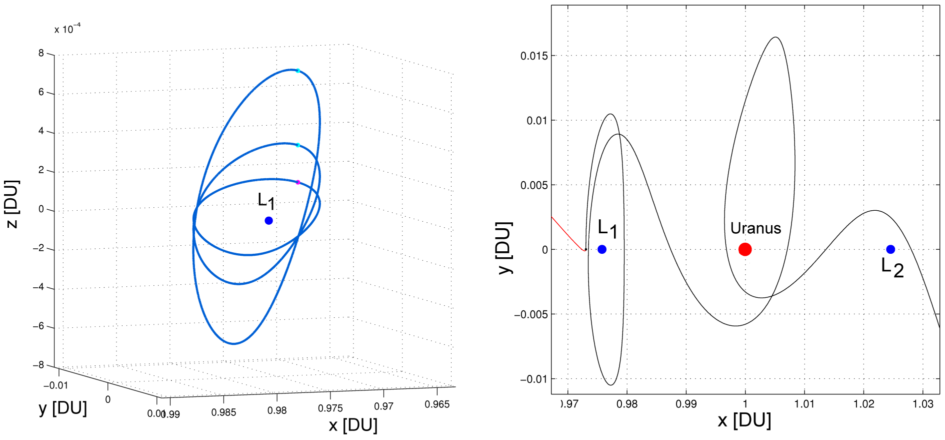

(a) (b)

Figure 5.8: (a) UL_1 Halo orbits for various values of A_z. (b) Ballistic transfer in the Uranus realm for $A_z = 5 \cdot 10^5$ km

The ballistic transfer shown in Fig. 5.8(b), identified by the black line, corresponds to a propagation of the transfer for almost 100 years, where the closest approach with the planet is obtained after approximately 60 years. These exorbitant transfer times decreased with increasing A_z. It turns out that these orbits remain infeasible for practical mission design.

These long transfer times are intrinsically associated with the method used to compute them, i.e. the ballistic continuation on the unstable manifold.

As this approach proved impractical, a different methodology was implemented where the optimization process was constrained to reach the libration point position, but this time with an excess in velocity along the positive x-direction. This resulted in a faster ballistic continuation of the trajectory diminishing the transfer times towards the planet. Theoretically this also introduced a propellant mass saving as less ΔV was needed to dissipate the excess energy. However, this proved very little with respect to the total propellant mass budget, so that this did not have a significant effect on the interplanetary phase design. Again, a parametric study was performed defining an excess velocity envelope along the positive x-axis, Δu, where the distance of closest approach and its associated transfer time were investigated. This showed the chaotic behaviour close to the planet in the CR3BP, particularly present for small values of Δu, for larger values the ve-

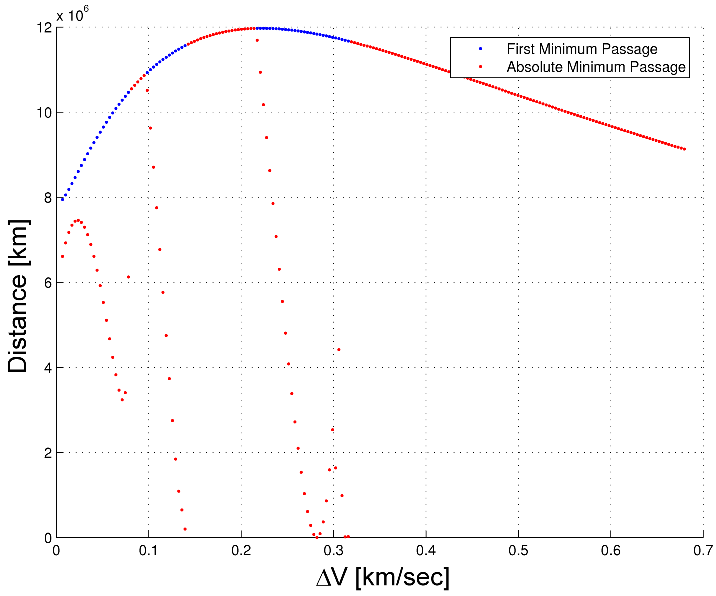

Figure 5.9: Minimum distance with respect to excess velocity.

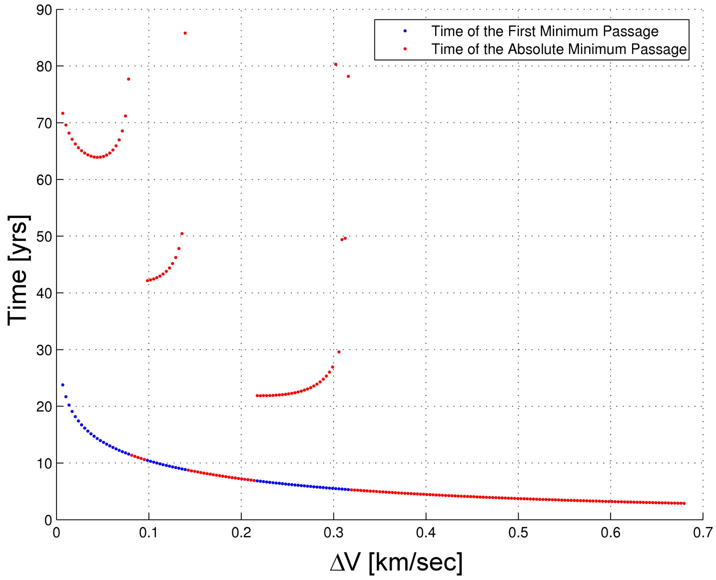

Figure 5.10: Ballistic time with respect to excess velocity.

locity dominated resulting in direct escape trajectories towards the second libration point UL_2.

Figure 5.9 and Fig. 5.10 present both the minimum planetary distance and the associated transfer time to reach the minimum distance with respect to the velocity excess. Both the first minimum and the absolute minimum were studied, because for low values of Δu the ballistic trajectory performed multiple closed orbits around Uranus. With respect to the first minima, a continuous curve is observed where its maximum lies around 0.2 km/s. Considering the chaotic behaviour, between 0 and 0.3 km/s, large advantages can be obtained for certain Δu values bringing the spacecraft very close to the planet, involving an extreme case showing an impact trajectory. The trend of minimum distance for the absolute minima shows discontinuities that correspond to the number of closed orbits performed. This number tends to decrease with Δu and from a value of approximately 0.3 km/s onwards the trajectory does not perform any closed orbit anymore and the two minima coincide.

Associated with the minimum distances are the transfer times, as seen in Fig. 5.10, where a monotonously decreasing trend is observed. This is due to the decreasing transfer times with increasing Δu. Again chaotic behaviour is present for low values of Δu. The same considerations with respect to the discontinuities apply as discussed for the minimum distance.

It was furthermore observed that the impact case marked the boundary between trajectories that perform at least a single, complete orbit and trajectories that are deflected but are not able to perform a closed orbit around Uranus.

In order to demonstrate the feasibility of a mission with planetary capture, ballistic continuation of an escape trajectory was performed, where upon approaching the minimum distance, a low thrust capture was performed. The capture is shown in Fig. 5.11 and Fig. 5.12, where $\Delta u = 0.3194$ km/s, which is just outside of the chaotic regime.

Departure Angle [deg]	230
Departure ΔV [km/s]	11.6
Initial Mass [kg]	1000
Final Mass [kg]	650
Transfer Time: Earth-UL1 [yrs]	10.13
Transfer Time: UL_1-min radius [yrs]	5.28
EP deceleration Time for final capture [yrs]	0.4

Table 5.2: Optimum transfer characteristics

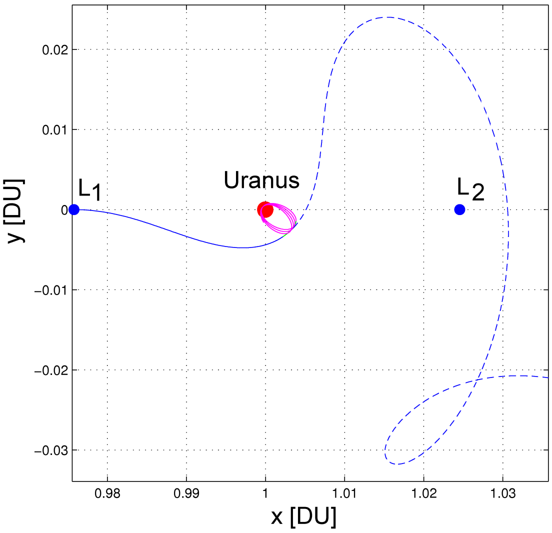

Figure 5.11: Transfer from UL_1 to the capture orbits (ballistic continuation without EP deceleration also shown with the blue broken line).

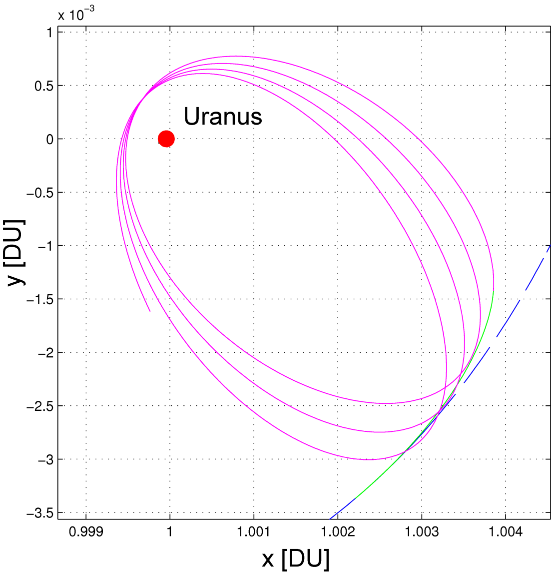

Figure 5.12: Transfer from UL_1 to the capture orbit - zoom on the capture orbits (green line = deceleration phase, magenta line = ballistic capture orbits).

Thrust was applied for 4 months in a direction opposing the velocity vector, establishing a highly elliptic orbit, with a semi-major axis of approximately $6.8 \cdot 10^6$ km. Refinement of the final orbit was beyond the scope of this study, therefore the mission feasibility was considered demonstrated. Optimizing the thrust vector and thrust duration may enable improvement of the final orbit with a relatively small amount of propellant mass.

Table 5.2 gives an overview of the main parameters describing this optimal transfer to Uranus.

5.3 Earth-Uranus Transfers: Alternative Strategies in the 2-Body Model

Additional studies[48][50][51] were performed in order to investigate the possibility to accomplish outer planetary missions based on small, power constrained spacecrafts that combine Electric Propulsion with Radioisotope Thermoelectic Generators (RTGs).

In particular, two strategies were investigated: a direct transfer to outer planets by means of a high energy launch and a multiply gravity-assist trajectory with a lower energy launch. In fact, objectives of these studies are to assess the feasibility of power constrained direct outer planetary transfer trajectories covering a large range of specific impulse and to explore the possibility to accomplish gravity-assist missions with a medium class launcher in order to reduce missions costs.

In both cases, total transfer time and spacecraft final mass at destination were considered the mission constraints.

For all destinations considered in both strategies, a constant RTG electrical power of 1 kW is hypothesized, where recent studies[52] give the RTG state-of-the-art specific mass as approximately 200 kg/kW. This would require the allocation of approximately 200 kg of the final mass to the power subsystem.

System Dynamics in both strategies In both strategies, the 2-Body model was applied to study the interplanetary transfer trajectories applying third body (Sun) effects only like a perturbative term in the planetary sphere of influence.

The characteristics of the transfer problem together with the limitations of the optimization techniques required for a definition of the system dynamics in a polar reference frame as shown in Fig. 5.13.

Description of the equations of motion based on the radial distance, r, the angle, θ, the radial and azimuthal velocities, u and v respectively, solved this problem. Equations (6.3) describe the spacecraft dynamics in the aforemen-

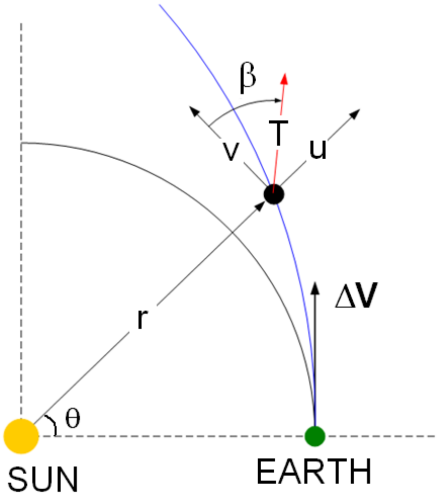

Figure 5.13: Definition of the System

tioned format, where the radial and azimuthal components have an additional accelerative term, representing the acceleration due to the thrust force.

$$\begin{cases} \dot{r} & = & u \\ \dot{\theta} & = & v \\ \dot{u} & = & v^2/r - \mu/r^2 + a\, sin(\beta) \\ \dot{v} & = & -uv/r + a\, cos(\beta) \end{cases} \tag{5.13}$$

Here a represents the istantaneous acceleration which is given by the values for power, specific impulse and the istantaneous spacecraft mass, as given in Eq. (5.14).

$$T = \frac{2\eta P}{g_0 I_{sp}} \quad \Rightarrow \quad a = \frac{T}{m_i - \dot{m}t} \tag{5.14}$$

At Earth departure, the escape energy provided by the launcher ($\Delta V_{launch} = \sqrt{C_3}$) is added to the Earth's orbital velocity given by Eq. (5.15).

$$V_{SC} = V_{Earth} + \Delta V_{launch} \tag{5.15}$$

Definition of the final states in the two cases is different. It will be done later in each specific paragraph.

5.3.1 Direct Transfers

Based on Oleson approach,[46][47][52][53] the spacecraft is directly placed on a highly elliptical or hyperbolic heliocentric transfer orbit towards its destination by means of a powerful launcher. The Electric Propulsion is exclusively used to decelerate and circularize the trajectory upon reaching the destination planet. This has been done for the three outermost planets: Neptune, Uranus and Saturn.[50]
Hereafter, in order to have comparable results with respect to other transfer strategies, only results obtained for Uranus capture will be discussed. Neptune and Saturn results are shown in Appendix A

In the transfer analysis, the effective mass at the destination is a function of the initial mass, which is in turn determined by the launcher C_3, the specific impulse and the coasting duration. Consequently, the final mass obtained by the optimization should cover all spacecraft subsystems and scientific payload.

As almost constant electrical power is available throughout the orbit transfer, the required propellant mass is only a function of specific impulse (I_{sp}) and thrusting duration. To cover an ample spectrum of EP thruster technologies, specific impulse values in the range from 1500s to 4500s, with a discretized step of 500s, are investigated.
Besides, during the propulsion phases, EP thrusters are constantly switched on in order to maximize the rate of change of spacecraft energy and then minimize the time to accomplish the desired final state.

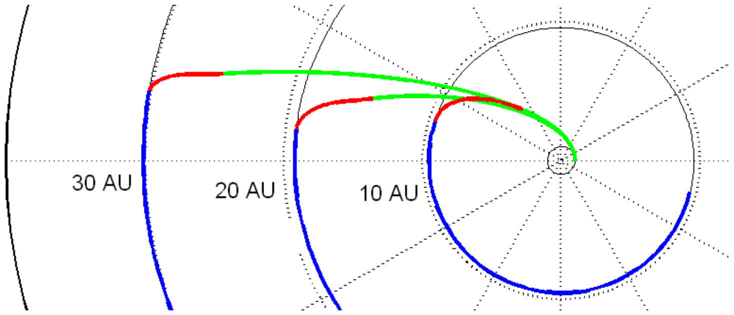

Figure 5.14: Typical geometry of direct transfers with initial coasting (green), propulsion (red) and ballistic continuation (blue)

The last parameter that influences the propellant mass requirement is the ballistic coasting phase duration that is indirectly related to the thrusting duration. It has been parameterized from zero up to more than 10 years and serves as a control parameter, because for identical C_3 and I_{sp}, different final masses and transfer times are obtained under variation of T_{bal}.

Therefore, based on the above discussed parameters, a trajectory optimization was performed, computing the optimal thrust angle to guide the spacecraft to a predefined final state, minimizing the required transfer time.

Initial and Final states The numerical routine computes time optimized transfers between a given initial state (a circular orbit with 1AU radius) and a heliocentric orbit with orbital radius equal to the planet under investigation.

The transfer from the end of the ballistic phase to the desired final orbit is computed using again two different, supplementary, optimization techniques. As said in Sec. 5.1, initially a gradient method is applied to provide a relatively accurate initial guess for a subsequently used forward shooting method. This combination of optimization techniques was able to provide a solution to all feasible scenarios investigated.

Mathematically, the final state can be expressed as a function of the three state parameters at the final time:

$$\begin{cases} r(t_f) &= r_{planet} \\ u(t_f) &= 0 \\ v(t_f) &= \sqrt{\mu / r_{planet}} \end{cases} \tag{5.16}$$

These final conditions will also serve to define the boundary conditions required by the optimization code.

Launcher C_3 [km^2/s^2]	Initial Mass [kg]
130	860
140	740
150	660
160	580
170	480

Table 5.3: Launcher Performance[4]

The spacecraft initial state, is a location on the Earth's orbit around the Sun. Due to the definition of the problem the exact location is not relevant as the model is symmetric.

Moreover, taking into account realistic high energy launcher performance (see for example the US Atlas 551 with Star 48V upper stage[4]), C_3 range considered goes from 130 to 170km^2/s^2 having an associated initial mass from 860 kg to 480 kg, respectively (see Table 5.3).

Results The range of possible spacecraft configurations, initial mass - specific impulse combinations, for a single planet is given by the product of C_3 values (5) and specific impulses (7), therefore a total of 35. For each of these configurations a different number of solutions exist governed by the number of parameterized ballistic coasting durations. This is not equal for all configurations as some *initial mass-*I_{sp} combinations did not converge to a final state adhering the imposed boundary conditions for all ballistic durations. In fact, the coasting phase could result either too short or too long, consuming all available mass or not decelerating in time, respectively.

Figure 5.15 and Fig. 5.16 show the results for the two extremes of launch energy, where the total transfer time and mass fraction are given as a function of different coasting durations and specific impulses. These are presented in three-dimensional figures for the two extremes of launch C_3. It is observed that for higher launch C_3, shorter coasting durations must be considered, especially for the higher specific impulses. The much larger excess energy transports the spacecraft towards its destination much faster, consequently for too long coasting durations the spacecraft is too close to its destination in order to decelerate and circularize the orbit.

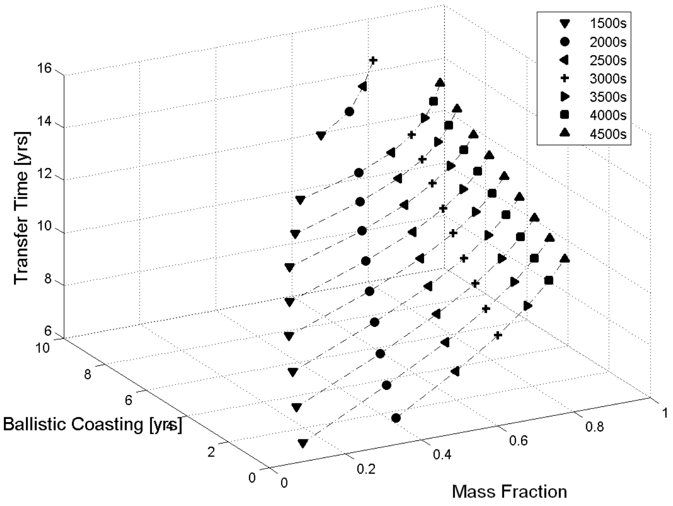

Figure 5.15: Transfer Time and Mass Fraction at the $C3 = 130[km^2/s^2]$ Launch Energy.

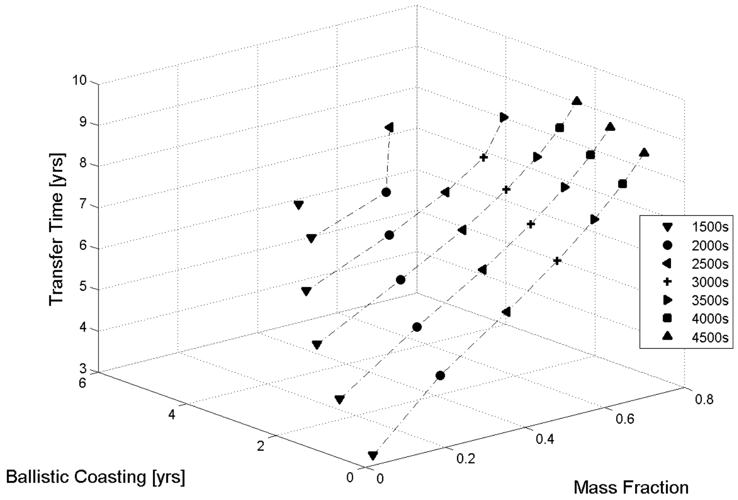

Figure 5.16: Transfer Time and Mass Fraction at the $C3 = 170[km^2/s^2]$ Launch Energy.

Figure 5.17 and Fig. 5.18 show two projections of the three-dimensional surface from Fig. 5.15, presenting the total transfer time and mass fraction as a function of coasting duration only. It is observed that for the lowest I_{sp} value a coasting duration of 1 year is taken as minimum. The low I_{sp} value and short coasting duration result in a very large propellant mass fraction. To minimize the transfer time the optimal trajectory has a long initial phase in which the thrust is mainly accelerating the spacecraft. Consequently the propellant mass fraction becomes very large, where in the extreme case this becomes unity. Higher I_{sp} values do not demonstrate this problem therefore coasting durations starting from zero years are also included.

An upper bound on the coasting duration is observed for the higher I_{sp} values. For longer durations the thrust force is no longer able to decelerate in time guiding the spacecraft towards the imposed boundary conditions. The higher I_{sp} values, for constant power, result in a lower thrust force, therefore more time is necessary to dissipate the excess energy.

A third order polynomial fit is applied to the computed data to obtain the trend lines. It is directly observed that a lower coasting duration results in a lower total transfer time, with the obvious mass fraction payoff. The transfer time decreases as the transfer includes an initial acceleration phase. As a result, increasing the coasting duration significantly increases the payload

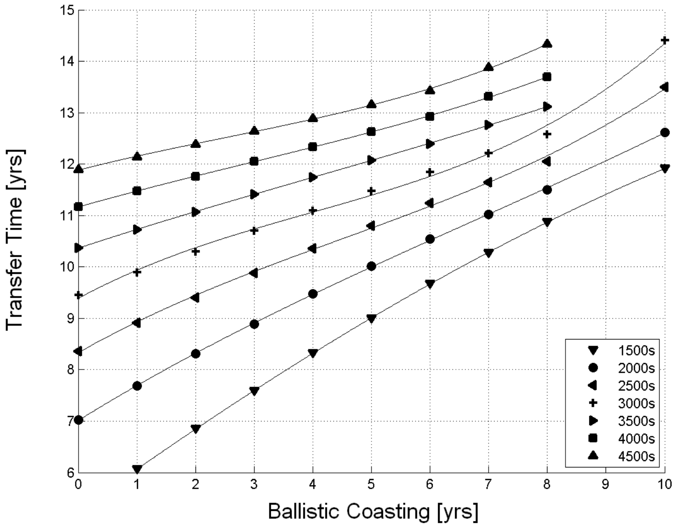

Figure 5.17: Transfer Time versus Coasting duration for various Specific Impulses at the fixed launch energy $C3 = 130[km^2/s^2]$.

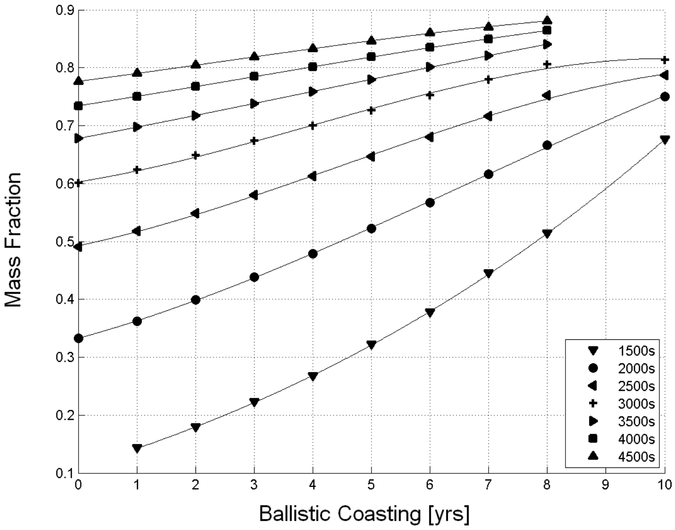

Figure 5.18: Mass Fraction versus Coasting duration for various Specific Impulses at the fixed launch energy $C3 = 130[km^2/s^2]$.

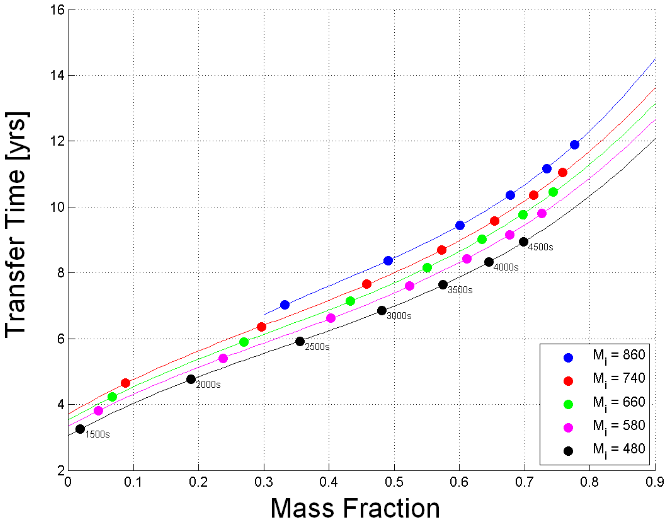

Figure 5.19: Transfer Time versus Mass Fraction for Coasting Duration $T_{bal} = 0$ years.

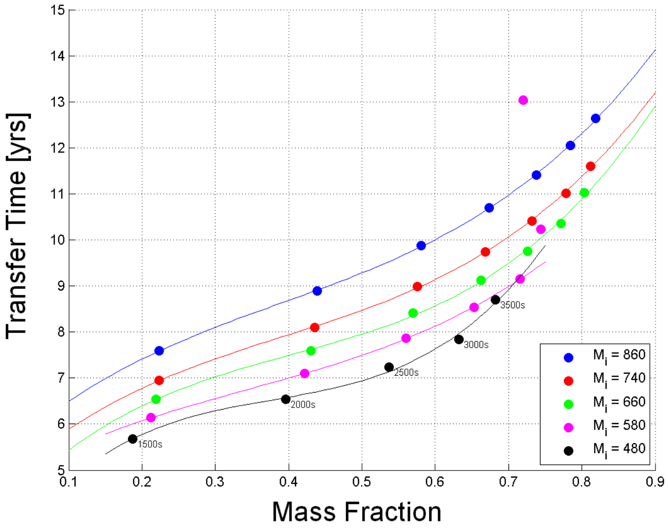

Figure 5.20: Transfer Time versus Mass Fraction for Coasting Duration $T_{bal} = 3$ years.

mass fraction, especially for the lower specific impulses. Moreover, in Fig. 5.18, it can be seen that the variation in mass fraction for subsequent specific impulses decreases with increasing I_{sp} for a constant coasting duration. To maximize the mass fraction for a given value of specific impulse, a coasting duration that does not cause the spacecraft to go beyond the final radius, should be considered.

Figure 5.19 and Fig. 5.20 show the results obtained for all initial masses considered and all specific impulses that lead to a successful transfer, for equal coasting duration. Coasting durations of zero and three years are shown, where the colours represent the initial masses and the dots the specific impulses.

The figure showing no ballistic phase demonstrates a regular behaviour for the different initial masses and impulses. Whereas the three year coasting duration shows the vertical shift in transfer time, as mentioned previously. For the highest C_3 value the two highest specific impulses show a deviation from this behaviour, which results in the fit to bend upwards. This is explained by the spacecraft going beyond the final heliocentric radius before coming back. This effect is even more prominent for the $M_i = 560$ kg case, where the $I_{sp} = 4000$s data point has been omitted for the data fit.

The zero coasting duration case is associated with the minimum total transfer time. When considering this for all evaluated initial masses, as given in Fig. 5.19 the performance envelope under certain mission constraints can be defined.

5.3.2 Multiply Gravity-Assist Transfers

The basic idea of this strategy is to obtain preliminary results about the possibility to use medium class, and thus cheaper, launch vehicles for transfer towards Uranus. However, as the high ΔV budget required is no more totally supplied by the launch vehicle as did in the previous section, additional multiple planets swing-bys are necessary if we want to accomplish such a transfer with comparable transfer times with respect to direct transfer strategy.

Therefore, if on one hand the mission scenario becomes more complex cause the necessity of gravity-assist maneuvers, on the other hand the use of less expensive launchers would result in mission costs reduction.

Mission Constraints According to previous works[48] a RTG-EP small spacecraft designed with all state-of-the-art technologies has been considered as baseline mass budget. Its preliminary dry mass budget is about 500 kg and this value will represent the minimum acceptable mass value at target planet capture throughout the investigation.

On the other hand, the spacecraft mass at departure will be given by the performance of the selected launch vehicle. In particular, a Delta II 7925H or Falcon 9 launch vehicle can be considered as viable options which are able to provide, for an initial mass of 750 kg, a launch C_3 of about $30 \div 35$ km^2/s^2.[54], [55] While this second constraint on the maximum initial mass was chosen to maximize launch escape velocity and thus to reduce transfer time, the first constraint on the minimum arrival mass affects above all the choice of the minimum specific impulse to be considered during the overall transfer and then, indirectly, the transfer time. Concerning the electrical power, a RTG able to provide 1 kW until end of life is hypothesized with a specific mass as approximately 200 kg/kW.[52] It turns out that the transfer problem is also power constrained. The principal mission constraints are summarized in Table 5.4.

Regarding gravity-assist maneuvers, under specific conditions Jupiter fly-by provides the necessary ΔV to reach Uranus orbit distance. However, in order to fulfil mass constraints and reduce transfer times, at least an additional gravity-assist maneuver is needed between the medium energy launch and Jupiter encounter. Thus, following the launch, a ballistic phase was performed till the first gravity-assist maneuver with Mars resulting in an additional ΔV able to increase transfer orbit energy. Then, an optimized phase started to accelerate the spacecraft and perform Jupiter gravity-assist maneuver. As spacecraft velocity vector is required to increase during gravity-assist maneuvers, both encounters were performed in the way that the planet-centered hyperbola passes behind the planet. In the end, a final EP optimized deceleration phase was performed for Uranus capture.

Besides, it should be noted that, as the transfer strategy includes multiple planets fly-bys, launch windows considerations shall impose additional mission constraints. However, this was beyond the scope of this study.

Launch $C3$ Energy [km^2/s^2]	35
Initial S/C Mass [kg]	750
Power [W]	1000
S/C mass @ Uranus capture [kg]	> 500

Table 5.4: Mission Constraints

As said previously, at Earth departure, the escape energy provided by the launcher ($\Delta V_{launch} = \sqrt{C_3}$) is added to the Earth's orbital velocity given by Eq. (5.15).

Both Mars and Jupiter encounters were determined fixing the fly-by altitude, respectively 250 km and $2 \cdot 10^6$ km, and a hyperbolic excess velocity

(V_{HE}). Both these two data determined the geometry of the planetocentric escape hyperbolic orbit and thus the initial and final states in the heliocentric system of reference for the optimization scheme hereafter discussed.

After the ballistic Mars fly-by at 250 km of altitude with a hyperbolic excess velocity $V_{HE} = 11.23$ km/s (see planetocentric encounter in Fig. 5.21), a first optimized low thrust transfer was performed in which final state was fixed by Jupiter fly-by inlet conditions resulting from $2 \cdot 10^6$ km fly-by altitude with a parametrized hyperbolic excess velocity (Fig. 5.22). In particular, a higher Jupiter excess velocity allows spacecraft to minimize transfer times but, on the other hand, it must be in a suitable range of values that guarantee both the matching conditions with the final state of the optimized phase and the capability for the EP thruster to decelerate with an acceptable amount of propellant before Uranus capture. In this study, discrete values of Jupiter excess velocities in the range $V_{HE} = 5 \div 7$ km/s were considered as they satisfied both the above mentioned conditions.

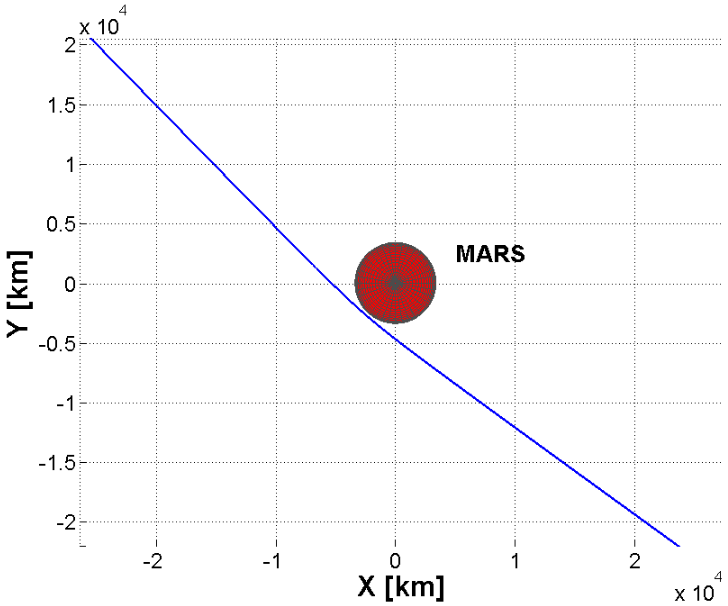

Figure 5.21: Mars fly-by in the planet-centered coordinates.

The transfer from the end of the ballistic phase after Mars fly-by to the desired final state before Jupiter gravity-assist is computed using again the two different, sequential, optimization techniques. Initially a gradient method was applied to provide a relatively accurate initial guess for a subsequently used forward shooting method. The same scheme was applied for the final

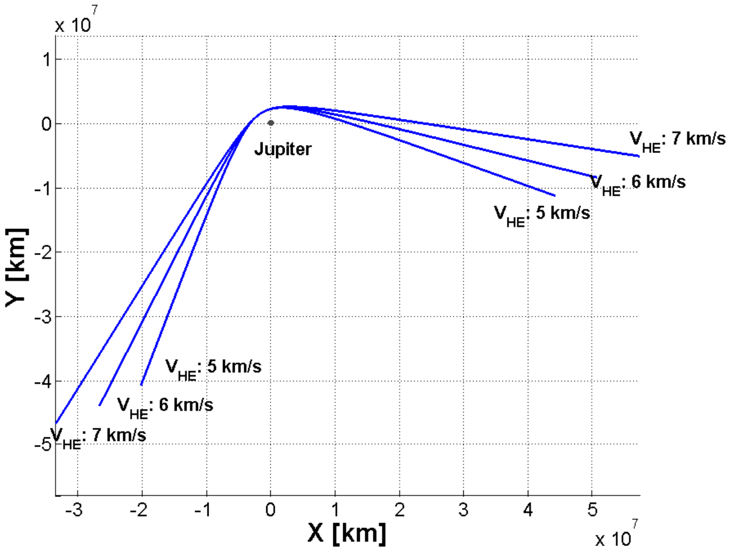

Figure 5.22: Effect of the hyperbolic excess velocity in Jupiter-centered coordinates with a fixed fly-by altitude.

EP deceleration phase.

To maintain feasible mission durations, transfer time and thus the propulsion phase was subjected to minimization.

This combination of optimization techniques was able to provide a solution to all feasible scenarios investigated.

Results According to mission constraints and transfer strategy outlined in previous paragraph, complete Earth-Uranus transfers were computed. Nevertheless, before doing that, another important assumption was made about the thruster specific impulse. In fact, for a power constrained transfer, a high specific impulse with consequent propellant mass saving results in lower thrust level and thus longer transfer times.

Jupiter V_{HE} [km/s]	5	6	7
Tot Transfer Time [dys/yrs]	5767/15.8	5365.5/14.7	5110/14
Tot Propellant Mass [kg]	208	223	235.5
S/C Mass @ Uranus capture	542	527	514.5
S/C Mass Fraction @ Uranus capture	0.723	0.703	0.686

Table 5.5: Overall transfer main results with respect to Jupiter excess velocity

Vice versa, a lower specific impulse reduces transfer times but increases

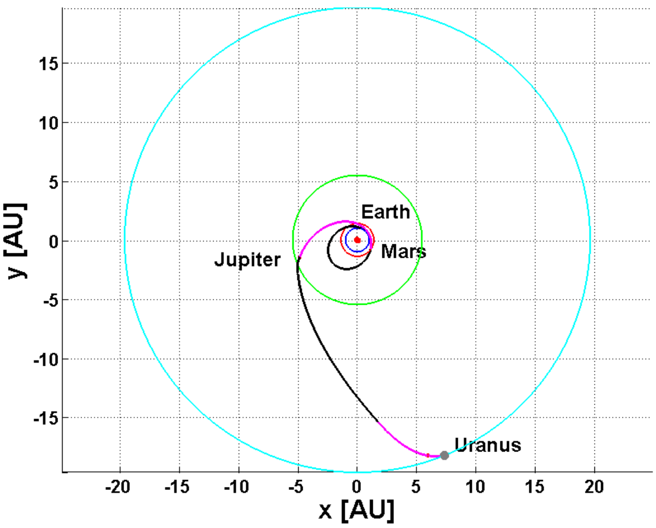

Figure 5.23: Complete Earth-Uranus transfer in Heliocentric coordinates (Jupiter $V_{HE} = 7$ km/s - magenta line=optimized phase, black line= ballistic phase).

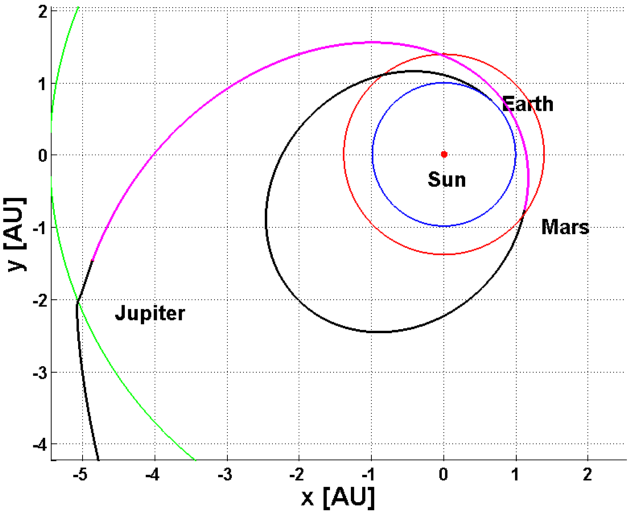

Figure 5.24: Zoom of the complete transfer between Earth and Jupiter (Jupiter $V_{HE} = 7$ km/s - magenta line=optimized phase, black line= ballistic phase).

propellant mass needed to perform the transfer. Therefore, in order to minimize transfer times, the idea was to find the minimum value of specific impulse able to fulfil mass constraints. Thus a $I_{sp} = 3200s$ was selected.

Regarding Jupiter gravity-assist maneuver, complete transfers were computed for all the excess velocities selected. Results are summarized in Table 5.5. Nevertheless, Jupiter excess velocity of 7 km/s was chosen for the reference transfer trajectory as it minimizes transfer time. The complete transfer is shown in Fig. 5.23 and Fig. 5.24 Instantaneous values of spacecraft mass, heliocentric position, heliocentric velocity and thrust angle β (see Fig. 5.13 for its definition) during the optimized phases are shown respectively in Fig. 5.25, Fig. 5.26, Fig. 5.27 and Fig. 5.28. Blue lines represent the ballistic phases while magenta lines the optimized ones.

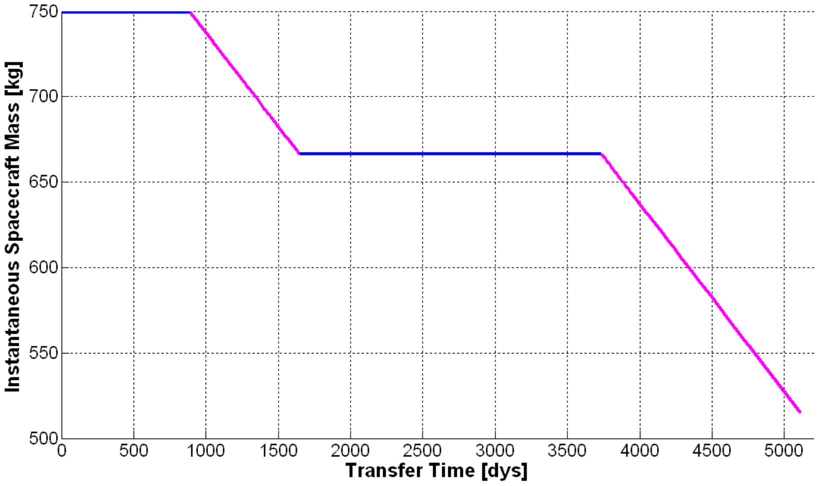

Figure 5.25: Instantaneous spacecraft heliocentric position vs Transfer Time (blue lines=ballistic phase, magenta lines=optimized phase).

Moreover, the main results for the reference trajectory launched with a medium class launcher combined with Mars and Jupiter fly-bys are summarized in Table 5.6. It can be noted that the overall transfer time results to be longer than the ones obtained in the direct transfer by means of a high energy and expensive launch. Nevertheless, if a longer transfer time is accepted, this approach allows to reduce launch costs that represent one of the major cost drivers in mission budgets.

Therefore,results showed the possibility to accomplish RTG-EP small spacecraft missions towards Uranus combining multiple gravity-assist transfer strategies with a medium energy launch performed by less expensive launch

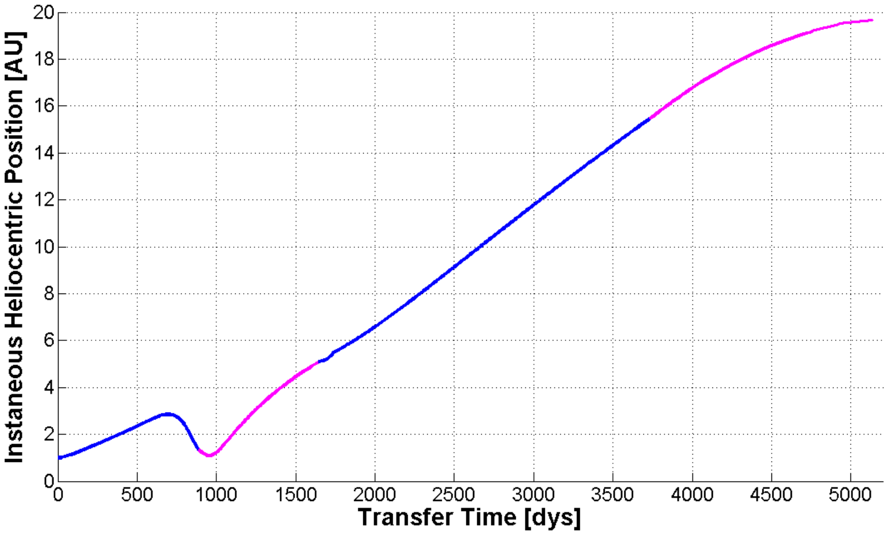

Figure 5.26: Instantaneous spacecraft heliocentric position vs Transfer Time (blue lines=ballistic phase, magenta lines=optimized phase).

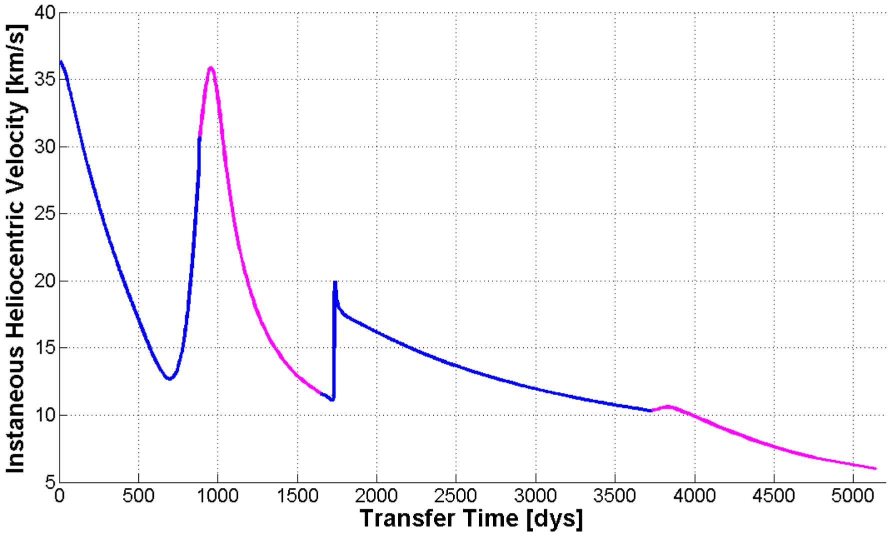

Figure 5.27: Instantaneous spacecraft heliocentric velocity vs Transfer Time (blue lines=ballistic phase, magenta lines=optimized phase).

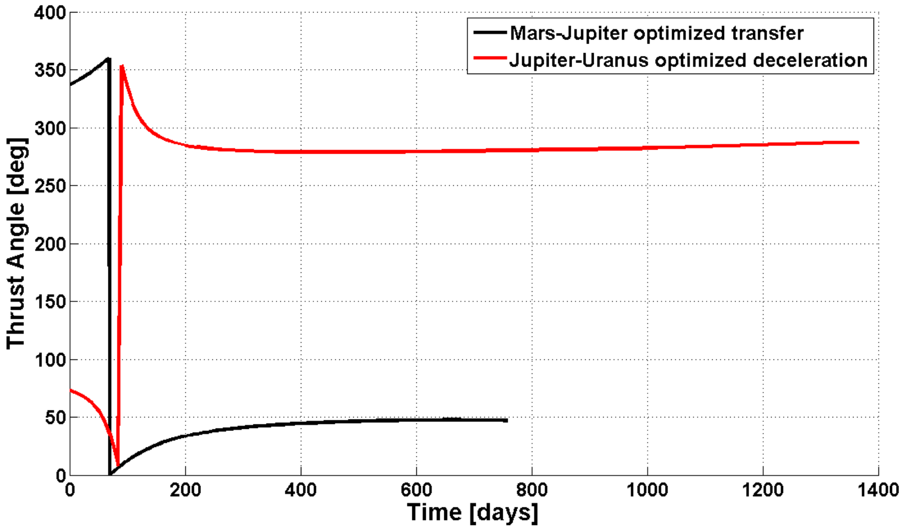

Figure 5.28: Thrust angle in the optimized phases vs Transfer Time.

Launch C_3 $[km^2/s^2]$	35
S/C Departure Mass [kg]	750
Power for EP subsystem [W]	1000
Specific Impulse [s]	3200
Earth-Mars ballistic transfer [dys/yrs]	883.2/2.42
Mars-Jupiter optimized transfer [dys/yrs]	758.22/2.08
Mars-Jupiter propellant mass consumption [kg]	83.48
Jupiter-Uranus coasting phase [dys/yrs]	2084.4/5.72
Optimized deceleration Phase and capture [dys/yrs]	1383.14/3.79
Deceleration propellant mass consumption [kg]	152.02
Total Transfer Time [dys/yrs]	5110/14
Total Propellant Mass [kg]	235.5
S/C Mass @ Uranus	514.5
S/C Mass Fraction @ Uranus	0.686

Table 5.6: Overall transfer main results

vehicles in order to reduce mission costs. Besides, results showed that missions compatible with the assumed mass budgets and launcher constraints are feasible within acceptable transfer times.

Nevertheless, the results obtained also pointed out the disadvantages associated with longer transfer times with respect to studies based on the assumption of a high energy launch followed by direct transfer to outer planets. Therefore, it should be noted that, even if the possibility to use medium class and thus cheaper launchers would result in mission costs reduction, the cost effectiveness of such alternative transfer strategies towards outer planets should be assessed for each particular case.

Chapter 6

Application of EP Low-Energy Transfers to a Reference Mission: Trajectory and Spacecraft Preliminary Design

During the last years, several studies[56] [57] [3] have investigated the possibility to develop tours in planetary systems, often performed in the Jovian system, based on the exploitation of three-body dynamics where the necessary velocity changes are provided by conventional propulsion systems.
From the mission design point of view, these mission scenarios are very interesting as they give the possibility to orbit several moons of an entire planetary system requiring only a minimum of onboard resources and increasing significantly the scientific outcome of a mission.

A similar approach is implemented in this study but Electric Propulsion (i.e. low-thrust) is considered for the execution of the required manifold transition. A similar strategy was also investigated by Topputo.[58]

In detail, a tour of the Uranian system and the required interplanetary trajectory in the CR3BP model are studied.
In fact, the Uranus vicinity provides an interesting dynamical environment because its main moons are sufficiently massive and near enough to form several three body models with the planet acting as the principal body. In this framework, a low energy passage from one moon to another is possible, where propellant requirements can be further reduced under consideration of an electric thruster.

The main purpose of this proposed reference mission is to develop a tour within the Uranus system that visits each one of the selected moons, including a temporary capture obtained by a ballistic arrival and departure arc.

Not only a planetary tour of the Uranian system orbiting consecutively

Oberon, Titania, Umbriel, Ariel and Miranda is designed, but also the required interplanetary trajectory transporting the spacecraft from the Earth to Uranus. Both the interplanetary trajectory as the planetary tour are computed in different three-body environments, where the start of the interplanetary phase is assisted by a high energy launch to limit the transfer time.

Moreover, because of the basic hypothesis of Electric Propulsion, another important aspect discussed in this chapter is the availability of an adequate power source for the spacecraft not reliant on the Sun. In fact, the increasing distance from the Sun results in the fading of solar power and therefore alternative power sources are needed, as solar arrays become ineffective.
A state-of-the-art viable option for power generation purposes, if power requirements remain within few kWs, are the Radioisotope Thermoelectric Generators (RTGs).

In the end, taking into account this aspect and all considerations made in the previous chapter on launchers performance, a preliminary spacecraft configuration is also developed and shown.

6.1 The Planetary Realm

During the complete planetary system tour, the spacecraft is unstable captured by the five moons for different periods of time. Several closed orbits around Oberon, Titania, Umbriel, Ariel and Miranda are executed and, in the end, a stable Uranian orbit as a final state is obtained. This would enable scientific studies of the main moons for a considerably longer duration when compared with fly-by's.
The developed tour is schematically represented in Fig. 6.1.

The orbital characteristics of the five main moons present in the Uranus system are shown in Table 6.1. It is worth noting that the inclinations presented in the Table 6.1 are referred to the Uranus equatorial plane. Due to the unique inclination of the axis of rotation of the planet, which has an axial tilt of 98 degrees and thus lies approximately in the ecliptic plane, the moons are orbiting almost perpendicular to this plane.

All trajectories calculated in this study are with reference to the Uranus equatorial plane, where the moons are considered to move in circular, equatorial orbits. Therefore application of different, coupled Planar Restricted Three Body Problems (PCR3BP) is considered a valid approximation.

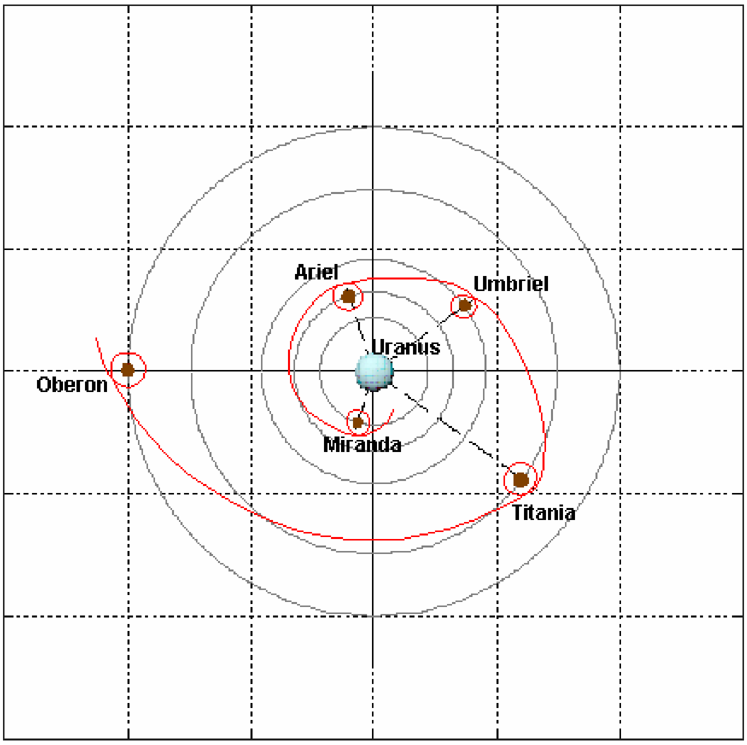

Figure 6.1: Schematic representation of the Uranus Moons Tour

Uranus Moon	Mass [kg]	Semi-major Axis [km]	Eccentricity	Inclination [deg]
Oberon	$3.014 \cdot 10^{21}$	583519	0.0016	0.700
Titania	$3.526 \cdot 10^{21}$	435910	0.0011	0.340
Umbriel	$1.200 \cdot 10^{21}$	266300	0.0039	0.205
Ariel	$1.350 \cdot 10^{21}$	190020	0.0012	0.260
Miranda	$6.590 \cdot 10^{19}$	129390	0.0013	4.232

Table 6.1: Uranus Moons characteristics

6.2 Reference System Transformation

Consideration of both the interplanetary and planetary phase of the mission requires for an appropriate reference system transformation. The planetary tour is computed subsequently considering, as said before, planar models formed by Uranus and one of its moons, where the initial state must be computed with respect to the outermost moon Oberon.

The Uranian tour initiates on the exterior invariant manifold leading toward the second libration point in the Uranus - Oberon system. This initial state in the Uranus - Oberon system is transformed to the Sun - Uranus system and forms the boundary condition for the interplanetary trajectory optimization. The transformation provides for a decoupling of the two systems with the advantage that both mission phases can be computed and optimized independently.

The high inclination of Uranus' spin axis and its moons having approximately equatorial orbits, results in an offset of the orbital plane of the moons with respect to the fundamental Sun - Uranus plane.[59] This is schematically shown in Fig. 6.2. A generalization is applied where Uranus' axis of rotation is assumed to coincide with the orbital plane of Uranus. Moreover, the moons are all considered to have circular, equatorial orbits, thus being exactly perpendicular to the Sun - Uranus plane. The system of reference transformation takes into account both this rotation of the principal axes, in addition to the velocity conversion. Due to this rotation the initial conditions of the planetary tour have components of the position and velocity only in the x-z plane.

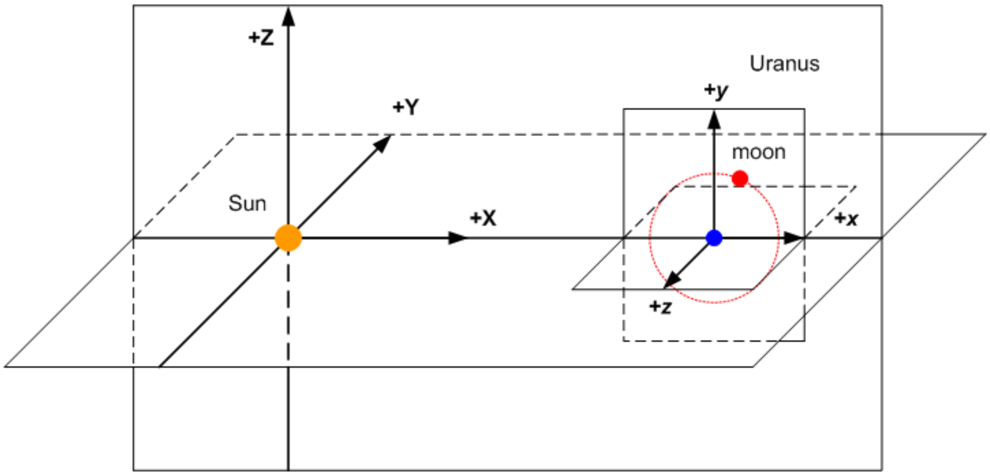

Figure 6.2: Schematic overview of the two principal reference systems

6.3 Interplanetary and Conjunction Phases

The initial conditions for the interplanetary phase are derived from the position and velocity that correspond with a 1AU circular orbit around the Sun (i.e. the Earth orbit). The position of departure on the circular orbit, together with the excess energy, has a strong effect on the shape of the trajectory. Erroneous selection of initial position or excess energy might render the transfer impossible or excessively long in duration. As shown in Sec. 5.2, the angular region giving the minimum transfer times was identified, in which a low sensitivity to excess energy magnitude for the range investigated was shown. This angle has been adopted in the current study and equals 230 degrees from the x-axis in anti-clockwise direction.

Equations of motion are:

$$\left\{\begin{array}{rcl} \ddot{x} - 2\dot{y} & = & -\bar{U}_x + a_x \\ \ddot{y} + 2\dot{x} & = & -\bar{U}_y + a_y \\ \ddot{z} & = & -\bar{U}_z + a_z \\ \dot{m} & = & -(T)/(I_{sp} \cdot g_0) \end{array}\right. \tag{6.1}$$

where the acceleration vector is given by $\mathbf{a} = \mathbf{T}/m$ and thrust modulus T is given by:

$$T = \frac{2\eta P}{I_{sp} \cdot g_0} \tag{6.2}$$

Following launch the EP must modify the velocity in all three dimensions in order to adhere the imposed final conditions: the initial state is in the x-y plane, whereas the final state which corresponds with the start of the Uranian tour is in the x-z plane. The optimization algorithm therefore computed both in- and out of plane thrust components, while minimizing the required time to arrive at the final state.

The interplanetary transfer is computed in two step, in a first phase a gradient method implements the transfer acting on the in plane and the out of plane thrust angles. This approach is less reliant on a precise initial guess and was applied to generate an accurate initial guess. Based on the results of the gradient method a forward shooting algorithm is implemented. It considers the Lagrange multipliers obtained by the former optimization to design the thrust law (see Sec. 5.1 for details).

To maintain feasible mission durations the transfer time (i.e. the functional) is subjected to minimization, where a limit on the final mass after the interplanetary transfer is imposed indirectly by ensuring departure with an initial mass that results in a final mass $m_f \geq 500$kg, this to ensure sufficient spacecraft and propellant mass for the planetary tour. This mass constraint is respected by applying a numerical scheme that ensured an initial mass sufficient to arrive at the final state with the required mass.

The interplanetary trajectory is connected with the Uranian tour by the previously discussed transformation of reference system. However, in addition a conjunction phase is required to dissipate the spacecraft's energy in order to adhere the tours initial conditions. The conjunction phase resembles a classical low-thrust planar orbit transfer, where a spiraling motion is performed gradually closing in on Uranus. The duration of the conjunction phase was arbitrarily chosen as the time required to reach a distance from Uranus equal to the sphere of influence (SOI).

The thrust vector orientation during this phase is opposing the velocity vector, thus decreasing the velocity magnitude and consequently approaching Uranus. The conjunction phase is computed by a backward integration in the Sun - Uranus system. The integration starts from the first Poincarè section of the L2 stable manifold of Oberon that represents the tour's initial conditions and ends at the Uranus SOI radius. This state is taken as the boundary condition for the interplanetary optimization code.

Results First of all, some initial spacecraft characteristics are given as input. In Table 6.2, an overview is given:

Power [W]	1000
Specific Impulse [s]	3200
Thrust Efficiency [-]	0.5
C3 Energy [$\mathrm{km}^2/\mathrm{s}^2$]	130

Table 6.2: Transfer Inputs

As already mentioned, the excess velocity corresponding with the excess energy has been summed to the Earth's velocity on a 1AU circular orbit in the Sun-Uranus system.

Figure 6.3 presents the interplanetary transfer shown in the Sun-Uranus synodic system. The visualization in the x-z plane shows a large excursion below the x-y plane. Nevertheless, it must be noted that the scaling along the z-axis is two orders of magnitude smaller than along the x-axis.

Figure 6.4 shows the instantaneous values for the radius as measured from the Sun, the velocity with respect to the synodic reference system and the mass decrease during the transfer. Results are shown both for the solution obtained by the gradient method as well as for the forward shooting method, represented by the blue and red lines, respectively. The continuation represented by the black line is the conjunction phase, which is shown only for the more precise forward shooting solution. The spiraling motion can be observed from the subfigure showing the spacecraft velocity, where the black line oscillates. This oscillation is also present in the Sun radius, however, due to scaling this less pronounced in the figure. The propellant mass consumption equates to a linear decrease in spacecraft mass as no coasting phases are foreseen by the optimization scheme.

The conjunction phase is shown in more detail in Fig. 6.5 where the final state of the forward shooting optimization is continued by the conjunction

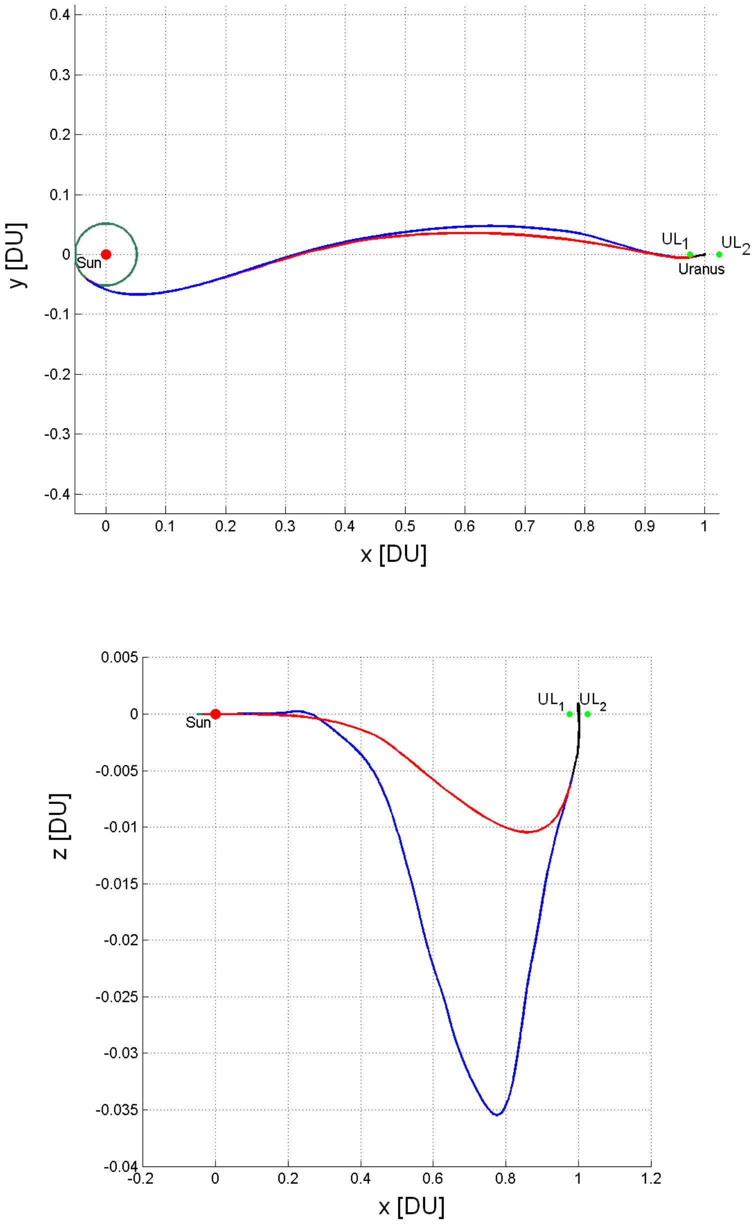

Figure 6.3: Overview of the Interplanetary Trajectory in the Sun-Uranus synodic frame (blue line=gradient method, red line=forward shooting method)

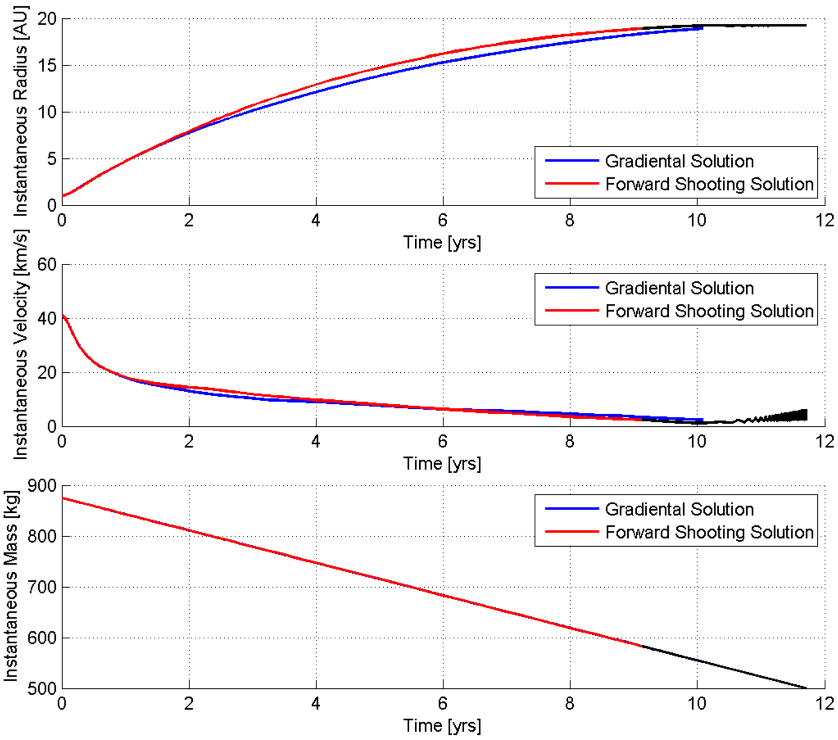

Figure 6.4: Instantaneous Radius, Velocity and Mass

phase shown in black. During the conjunction phase the spacecraft energy gradually decreases leading to a closure of Hill's region. In addition, the spacecraft is closing in on Uranus aligning the position and velocity to the requirements imposed by the planetary tour, discussed in the next section. The duration equals approximately 2.56 years with a mass consumption of 83kg. This in addition to the 9.14 years required to reach the SOI of Uranus with a mass consumption of 292.7kg.

Figure 6.6 shows the in- and out-of plane thrust angles computed by the forward shooting optimization scheme. It can be seen that after approximately 2.35 years thrust angles demonstrate a rapid variation of the thrust direction. The α-angle represents the in-plane thrust angle measured positive in anti-clockwise direction from the x-axis, whereas the β-angle represents the out-of-plane thrust angle measured positive along the positive z-axis. Before the variation in direction the α-angle contains an accelerative component in the positive x-direction, where this changes into a decelerative behavior afterward. The β-angle demonstrates only a slight out-of-plane excursion, which is explained by the fact that the velocity component along z at the final state

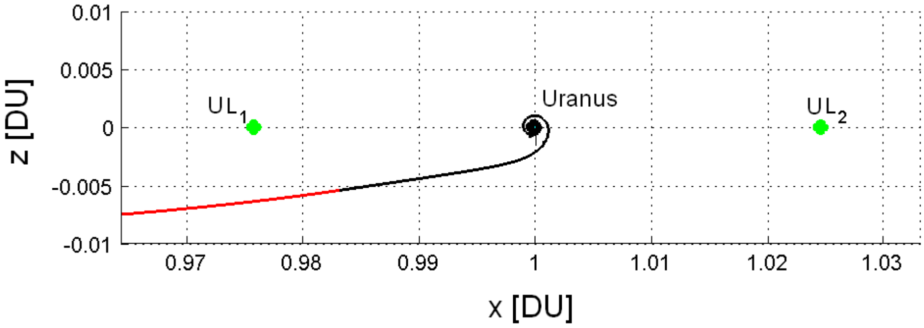

Figure 6.5: Detail of the Conjunction Phase

is relatively small and the a total distance of 19.2 AU is available to achieve this.

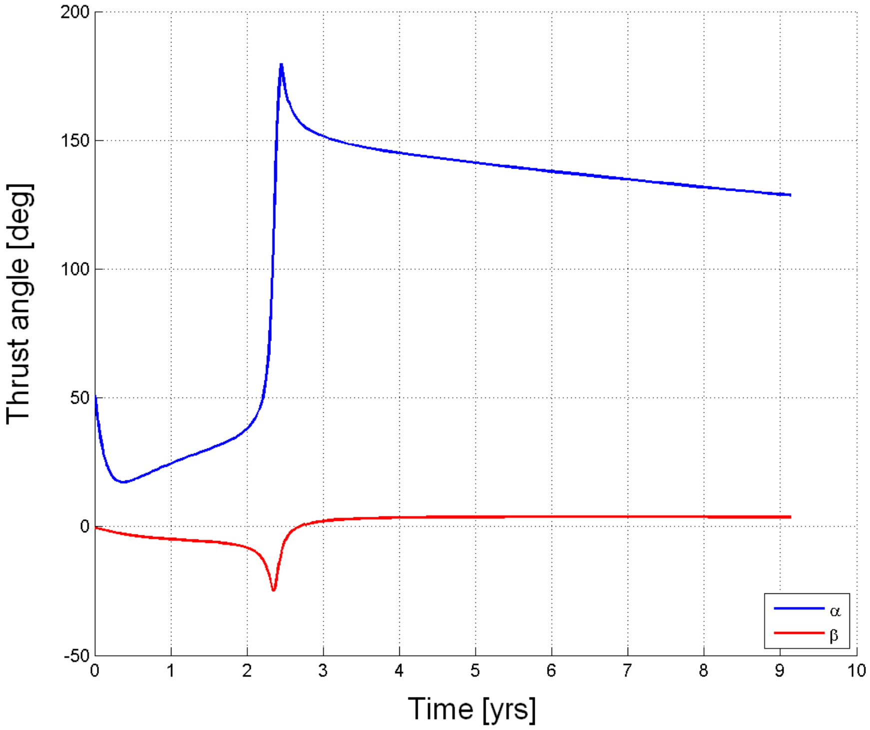

Figure 6.6: Time Variation of the Thrust Angles by the Forward Shooting Method (α=in-plane, β=out-of-plane)

The general outputs of the interplanetary phase are summerized in Table 6.3:

Outputs:	
Interplanetary Transfer Time [yrs]	11.7
Initial Mass [kg]	875
Propellant Mass [kg]	375
Fuel Mass Fraction [-]	0.417
Transfer ΔV [km^2/s^2]	17.57

Table 6.3: Transfer Outputs

After some numerical iteration the initial spacecraft mass at launch equals 875 kg, this, coupled with the assigned excess energy of $C_3 = 130km^2/s^2$, is compatible with the Atlas launcher performance equipped with the Star 48V upper stage.

6.4 Uranian Tour

The second part of the study investigated the possibilities to continue the interplanetary transfer with a tour of the Uranian system, advantageously exploiting the three-body low energy ballistic trajectories. This results in a tour with a scientifically interesting character as many different environments are experienced and a technically interesting as the propellant requirements are be limited.

System Dynamics The tour is computed within the PCR3BP, based on which the stable and unstable manifolds associated with the libration points of that system are computed. The connection of two states on an unstable and stable manifold, respectively, enables the passage from one system to the other.[60] The connection of two states requires an energy change provided by the Electric Propulsion, where the thrust direction and modulus are two parameters of optimization, explained in more detail further on.

If the manifolds intersect in the position space a single ΔV can suffice to establish transition, however, for the system studied in this work this is not possible. Due to the low mass parameters of the different systems (Table 6.4), no intersections in the position space are present (Fig. 6.8). Thus, the only approaches feasible to perform the tour are either using a multi-burn strategy or a continuous thrust, which modifies the spacecraft energy during propelled arcs.

The moons, together with the planet Uranus itself, form different three body environments in which the motion of the spacecraft is studied. Here, the planet and its specific moons are the *primaries* of the relative dynamic system. The dynamics of the PCR3BP and its governing equations are briefly recalled:

$$\left\{ \begin{array}{rcl} \ddot{x} - 2\,\dot{y} & = & -\bar{U}_x \\ \ddot{y} + 2\,\dot{x} & = & -\bar{U}_y \end{array} \right. \tag{6.3}$$

where, as said in chap. 2, the subscripts denote the partial derivates and $\bar{U}$ is the *effective potential* (see Eq. (2.22)), the x and y coordinates and their derivates are computed with respect to a non dimensional, synodic reference frame centered in the center of mass of the two main attractors and rotating with their relative angular velocity. The distances between the two primaries and the third body are given by:

$$\left\{ \begin{array}{rcll} r_1^2 & = & (x+\mu)^2 + y^2 & \text{Uranus} - \text{Spacecraft distance} \\ r_2^2 & = & (x-1+\mu)^2 + y^2 & \text{moon} - \text{Spacecraft distance} \end{array} \right. \tag{6.4}$$

As already mentioned in chap. 2, the CR3BP (or PCR3BP) has one first integral of motion, the *Jacobi integral* (C), which represents the energy (E) in the rotating non-dimensional frame. This is given by:

$$\begin{array}{rcl} C & = & -(\dot{x}^2 + \dot{y}^2) - 2\bar{U}(x,y) \\ E & = & -C/2 \end{array} \tag{6.5}$$

The *mass parameter* (μ) of the system is the only parameter necessary for the characterization of the specific three body system, which in this case depends on the second primary (moon) selected.
This parameter and the non-dimensionalizing quantities are different for each three body systems and are dependent on the specific moon involved in the trajectory arch (Table 6.4).

As discussed in Sec. 2.3, any set of $(x, y, \dot{x}, \dot{y})$ satisfying the Jacobi constant will represent a possible motion for a given energy level and, once initial condition is given, the Jacobi integral can be used to establish some allowed and forbidden regions for the motion of the spacecraft bounded by the *zero velocity surfaces* or *Hill's surfaces* on which the kinetic energy is zero.

However, during the transfer, the electric thruster modifies the energy of the spacecraft and during the passage from one manifold to the other the zero velocity curves can be crossed.

For increasing spacecraft energy the forbidden region opens a neck around each equilibrium point. In Fig. 6.7, the Hill regions for each Uranus-moon

Primaries	μ	Distance Unit [km]	Time Unit [sec]	Mass Unit [kg]
Uranus-Oberon	$3.4792 \cdot 10^{-5}$	583519	$1.8539 \cdot 10^{5}$	$8.6628 \cdot 10^{25}$
Uranus-Titania	$4.0703 \cdot 10^{-5}$	435910	$1.1970 \cdot 10^{5}$	$8.6629 \cdot 10^{25}$
Uranus-Umbriel	$1.3853 \cdot 10^{-5}$	266300	$5.7157 \cdot 10^{4}$	$8.6626 \cdot 10^{25}$
Uranus-Ariel	$1.5584 \cdot 10^{-5}$	190020	$3.4452 \cdot 10^{4}$	$8.6626 \cdot 10^{25}$
Uranus-Miranda	$7.6075 \cdot 10^{-7}$	129390	$1.9358 \cdot 10^{4}$	$8.6625 \cdot 10^{25}$

Table 6.4: Uranus-moon identification parameters

system investigated are shown. These are produced for an energy value that assures an opening being present even for the smallest μ, Miranda, considered.

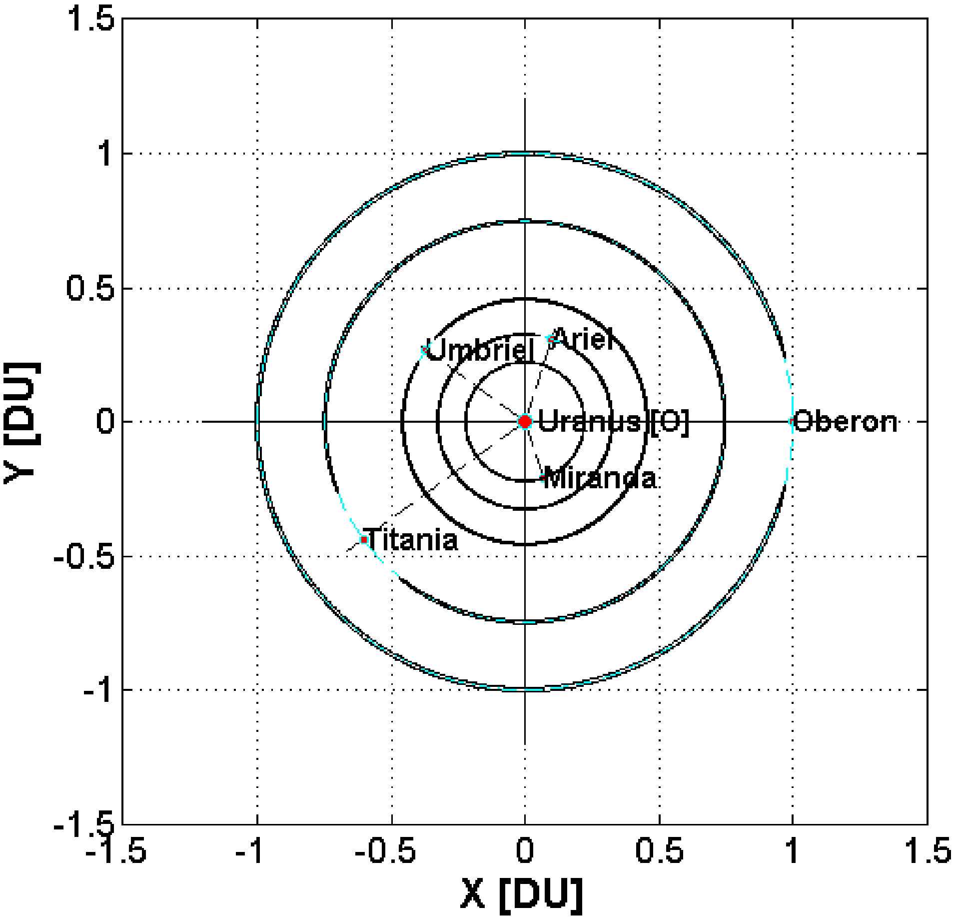

Figure 6.7: Hill regions of the chosen moons

Using the passages provided by the opened Hill region, transits can be established going from one realm to the other. The lowest energy value that permits a transit from the outer realm, traversing the moon and going to the inner realm is the energy value associated with the second libration point L_2, therefore the manifolds computed in this study are based on this libration point, thus its energy level.

As discussed in chap. 3, these manifolds are given by the stable and unstable eigenvalues of the coefficient matrix of the linearized dynamics, and compute two one dimensional manifolds associated with the libration points.[49] The manifold associated with the stable eigenvalues computes to a ballistic trajectory leading towards the libration point, whereas the unstable eigenvalues compute to ballistic trajectories going away from the libration points.

Recalling the linearized equtions of motion near collinear libration points, and the computation of invariant manifolds associated to collinear libration points discussed in Sec. 3.2, the manifolds associated with L_1 and L_2 can be obtained by propagating a small perturbation d in the direction of $\mathbf{u}_s$ and $\mathbf{u}_u$ the eigenvectors associated to the stable and the unstable eigenvalues ($\lambda_s < 0$ and $\lambda_u = -\lambda_s$) starting from the state $\mathbf{x_0}$ of the libration point of interest:

$$\begin{aligned} \mathbf{x_0}^s &= \mathbf{x_0} \pm d\,\mathbf{u}_s \\ \mathbf{x_0}^u &= \mathbf{x_0} \pm d\,\mathbf{u}_u \end{aligned} \qquad (6.6)$$

The first of Eqs. 6.6 must be propagated backward and the second forward, where there are two legs for each manifold. The manifolds associated with L_1 and L_2 for each of the five moons are shown in Fig. 6.8. It is worth noting that in the figure only the planetary distance is scaled, moreover the manifolds are shown as seen each in their rotating reference frame.

In order to perform the passage among the different three body systems, an in-plane thrust has been included adding an acceleration term to the equations of motion (Eq. 6.3). Again, to modulate the thrust value $\vec{T}$ a scaling parameter, $\tau \in [0, 1]$, and a thrust angle (α) have been included as shown below.

Furthermore an equation for the mass variation has been added.

$$\vec{a} = a\,cos(\alpha)\,\hat{T} + a\,sin(\alpha)\,\hat{N} \qquad (6.7)$$

$$\begin{cases} \ddot{x} - 2\,\dot{y} &= -\bar{U}_x + \vec{a} \cdot \hat{\imath} \\ \ddot{y} + 2\,\dot{x} &= -\bar{U}_y + \vec{a} \cdot \hat{\jmath} \\ \dot{m} &= -(|\vec{T}| \cdot \tau)/(I_{sp} \cdot g_0) \end{cases} \qquad (6.8)$$

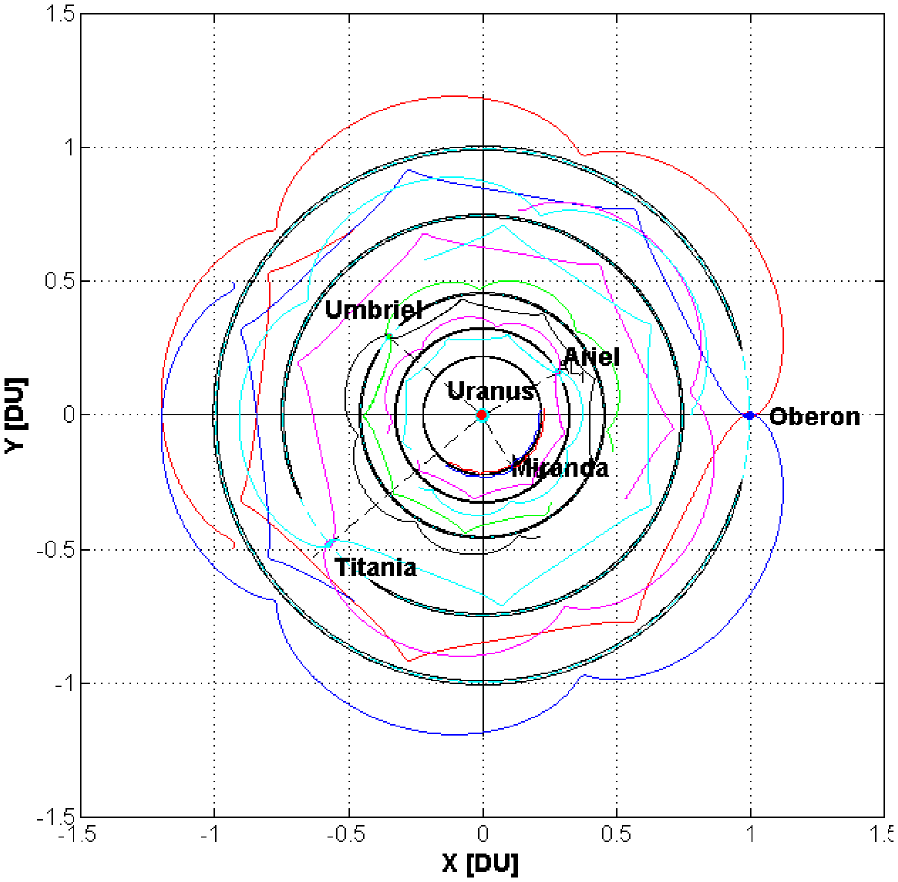

Figure 6.8: Manifolds of the libration points of the chosen moons

where

$$a = \frac{|\vec{T}| \cdot \tau}{m} \qquad |\vec{T}| = \frac{2\,\eta\,P}{I_{sp} \cdot g_0} \tag{6.9}$$

The thrust angle α is measured counterclockwise from the velocity direction, $\hat{\imath}$ and $\hat{\jmath}$ are the unit vectors of the synodic frame and $\hat{T}$ and $\hat{N}$ are the unit vectors tangent and normal to the trajectory, respectively.

Design Approach The state obtained by the spacecraft after the execution of the interplanetary transfer and the subsequent conjunction phase is the intersection between the exterior, stable manifold of Oberon and the first Poincare section. This stable manifold will transport the spacecraft ballistically to the second libration point, L_2, in the Uranus - Oberon system. Moreover, more generally, the manifolds associated with the libration points of each moon are computed in the relative synodic frame and subsequently translated and scaled to the Uranus - Oberon system, which is chosen as the main system of reference for the tour construction as it is the outermost moon considered.

The transformation between the two systems takes into account the initial phase of the moons and the associated non-autonomous phase difference during the entire transfer. A manifold of a generic moon, in this system, appears as a trajectory that flows from a radius greater than the radius of the circular orbit of the moon, wraps around the moon's orbit and finally arrives inside the moon's circular orbit. In the main reference frame the manifolds of Oberon are time independent, whereas the manifolds associated with the other moons are time dependent (periodic).

It is worth noting that the manifold used for the construction of the capture arc of each moon is the stable manifold associated with L_2, because this is the ballistic trajectory that leads the spacecraft towards the moon from the outer realm. Its computation requires a propagation of the initial conditions (Eq. (6.6)) for a time span that must begin at the same final time as the powered phase of the previous step. The propagation is performed backward for a time span that identifies the time duration for which the spacecraft lies on the stable manifold. The duration of this time span (t_{man}) and the initial position of the relative moon (θ) are terms of the control vector. Furthermore, the exit time from the previously considered unstable manifold of L_1, (t_0), is also considered a term of the control vector.

As opposed to the interplanetary trajectory, optimization with respect to the required transfer time is not applied anymore. Time optimization results in a continuous, maximized thrust modulus, whereas this is not necessarily the case when minimizing the required propellant mass as applied for the tour optimization scheme. An appropriate thrust law, based on (α,τ) which are the thrust angle and modulus, respectively, is required in order to establish the connection between the final conditions of the propulsion phase and the insertion conditions on the manifold of the target moon. The thrust must be considered for a time span to be determined, being (t_{EP}), where these parameters are determined by the optimization scheme. The definition of the control vector elements for the first passage are shown in Fig. 6.9.

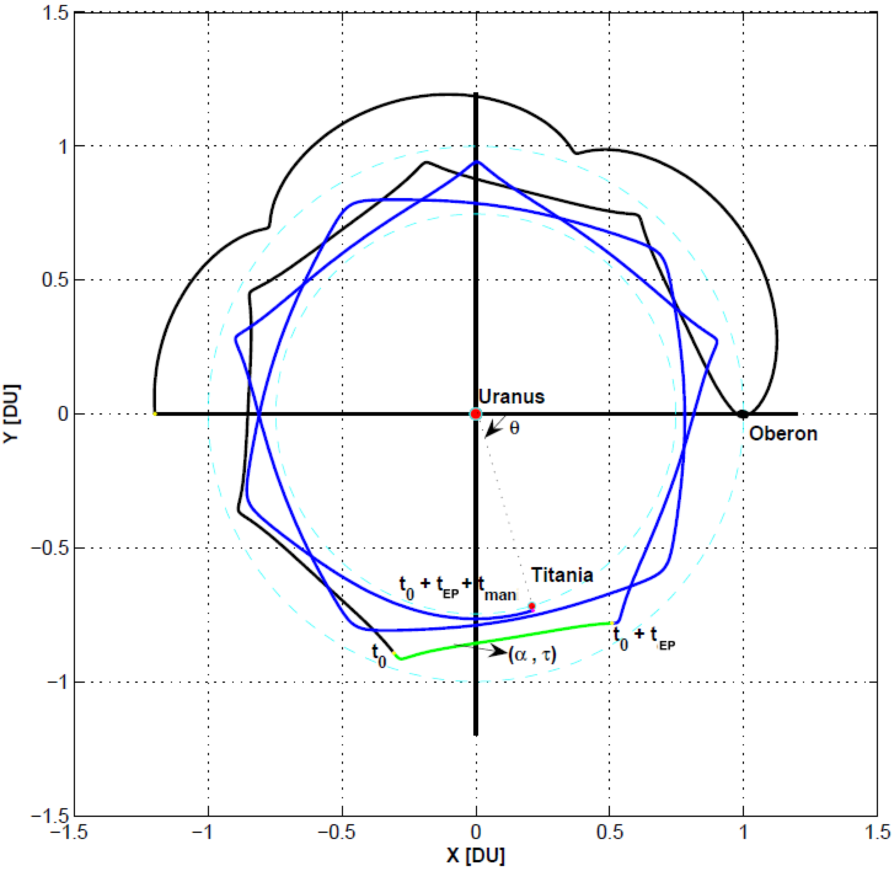

Figure 6.9: Representation of optimization parameters for the Oberon-Titania transfer

The complete control vector ($\mathbf{u}$) used for each passage of the tour is:

$$\mathbf{u} = \{t_0, t_{EP}, t_{man}, \alpha, \tau, \theta\} \tag{6.10}$$

The control vector elements are determined by an optimization process that must compute the passage using minimum propellant mass, subjected to the constraint that the final state of the propulsion phase must match with the initial state of the L_2 stable manifold of the target moon. It must be noted that the stable manifold associated with the second libration point of the specific moon, when propagated for a ballistic time greater than t_{man}, performs various closed orbits around that moon after which it passes onto the unstable manifold of L_1 of the same moon. This transition is the so called *heteroclinic connection* already discussed in Sec. 3.3 and is used to obtain the starting conditions for the subsequent passage. In fact, t_0 is the exit time from the unstable manifold associated with the first libration point of the previous moon considered.

Tour Optimization The problem is stated as a constrained minimization approach with equality constraints on the final state function of the control vector and with inequality constrains on the elements of the control vector, which has an upper and a lower bound (u_{ub}, u_{lb}), these identify the feasibility envelope (U) for $\mathbf{u}$.

$$\begin{aligned}&\min_{U} f(\mathbf{u}) \ \ \textit{subjected to}:\\ &c_{eq}(u) = 0\\ &u_{lb} \leq u \leq u_{ub}\end{aligned} \tag{6.11}$$

This is a nonlinear programming problem with only active constraints[29] . The functional to be minimized, $f(\mathbf{u})$, is the propellant mass required during the propulsion phase, which is a nonlinear objective function with multiple nonlinear constraints.

A sequential quadratic programming technique has been implemented to find the optimal solution. This technique converts the objective function in a quadratic form and linearizes the constraints. Moreover, at each iteration an approximation of the Hessian of the Lagrangian is made using a Quasi-Newton updating method. This type of optimization process is strongly dependent on the quality of the initial guess and possible results in a high computational load due to a poor initial guess or when it lies on the boundary of the feasible region.

Using this method the thrust law (α,τ) is included in the control vector by a time discretization of the propulsion phase. It has been divided into N-mesh points and at each point the thrust modulus and angle have been considered as elements of the control vector. So the total dimension of $\mathbf{u}$ equals: $2 \cdot N + 4$. The thrust law between two consecutive mesh points has been linearly interpolated.

Due to the extreme sensibility of the three body system to the initial conditions this kind of approach is not sufficient to assure the passage between two manifolds. In fact, the chaotic dynamics of the model lead to completely different solutions even for very similar initial conditions.

Therefore, in order to improve the precision of the conjunction points, a further optimization process has been implemented starting from the solution of the nonlinear programming problem. In this second step the function to be minimized is only the distance in the phase space between the end point

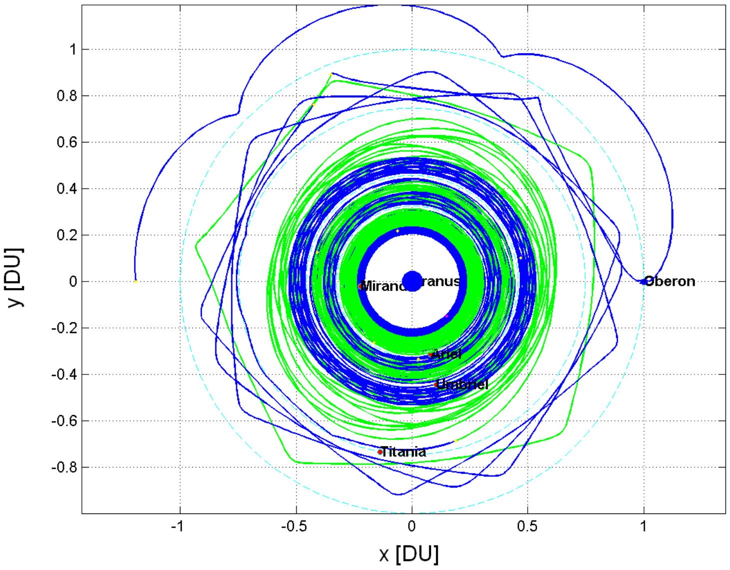

(a) Uranus - Oberon Synodic System

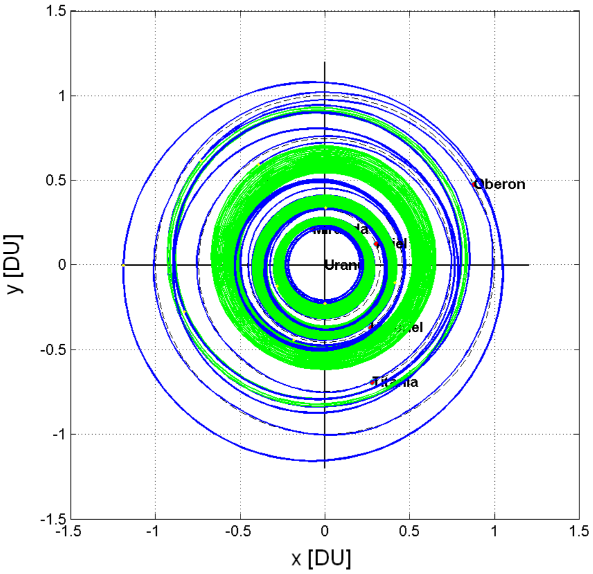

(b) Uranus Inertial System

Figure 6.10: The Planetary Tour

of the propelled phase and the initial condition required for the insertion onto the stable L_2 manifold. A simplex algorithm has been used taking the output of the previous step as initial guess. This approach assures a local solution that requires approximately the same propellant mass as given by the minimization process.

The value of the small perturbation introduced in Eq. 6.6 has been subjected to a numeric iteration in order to obtain a value that corresponded with a minimum altitude not less than 50km above the surface.

Results The computation of the different legs of the planetary tour initiated by the determination of the optimized thrusting law as described in the interplanetary phase. For all manifold transitions, the initial guess constituted an angle of approximately 180 degrees with respect to the velocity vector. This corresponds with an anti-tangential thrust dissipating the spacecraft's energy, justified by the fact that all transitions performed corresponded with a decrease in orbital altitude with respect to Uranus.

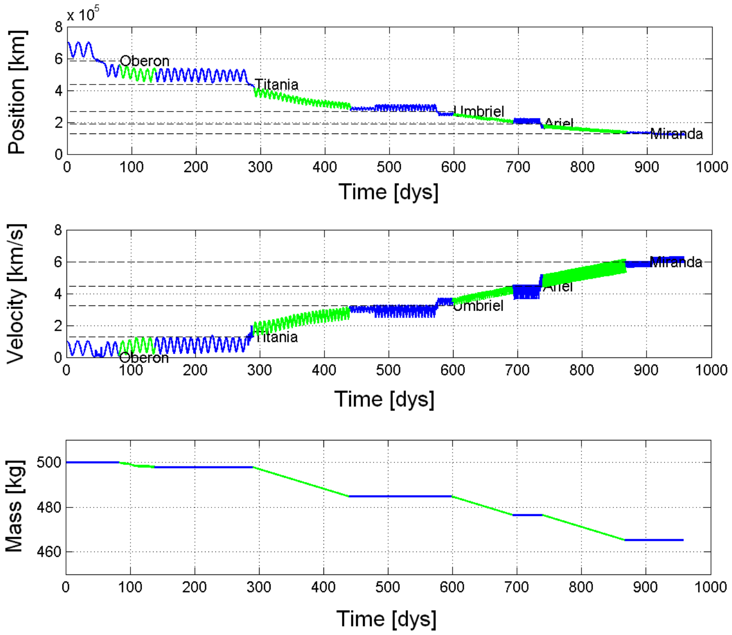

Figure 6.11: Instantaneous Position, Velocity and Mass during the Tour

The starting point of the tour, the position on the exterior L_2 Uranus - Oberon manifold, has been arbitrarily fixed on the intersection with the x-axis, where it is considered that $t_0 = 0$. A fixed number of mesh point,

Tour Transfer Time [dys]	957.6
Tour Mass Fraction [-]	0.070
Propellant Mass [kg]	35
Tour ΔV [km^2/s^2]	2.26

Table 6.5: Tour Outputs

$N = 10$, has been arbitrarily chosen for normal transfers and this is doubled for long propulsion phases to limit the computational time.

A sequential quadratic programming scheme has been applied to compute the solution, corresponding with convergence of the relative error of the equality constraints. In order to constrain the computational time, a tolerance of 5% has been imposed on the phase-distance of the conjunction states. The main system of reference to which all other, coupled systems are

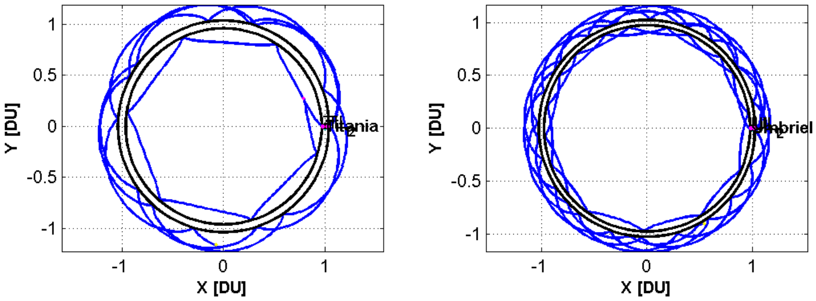

(a) Manifold Transitions in Uranus-Titania (left) and Uranus-Umbriel (right) synodic frame.

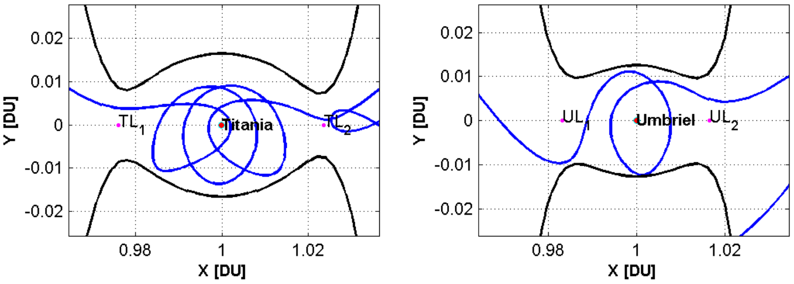

(b) Ballistic captures and escapes in Titania and Umbriel realms.

Figure 6.12: Detail of the Heteroclinic Connections for Titania and Umbriel

scaled is the Uranus - Oberon system. Figure 6.10 shows the entire tour with respect to this reference frame, together with a transformation to the inertial reference frame.

In the figure the propulsion phases are represented by green lines and the ballistic arcs by blue lines. Maintaining this convention the position, velocity and mass are shown in Fig. 6.11. It is noted that the velocities are with respect to the principal reference frame where the velocity of Oberon equals zero. The passages near one of the moons are indicated by the rapid oscillations in the velocity and position plots.

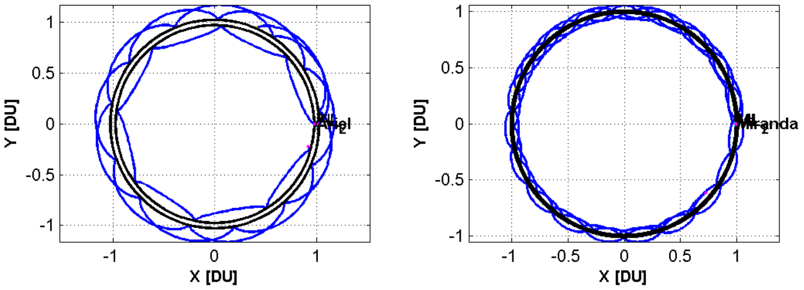

(a) Manifold Transitions in Uranus-Ariel (left) and Uranus-Miranda (right) synodic frame.

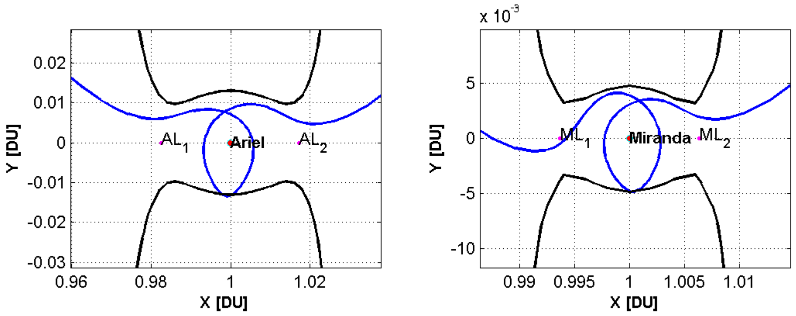

(b) Ballistic captures and escapes in Ariel and Miranda realms.

Figure 6.13: Detail of the Heteroclinic Connections for Ariel and Miranda

The transition from the Oberon to the Titania system requires only a relatively short propulsion phase of approximately 56 days due to the close proximity of the two moons and their similar physical conditions. This with respect to the transition to Umbriel and Miranda, requiring approximately 150 and 128 days respectively. This is explained by the large physical and radial difference with respect to the preceding system.

The transitions from the outer to the inner Lagrange point, L_2 to L_1 respectively, for a certain system, correspond to the so called heteroclinic connections between the two manifold associated with the Lagrange points.

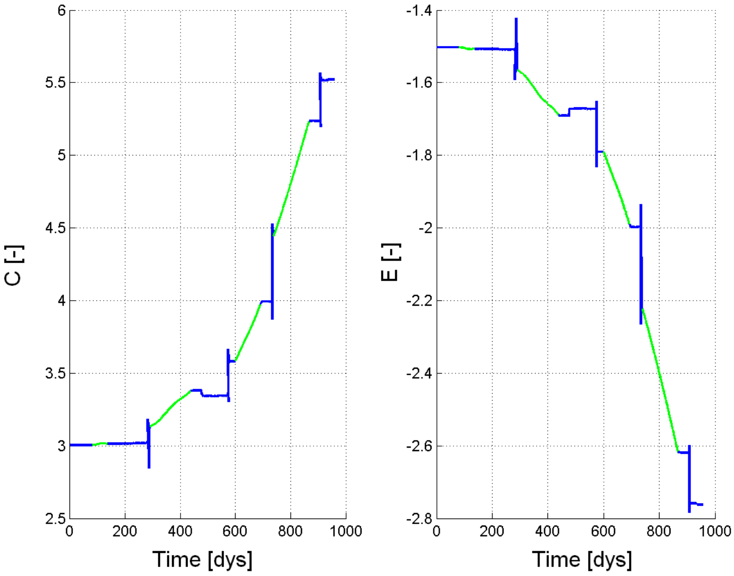

Figure 6.14: Value of the Jacobi Constant (left) and of the Energy (right)

These connections are shown in Fig. 6.12(a) and Fig. 6.13(a). The figures display the ballistic trajectories within the appropriate synodic system, the Hill region associated with the L_2 energy and are propagated for the effective time that the spacecraft follows the heteroclinic connection. The minimal orbit altitude for each moon is set to be equal or greater than 50km. This is achieved by numerical iteration of the small perturbation factor, d, discussed in the previous section.

Moreover, the number of closed orbits around each moon and the associated duration of the unstable ballistic capture are also strongly dependent on the value of the perturbation used to compute the manifold. Neither the number of closed orbit nor the capture duration have been parameters of optimization in this study, merely the constraint of minimum altitude has been imposed. This resulted in a capture duration ranging from several days to almost a month.

Figure 6.12(b) and Fig. 6.13(b) show a zoom of the closed orbits performed around the different moons, together with the incoming and outgoing ballistic arcs. The trajectories flow from right to left where in neck regions the spacecraft closely passes the libration points.

6.5 Spacecraft Preliminary Design

In the previous section, a reference low-thrust interplanetary transfer in the CR3BP from Earth to Uranus planetary system for an Electric Propulsion powered spacecraft has been designed.

Based on results obtained from the trajectory design and taking into account design constraints imposed by the transfer, the system analysis now is conducted enabling the sizing of the spacecraft subsystems, which will be briefly outlined in this section.

Advantages of RTG-EP combination Because of the basic hypothesis of Electric Propulsion, another important aspect to be discussed in this section is the power generation.

In fact, feasibility of outer planetary missions with Electric Propulsion is strongly dependent on the availability of an adequate power source not reliant on the Sun.

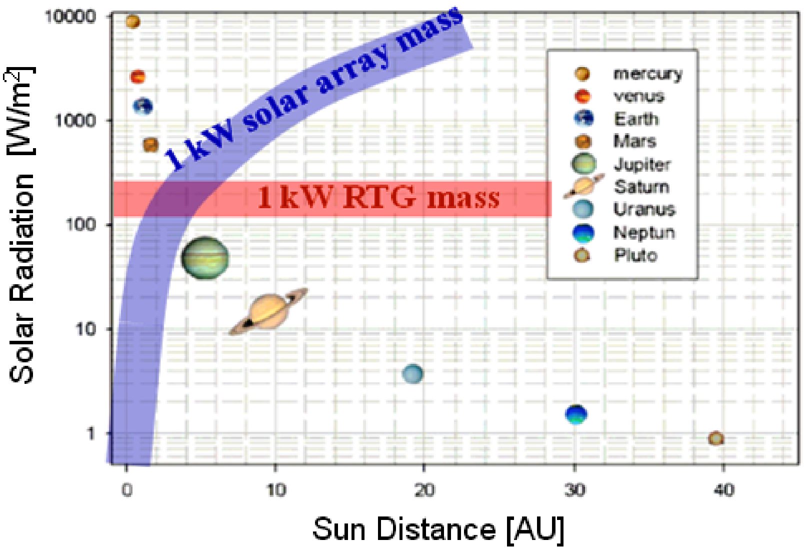

Figure 6.15: Solar array and RTG specific mass vs. Sun distance

Besides, without adequate sunlight for solar electric power in the outer Solar System, the only near-term power sources available to generate electricity are of nuclear nature.

If spacecraft power requirements remain within few kWs, a viable option to solve this problem is the use of Radioisotope Thermoelectric Generators (RTGs). As shown in Fig. 6.15, the rapid decrease of solar power density at increasing distance from the Sun, makes the RTGs more efficient than solar arrays from the ponderal point of view at distance beyond Mars.

Furthermore, in recent years the possibility of coupling advanced low power EP technology with RTGs has been considered by NASA and other space agencies, as a way to enable small spacecraft exploration of multiple targets in deep space. In fact, in several past works, Noble[43][44][45] and Oleson[46][47][52] noted the potential advantages of using radioisotope-powered EP for outer planet exploration; in particular, main beneficial factor of a RTG-EP system is the diminished propellant requirement compared with chemical propulsion, which in turn poses less stringent requirements on the launch vehicle performance.

RTGs Technology Description An RTG is a simple electrical generator which obtains its power from radioactive decay. In such a device, the heat released by the decay of a suitable radioactive material (typically Plutonium-238) is converted into electricity either using an array of thermocouples (Seebeck effect) or by means of a thermodynamic cycle (e.g. Stirling cycle).

In the first case, the thermocouple is a semi-conductor device with ”N” and ”P” type material in legs. The heat is applied to a hot junction while the cooling side produces electrical potential difference between materials. Connecting cold side terminals through a resistive load causes current to flow in the electrical circuit (see Fig. 6.16).

Thermocouples, though very reliable and long lasting, are very inefficient; efficiencies above 10% have never been achieved and most RTGs have conversion efficiencies between $3 \div 7\%$. On the other hand, conversion efficiency is improved if a thermodynamic cycle is used (about $28 \div 32\%$).

It is worth noting that higher efficiency means less radioactive fuel needed and therefore also a lighter overall weight for the generator, a critically important factor in spaceflight launch cost considerations.

State-of-the-art technology is the General Purpose Heat Source (GPHS) module (Fig. 6.17 on the left) containing 4 fuel pellet. It is the building block for constituing the heat source of the GPHS-RTG with a total of 18 modules (Fig. 6.17 on the right).

The GPHS-RTG mass is about 55 kg, with a total nominal thermal power of 4400 W and an electric power of about 300 W (specific power of about 5 W/kg). This technology flew on many past missions such as the Pioneer 10 and 11 (1972/73) to Jupiter and Saturn , the Viking 1 and 2 (1975) to Mars , the Voyager 1 and 2 (1977) to the outer solar system , Galileo (1989) and Ulysses (1990) missions to Jupiter and Cassini (1997) to Saturn. Nowadays, one GPHS-RTG is flying on the New Horizons mission (2006) to Pluto and beyond.

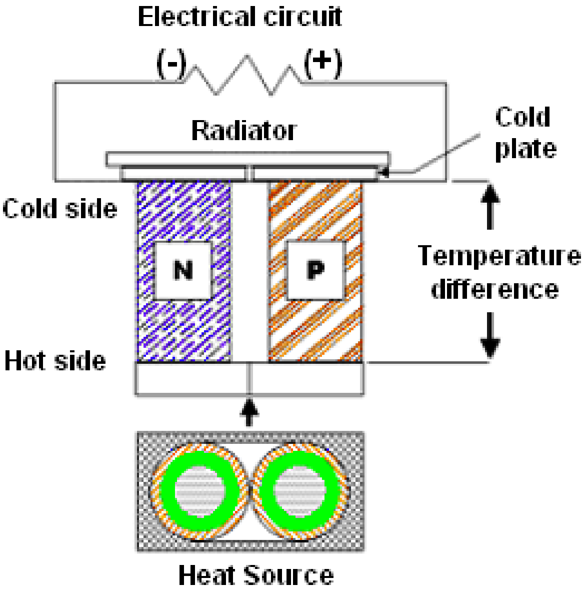

Figure 6.16: Sketch of the Seebeck effect

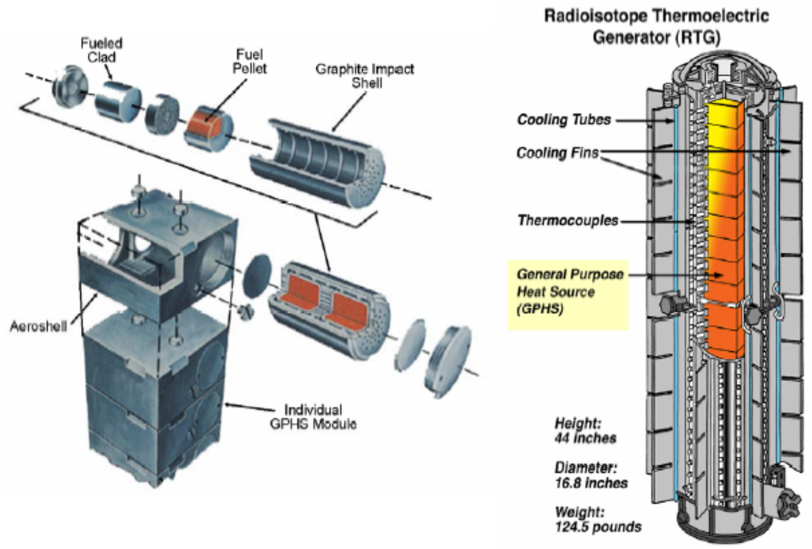

Figure 6.17: General Purpose Heat Source (GPHS)-RTG

However, recently many efforts have been done by NASA Glenn Research Center in developing next generation Radioisotope power systems for potential use on future NASA space science and exploration missions.
In particular, they are developing a high-efficiency Advanced Stirling Radioisotope Generator (ASRG) (Fig. 6.18) with a conversion efficiency of about $28 \div 32\%$ that reduces the required amount of radioisotope by a factor of four with consequent reduction of costs.
An ASRG engineering unit mass is about 20 kg with a total nominal thermal power of 500 W and an electric power of about 140 W/160 W according to the hot-end temperature (650°C/850°) (specific power of about $7 \div 8$ W/kg).

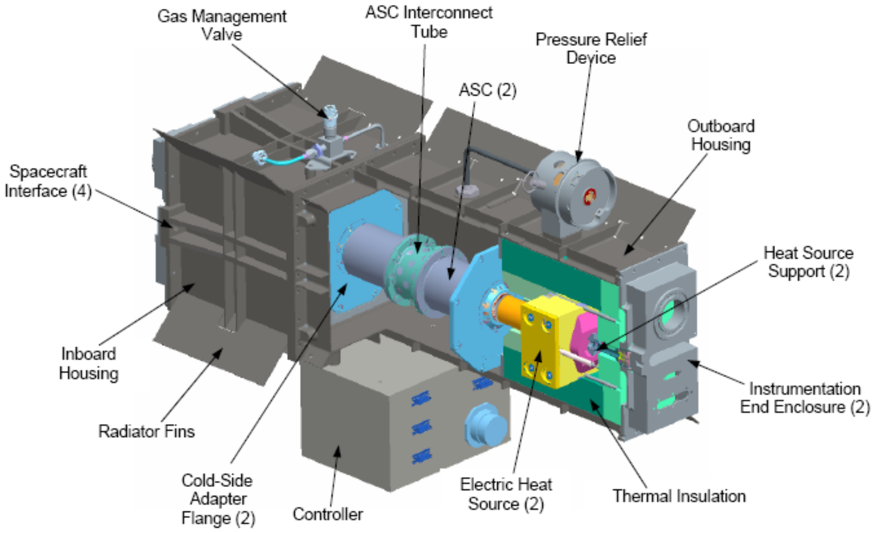

Figure 6.18: Advanced Stirling Radioisotope Generator (ASRG)

Spacecraft Design According to mission constraints outlined in the trajectory design section, the power subsystem is required to continuously provide a minimum of 1000 W of electrical power until end of life and the RTG systems assure an almost constant power level for decades and only a slight degradation of performance occurs (thermal to electric conversion degradation is about 0.8% per year).

Considering the transfer time plus an operative lifetime the number of RTG modules required was computed. In particular, the GPHS-RTG has been considered as candidate since it is a space proven technology. However, we shall take in mind that, at system level, the alternative choiche of near-term next generation RTGs such as the ASRG allows to reduce the spacecraft mass budget.

In order to obtain 1 kW of available on-board power and because of the low conversion efficiency of these devices, the modules generate a large amount of thermal power, which must be taken into account in the spacecraft design. Furthermore, the part of the spacecraft body housing the instrumentation and electronic apparatus must also be protected from the emission of radioactive particles and EMI.

The Power Subsystem is completed with the mass of the power conditioning and distribution unit (PCDU) that accomplishes the conversion and distribution towards the various subsystems of the power generated by the RTG modules. The PCDU is sized based on mass budgets found in the literature for similar power levels. A complete mass budget for the power subsystem is shown in Table 6.6.

Required Power @ EOL [W]	1000
Power produced by 1 GPHS-RTG @ EOL [W]	242
Number of GPHS-RTG needed [-]	4
Mass of 1 GPHS-RTG [kg]	55
Total GPHS-RTGs mass [kg]	220
PCDU mass [kg]	10
Total power subsystem mass [kg]	**230**

Table 6.6: Power subsystem mass budget

The Electric Propulsion subsystem requires a thruster that provides a specific impulse of approximately 3200s at an input power of 1 kW. The well-proven Xenon fed gridded ion engine RIT-10 shown in Fig. 6.19 was selected for reference,[61] as this thruster is designed for an operating power of 500 W providing the required specific impulse. Hence, a combination of two thrusters satisfies the propulsion requirements. Four thrusters (2 + 2 for cold redundancy) have been considered in the preliminary design of the spacecraft in order to obtain a sufficient level of reliability. Apart the thrusters, the subsystem also includes the propellant tank, the feeding system and the Power Processing Unit (PPU). Tank mass was estimated as 10% of the propellant mass. It must be noted that this is a precautionary sizing estimate compared to data found in literature.[62]

Sizing of piping, harness, tank isolation system and the Xenon feeding system has been done based on statistical data available in literature[43] and taken from preliminary designs of similar missions.

In the preliminary mass budget of the Electric Propulsion subsystem, the

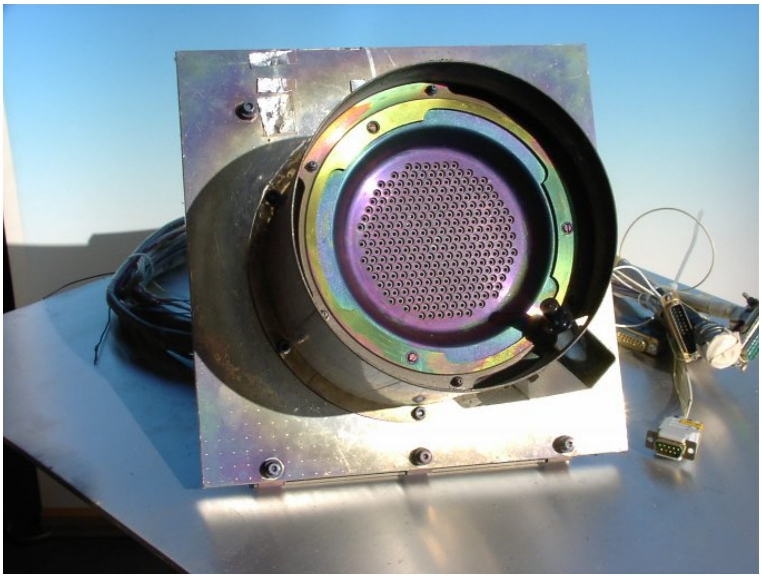

Figure 6.19: The RIT 10 (EVO) gridded ion engine

PPU is a heavy component since the ion engine requires a high voltage that must be processed by this device. Typically, the PPU is required to be able to operate in a wide dynamical power range for solar electric applications. However, in the RTG application, the only power level variation is due to the plutonium decay and to the converter efficiency decrease; thus the operative range is almost constant and the PPU design may be optimized for this particular application. Data available on state-of-the-art devices as found in literature has been used to size the PPU.[63]

The Attitude Control Subsystem (ACS) is subject to stringent tolerances as at the large distances accurate positioning of the antennas is required. These requirements are satisfied only with an active attitude control scheme; highest reliability and precision is given by a three axis stabilized configuration with reaction wheels where position maintenance is achieved by a combination of four reaction wheels and eight resisto-jet thrusters for desaturation purposes.

Taking into account the mission profile, worst case scenario for the ACS subsystem is during the planetary tour when the spacecraft is subjected to the perturbations of the target planet. During the interplanetary flight, perturbations are, indeed, very small and negligible, while in the Uranus realm capture phase the spacecraft can experience high perturbations due to Yranus magnetic field that is about 48 times more intense than the one of the Earth.

Therefore, a strong disturbance torque is foreseen.
Evaluation of disturbance torque acting on the spacecraft and computation of desaturation propellant needed during the planetary tour are carried out according to procedure outlined in Wertz[64]

The thermal control system experiences two extremes during the entire mission as in the initial phase it must dissipate the heat generated by the RTG and the surplus of generated electric power not required. In addition the close Sun distance does not require heating of internal components that could dissipate RTG heat. On the other hand, during Uranus tour the thermal control system must maintain acceptable internal temperatures. This can be achieved by using the RTG generated heat in addition to internal heaters.
Therefore, radiators'surface area has been computed in the worst case of external heating (closest distance from the Sun). Besides, sizing of the RTG's cooling system has not been considered since it is already included in the module itself.

The command and data handling subsystem must be able to communicate with the Earth both upon departure as during the operational life. This requires two antenna types, a high-gain antenna for long distance communication and a low-gain antenna for communication close to Earth. The former antenna has a diameter of 2.1 m and emits with an angle of only 0.3 degrees. Both antennas considered operate on the X-band, this being a typical solution for interplanetary missions. A store and forward approach is used to communicate and transmit data with the ground stations as long eclipse times can occur during operational life. This communication system's architecture allows a data-rate of 38 kbits per second at Jupiter distance and more than 1 kbits at Uranus distance.
The system is completed with transponders, amplifiers and cabling.

The spacecraft structure offers a mechanical support for the entire equipment, provides the thermal conductivity, provides shielding by micro-meteorites and protects against electromagnetic interferences coming from the RTGs and deep space. In addition, it must also provide the required interface to fit the fairing of the selected launcher.
The structure is based on a trussed frame with the subsystem components integrated. The structural mass is estimated as 8% of the total mass.[64] The propellant tanks are located close to the centre of mass to minimize shifting of the centre of gravity. The thrusters and the high gain antenna are mounted at opposite sides to enable communication with the Earth also during the deceleration phase. Moreover, thrusters must be aligned with the centre of mass of the spacecraft.

Subsystem	**Component**	**Qty**	**Mass [kg]**			**Total [kg]**
			Each	Cont. (%)	Total	
Power	RTG	4	55	-	220	
	PCDU	1	10	10	11	
						231
Propulsion	Thrusters	4	1.8	-	7.5	
	Tank	1	30	-	30	
	Feed System	1	6	20	7.5	
	PPU	2	9	-	18	
						63
ACS	Reaction wheel	4	2	-	8	
	Star tracker	3	0.3	-	1	
	Sun sensors	4	0.1	-	0.5	
	Resistojet	8	0.5	20	5	
	Electronics	2	3	10	7	
						21.5
Thermal	Radiators	1	3.5	30	4.5	
	PPU waste heat	1	0.6	30	1	
	MLI	1	14	20	16.8	
	heaters, sensors	1	1	20	1.2	
						23.5
CCDH	Transponder	2	3	10	6.5	
	Computer	2	5	20	12	
	Antenna HG	1	9	10	10	
	Antenna LG	3	0.15	10	0.5	
	TWTA	1	2.1	20	2.5	
	Amplifier	2	1.1	10	2.5	
	Memory 60GB	2	1	-	2	
	Cabling	1	10	10	11	
						47
Structure	8% M_{tot}					
						60
Payload	Imaging system	1	6.8	25	8.5	
	Spectrometer	2	5.5	30	7	
	Optics	1	2	30	2.5	
	Processing Unit	2	3.3	5	7	
						25
Spacecraft Dry Mass						471

Table 6.7: RTG-EP Spacecraft Mass Budget

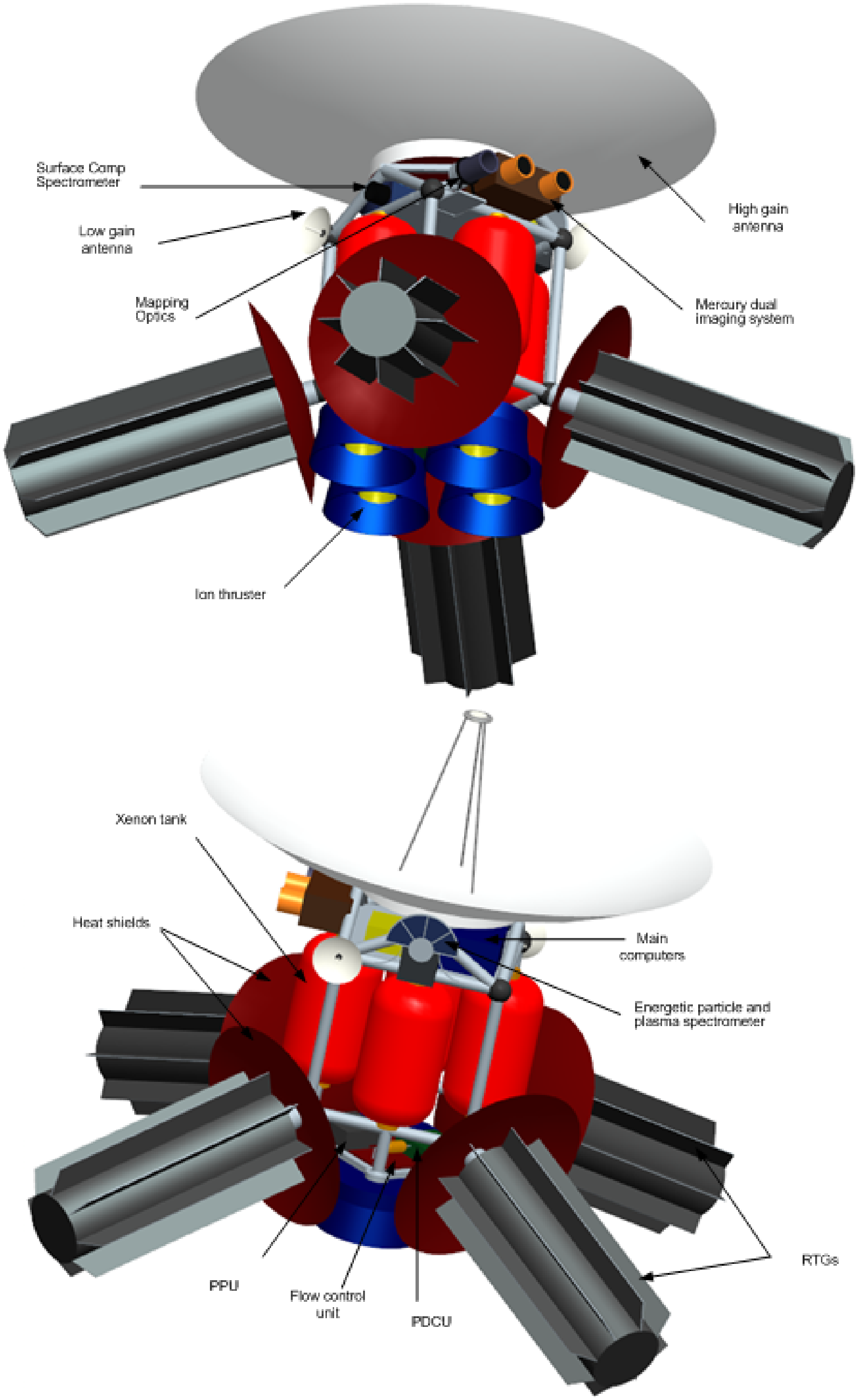

Figure 6.20: Preliminary Spacecraft Configuration

The scientific instrumentation mass allocated for the payload is 25 kg, which is considered sufficient taking into consideration scientific equipment similar to the New Horizons mission,[65] which is, moreover, comparable with the payload mass considered by Oleson.[46]

The specific mass for each subsystem and the total mass computed including contingency are summarized in the Table 6.7.

A preliminary configuration, based on the previously discussed considerations is shown in Fig. 6.20.

Chapter 7

Conclusions and Way Forward

Primary objective of this thesis was to investigate and outline the potential benefits deriving from the combination of low-energy trajectory transfers under the assumptions of the CR3BP with the Electric Propulsion. In fact, apart from making feasible missions which classical approaches could not, a non-Keplerian approach allows to perform orbit transfers by simply exploiting the simultaneous gravitational fields of two or more attarctors with consequent reduction of the ΔV necessary for the transition. Electric Propulsion is a high efficiency propulsion technology that can rely on specific impulses ten times higher than chemical propulsion.

Both optimal control theory and the field of Dynamical Systems Theory applied to the non-Keplerian model were investigated as optimization schemes were necessary to design low-thrust arcs subjected to boundary constraints and chaotic motion is the basis of the CR3BP.

Intention of the author was to develop an analytic approach in such amazing context in order to have the suitable tools to be applied in a more engineering way to the preliminary mission design of interplanetary transfers with EP powered spacecraft.

In detail, particular interest was focused on interplanetary transfers to outer solar system as they represent challenging targets and many efforts in terms of technologies improvement are still needed to let these sites become more accessible.

In the first part of the thesis, the theoretical background related to the CR3BP, the equations of motion, the orbit structures and the construction of periodic orbits and manifolds have been presented. The necessary ingredients to start the trajectory design connecting different realms of the main attractors were shown as basis for the design of prescribed itineraries.

Then, the optimal control problem and the optimization techniques used during this thesis have been introduced. A combination of the gradient method and the forward shooting method was used as the former is less sensitive to the initial conditions and provides a more accurate first guess solution to the latter that is much faster but requires more accurate initial guesses.

Analytical approaches were developed and low-thrust interplanetary transfers to Uranus in the CR3BP were obtained. In particular, in Chapter 5, the feasibility of outer planetary missions combining the advantages of a high energy launch plus the Electric Propulsion were presented. Although previous studies already demonstrated this, to the authors' knowledge this was never performed under the CR3BP assumption.

It was observed that advantages in mission design are obtained by the elimination of the planetary capture design considered in the conventional two-body approach. The capture obtained by the libration point entry in the planetary realm of the CR3BP provided a stationary point that must be targeted, which enabled the employment of dynamical optimization techniques.

The minimum transfer time to the Sun - Uranus libration point is in the order of 10 years, which is comparable with impulsive patched-conics solutions. The discussed approach, however, achieved a planetary capture with an increased mass fraction due to the higher efficiency of the Electric Propulsion.

In the end, a reference mission and the preliminary spacecraft configuration were designed. A tour of the Uranian system and the required interplanetary trajectory under the CR3BP model were studied.

Results demonstrated that by a combination of coupled three-body models and Electric Propulsion very interesting scientific missions to Uranus can be designed. Moreover, it is shown that inclusion of the interplanetary trajectory does not render the mission infeasible neither in terms of mission duration nor with respect to the mass budgets.

The interplanetary trajectory presented a time minimized solution adhering the appropriate conditions for the planetary tour to start. The optimization scheme computed a solution modifying the spacecraft's state in all 6 dimensions, with in addition a conjunction phase that dissipates the excess in energy in order to start the planetary tour.

The planetary tour designed combined the advantages of dynamical systems theory within the three-body model and the use of Electric Propulsion which opens a wide range of possible mission scenarios. The tour takes about 956 days to perform transitions between five different planetary three-body systems, realizing unstable captured orbits at each moon (Oberon, Titania, Umbriel, Ariel and Miranda respectively) where the spacecraft is finally guided into a stable, circular orbit around Uranus after departure from the ultimate moon considered. The propellant mass fraction required for the entire tour is about 7% that corresponds to a ΔV of 2.26 km/s.

Finally, taking into account constraints deriving from the trajectory design, the preliminary spacecraft configuration was developed in which, because of the basic hypothesis of Electric Propulsion, the availability of an adequate power source not reliant on the Sun was needed.
Within few kilowatts, a state-of-the-art viable option for power generation purposes are the Radioisotope Thermoelectric Generators (RTGs).

Future developments could invoke the evaluation of manifolds associated with periodic orbits instead of the libration point, giving more freedom in the manifold intersections and therefore the number and duration of closed orbits around the moons. Moreover, increasing the envelope of available ballistic trajectories could decrease the propellant mass requirements even further. Furthermore, considering a 3-dimensional environment for the Uranian tour would present a more realistic analysis.
It must be noted that the dynamics considered are very unstable and susceptible to gravitational perturbations. Therefore a detailed analysis evaluating the effects of the other gravitational bodies in the solar system during the interplanetary phase should be performed for a more refined mission design.

Furthermore, many aspects do impose very high technological demands such as the Electric thrusters total impulse and duration. For simplicity reasons, in this thesis EP technological issues have been omitted.

Appendix

Appendix A

Outer Planetary Missions: Results in the 2-Body model

A.1 Neptune

A transfer analysis as described in the previous section is also performed for Neptune, considering identical launcher and thruster performance ranges, however, in this case the maximum coasting duration is augmented due to the much larger distance. For brevity reasons the two-dimensional figures showing the total transfer time and mass fraction as a function of the coasting duration are omitted. This is directly presented by the two three-dimensional figures for the extremes in launch energy, as seen in figure A.1.

Trends similar to the Uranus case can be observed. The total transfer time increases with coasting duration, where this is accompanied with an increase in final mass fraction. This latter effect is more pronounced for the higher launch energies and lower specific impulses. Furthermore it is again observed that the lowest I_{sp} value has a minimum coasting duration significantly larger than the higher impulses and again the highest impulses are not capable to adhere the boundary conditions when considering long coasting durations. The overall shift in total transfer time and maximum coasting duration origin from the significantly larger Sun distance that must be reached.

Figure A.2 shows the total transfer times versus the final mass fractions for zero and seven ballistic years, for all considered launch energies. It is seen that for none of the launch energies at zero ballistic time, a specific impulse of 1500s achieved the imposed final state. For the coasting duration of seven years, only the $I_{sp} = 4500$ case for the lowest launch energy did not manage to obtain a successful transfer.

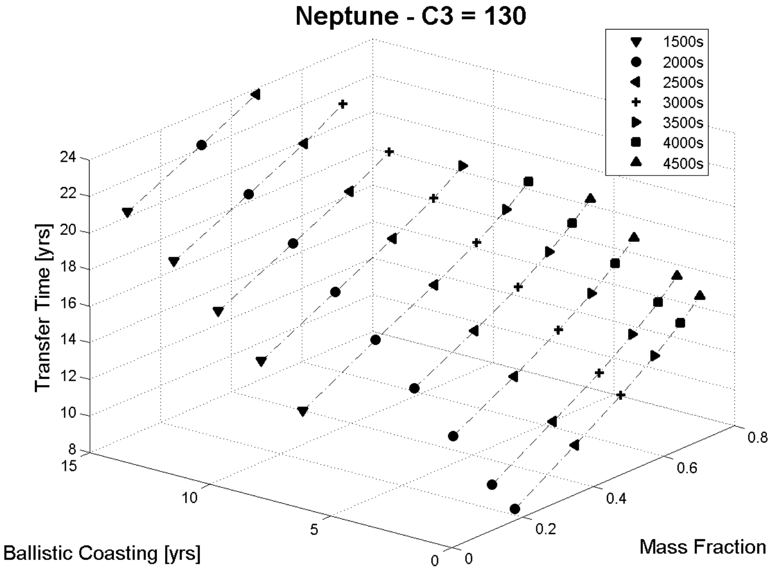

(a) Launch $C_3 = 130 \text{km}^2/\text{s}^2$

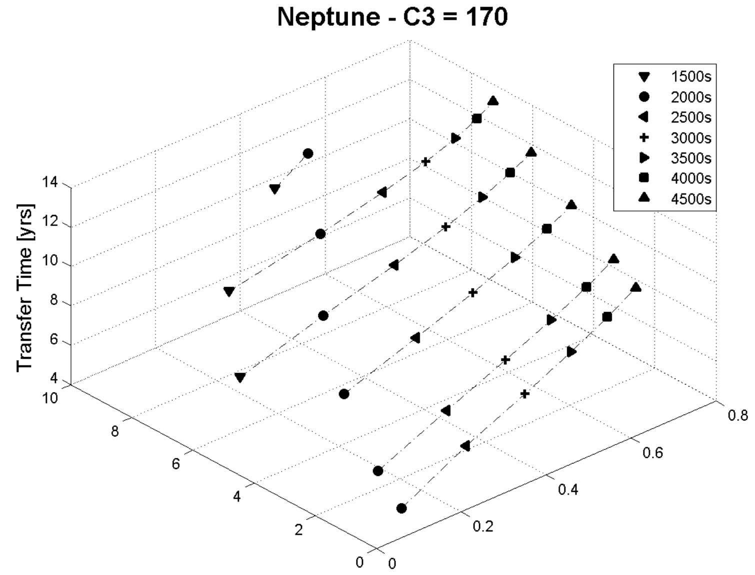

(b) Launch $C_3 = 170 \text{km}^2/\text{s}^2$

Figure A.1: Transfer Time and Mass Fraction for Different Launch Energy

It is clearly seen that the total transfer time always increases with specific impulse, for both coasting durations. However, for the shorter coasting durations, this increase in total transfer time, at constant specific impulse and different initial masses, goes together with an increase in mass fraction. The opposite behaviour is observed for longer coasting durations where the mass fraction actually decreases.

A.2 Saturn

A transfer analysis as described in the previous sections is also performed for Saturn, considering identical launcher and thruster performances, however, the maximum coasting duration is strongly decreased to 1.5 years due to the shorter planetary distance. Figure A.3 shows two three-dimensional surfaces giving the results for the two C_3 extremes.

For Saturn a much more pronounced increase in total transfer time with increasing specific impulse can be observed. Especially for the higher launch energy, only the two lowest specific impulses are able to generate a deceleration high enough to satisfy the final conditions for coasting durations exceeding zero years. For the $C_3 = 170$ case the vertical shift in transfer time with almost constant mass fraction for two higher specific impulses is again explained by the fact that the trajectory goes beyond the final radius, after which it returns inwards.

Figure A.4 shows the total transfer times versus the final mass fractions for zero and 0.25 ballistic years, for all considered launch energies.

The results indicate that the investigated strategy is less advantageous for a small spacecraft destined for Saturn. The planetary distance and high excess energy result in an unfavourable combination of spacecraft mass and required specific impulse, computing to low final mass fractions. A possible alternative could be a less powerful launcher, providing the spacecraft with less excess energy, or considering the lower C_3 values investigated as these are not as susceptible to this behaviour. This tendency is also reported in previous studies[48],[53] suggesting a slightly different strategy for closer planets, associated with a less powerful launch.

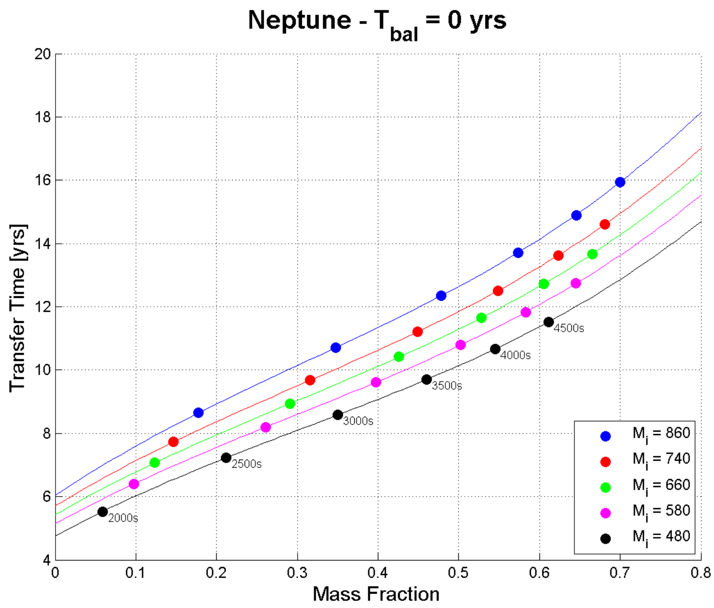

(a) Zero Ballistic Years

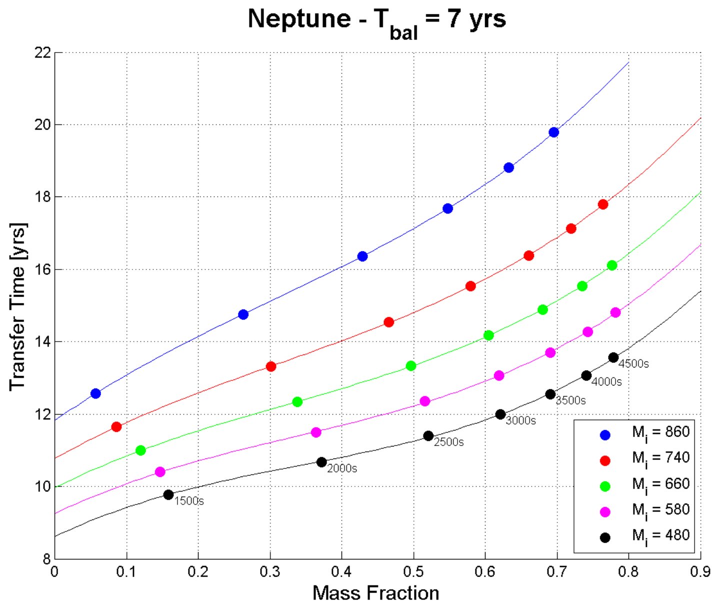

(b) Three Ballistic Years

Figure A.2: Transfer Time versus Mass Fraction for Different Coasting Durations

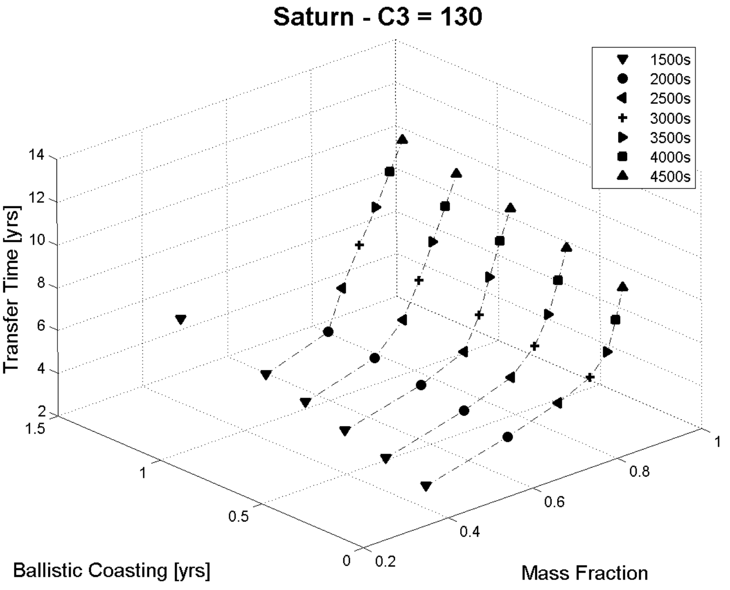

(a) Launch $C_3 = 130\text{km}^2/\text{s}^2$

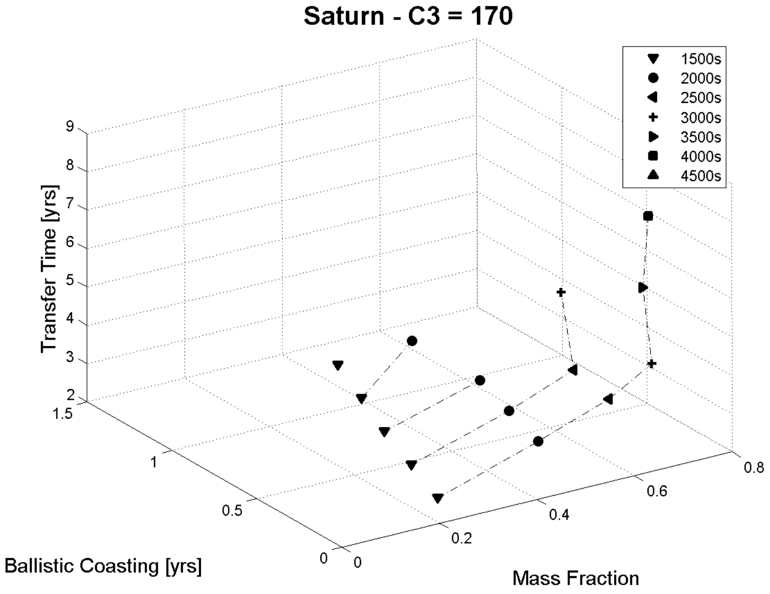

(b) Launch $C_3 = 170\text{km}^2/\text{s}^2$

Figure A.3: Transfer Time and Mass Fraction for Different Launch Energy

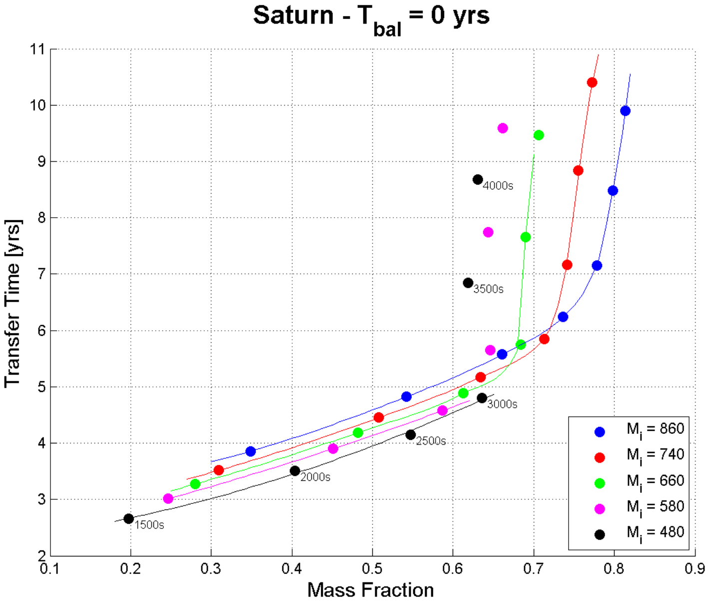

(a) Zero Ballistic Years

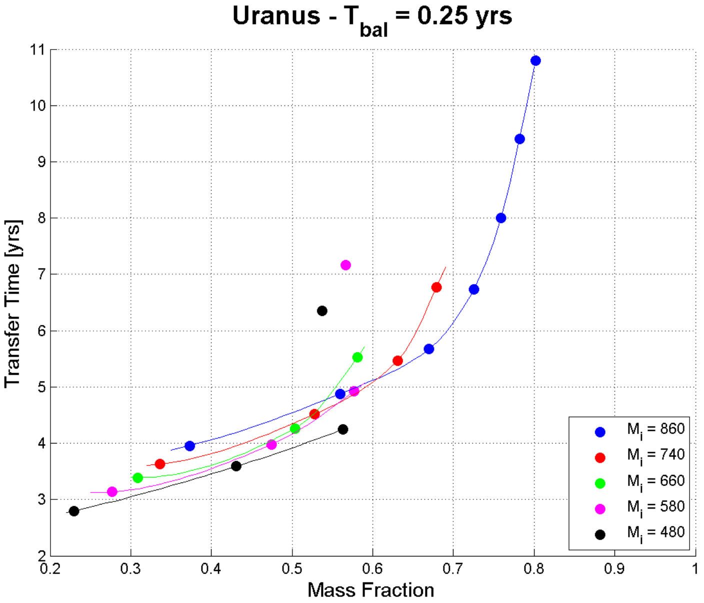

(b) Three Ballistic Years

Figure A.4: Transfer Time versus Mass Fraction for Different Coasting Durations

Bibliography

[1] Ross, S. D., *Cylindrical Manifolds and Tube Dynamics in the Restricted Three-Body Problem*, Ph.D. thesis, Ph.D. dissertation, California Institute of Technology, California, 2004.

[2] W. S. Koon, M. W. Lo, J. E. M. and Ross, S. D., "Heteroclinic connections between periodic orbits and resonance transitions in celestial mechanics," *Chaos*, Vol. 10(2), 2000, pp. 427–469.

[3] G. Gomez, W. S. Koon, e. a., "Invariant manifolds, the Spatial Three-Body Problem and Space Mission Design," *Advances in the Astronautical Sciences*, Vol. 109 part 1, 2001, pp. 3–22.

[4] Corporation, L. M., *Atlas Launch System Mission Planner's Guide*, Revision 10a, January 2007.

[5] Belbruno, E. A., "Lunar Capture Orbits, a Method of Constructing Earth Moon Trajectories and the Lunar Gas Mission," *AIAA-87-1054, 19th AIAA/DGLR/JSASS International Electric Propulsion Conference, Colorado Springs, Colorado*, 1987.

[6] Starchville, T. F. and Melton, R. G., "Optimal Low-Thrust Trajectories to Earth-Moon L2 Halo Orbits (Circular Problem)," *AAS 97-714, AAS/AIAA Astrodynamics Specialists Conference*, 1997.

[7] Starchville, T. F. and Melton, R. G., "Optimal Low-Thrust Transfers to Halo Orbits about the L2 Libration Point in the Earth-Moon System (Elliptical Problem)," *AAS 98-205, AAS/AIAA Space Flight Mechanics Meeting*, 1998.

[8] J. Senent, C. O. and Capella, A., "Low-Thrust Variable Specific Impulse Transfers and Guidance to Unstable Periodic Orbits," *Journal of Guidance, Control and Dynamics*, Vol. 28, 2005, pp. 280–290.

[9] Szebehely, V., *Theory of Orbits - The Restricted Problem of Three Bodies*, Academic Press Inc., Harcourt Brace Jovanovich Publishers, Orlando, Florida, 1967.

[10] Poincarè, H., "Sur le Problème des Trois Corps et les équations de la dynamique," *Acta Math.*, Vol. 13, 1890, pp. 1–271.

[11] Poincarè, H., "Les Methodes Nouvelles de la Mécanique Céleste," *Gautiers-Villars, Paris. Reprinted by Dover, New York, 1957*, Vol. 1-3, 1892-1899.

[12] M. W. Lo, W. S. Koon, J. E. M. and Murray, R. M., "Formation Flight near Libration Points: Survey and Recommendations," *Space Mission*, Fall 2000, pp. 35–48.

[13] Belbruno, E. A., "Examples of the Nonlinear Dynamics of Ballistic Capture and Escape in the Earth-Moon System,AIAA-90-2896-CP," *AIAA*, 1990.

[14] Belbruno, E. A. and Carrico, J. P., "Calculation of Weak Stability Boundary Ballistic Lunar Transfer Trajectories," *AIAA-2000-4142, AIAA/AAS Astrodynamics Specialist Conference, Denver, Colorado*, 2000.

[15] Moser, J., "On the generalization of a theorem of Lyapunov," *Comm. Pure Appl. Math.*, Vol. 11, 1958, pp. 257–271.

[16] Jorba, A. and Masdemont, J., "Dynamics in the center manifold of the collinear points of the Restricted Three Body Problem," *Physica D*, Vol. 132, 1999, pp. 189–213.

[17] G. Gomez, W. S. Koon, e. a., "Connecting orbits and invariant manifolds in the spatial restricted three body problem," *Nonlinearity, Institute of Physics Publishing*, Vol. 17, 2004, pp. 1571–1606.

[18] Conley, C. C., "Low energy transit orbits in the restricted three-body problem," *SIAM J. Appl. Math.*, Vol. 16, 1968, pp. 732–746.

[19] Richardson, D. L., "Analytic Construction of Periodic Orbits about Collinear Points," *Celestial Mechanics*, Vol. 22, 1980, pp. 241–253.

[20] Farquhar, R. W., *The control and use of Libration-Point satellites*, Ph.D. thesis, Ph.D. dissertation, Stanford University, California, 1968.

[21] Richardson, D. L., "A Note on a Lagrangian Formulation for Motion about the Collinear Points," *Celestial Mechanics*, Vol. 22, 1980, pp. 231–236.

[22] Thurman, R. and Worfolk, P., *The geometry of Halo orbits in the Circular Restricted Three-Body problem*, Ph.D. thesis, Geometry Center Research report, University of Minnesota, 1995.

[23] W. S. Koon, M. W. Lo, J. E. M. and Ross, S. D., "The Genesis trajectory and heteroclinic connections,AAS 99-451 103 part III," *Astrodynamics*, 1999, pp. 2327–2343.

[24] K. C. Howell, B. T. B. and Lo, M. W., "Application of dynamical systems theory to trajectory design for a libration point mission," *Astronautical Sciences*, Vol. 45(2), 1997, pp. 161–178.

[25] McGehee, R., *Some homoclinic orbits for the restricted three-body problem*, Ph.D. thesis, Ph.D. thesis, University of Wisconsin, Madison, 1969.

[26] J. R. Llibre, C. M. and Simo, C., "Transversality of the invariant manifolds associated to the Lyapunov family of periodic orbits near L2 in the restricted three-body problem," *Journal of Differential Equations*, Vol. 58, 1985, pp. 104–156.

[27] Deurloo, R., "A search for low-energy capture orbits around Jupiter using the influence of Galilean moons," 2003.

[28] Bryson, A. E. and Ho, Y.-C., *Applied Optimal Control*, Hemisphere Publishing Corporation, 1975.

[29] Betts, J. T., "Survey of Numerical Methods for Trajectory Optimization," *Journal of Guidance and Control, and Dynamics*, Vol. 21, No.2, 1998.

[30] von Stryk, O. and Bulirsch, R., "Direct and Indirect Methods for Trajectory Optimization," *Annals of Operations Research*, Vol. 37, 1992, pp. 357–373.

[31] Sun, K. and Yuan, Y.-X., *Optimization Theory and Methods - Nonlinear Programming*, Springer, 2006.

[32] E. Hairer, S. P. N. and Wanner, G., *Solving Ordinary Differential Equations, Nonstiff Problems*, Springer-Verlag, Berlin, Heidelberg, 1987.

[33] Shampine, L. F. and Reichelt, M. W., *The Matlab ODE Suite*, The MathWorks Inc., 1994.

[34] Betts, J. T., "Practical Methods for Optimal Control Using Nonlinear Programming," *Advances in Design and Control, Society for Industrial and Applied Mathematics*, 2001.

[35] Bock, H. G. and Plitt, K. J., "A Multiple Shooting Algorithm for Direct Solution of Optimal Control Problems," *Institut für Angewandte Mathematik, Report 09.2/A-5, SFB 72, University of Bonn, in Preprints of the 9th IFAC World Congress, Budapest, Hungary*, Vol. 9, 1984, pp. 242–247.

[36] Dickmanns, E. D. and Well, K. H., "Parametrization of Optimal Control Problems using Piecewise Polynomial Approximation," *AIAA 74-822, AIAA Mechanics and Control of Flight Conference, Anaheim, California, USA*, 1974.

[37] Hargraves, C. R. and Paris, S. W., "Direct Trajectory Optimization Using Nonlinear Programming and Collocation," *Journal of Guidance, Control, and Dynamics*, Vol. 10, No.4, 1987, pp. 338–342.

[38] Gath, P. F. and Well, K. H., "Trajectory Optimization Using a Combination of Direct Multiple Shooting and Collocation," *AIAA 2001-4047, AIAA Guidance, Navigation, and Control Conference, Montréal, Québec, Canada*, 2001.

[39] L. S. Pontryagin, V. G. B. e. a., *The Mathematical Theory of Optimal Processes*, Wiley-Interscience, 1st ed., 1962.

[40] Bryson, A. E., *Dynamic Optimization*, Addison-Wesley, California, 1999.

[41] Lewis, F. L. and Syrmos, V. L., *Optimal Control*, John Wiley and Sons, 605 Third avenue, New York, 2nd ed., 1995.

[42] R. F. Hartl, S. P. S. and Vickson, R. G., "A survey of maximum principles for optimal control problems with state constraints," *SIAM Review*, Vol. 37(2), 1995, pp. 181–218.

[43] Noble, R. J., "Radioisotope Electric Propulsion of Small Payloads for Regular Access to Deep Space," *AIAA 93-1897, 29th Joint Propulsion Conference, Monterey, California*, 1993.

[44] Noble, R. J., "Radioisotope Electric Propulsion for Small Robotic Space Probes," *British Interplanetary Society*, Vol. 49, 1996, pp. 445–468.

[45] Noble, R. J., "Radioisotope electric propulsion of science-craft to the outer Solar System and near-interstellar space," *Proceedings 2nd IAA Symposium on Realistic Near-Term Advanced Scientific Space Missions - Aosta (Italy), FERMILAB-Conf-98/231*, August 1998.

[46] S. R. Oleson, S. Benson, e. a., "Radioisotope Electric Propulsion for Fast Outer Planetary Orbiters," *AIAA-2002-3967, 38th Joint Propulsion Conference, Indianapolis, Indiana, July*, 2002.

[47] S. R. Oleson, L. Gefert, e. a., "Outer Planet Exploration with Advanced Radioisotope Electric Propulsion," *IEPC-2001-0179, 27th International Electric Propulsion Conference, Pasadena, California, October*, 2001.

[48] C. Casaregola, K. Geurts, P. P. and Andrenucci, M., "Radioisotope Low-Power Electric Propulsion Missions to the Outer Planets," *AIAA-2007-5234, 43rd Joint Propulsion Conference, Cincinnati, OH*, 2007.

[49] F. B. Zazzera, F. T. and Massari, M., "Assessment of Mission design Including Utilization of Libration Points and Weak Stability Boundaries," *Ariadna Study id: 03/4103.*.

[50] K. Geurts, C. Casaregola, P. P. and Andrenucci, M., "Power Constrained Electric Propulsion Missions to the Outer Planets," *IEPC-2007-304, 30th International Electric Propulsion Conference, Florence, Italy*, 2007.

[51] C. Casaregola, K. Geurts, P. P. and Andrenucci, M., "Cost Effective Electric Propulsion Missions to the Outer Planets," *AIAA-2008-4515, 44th Joint Propulsion Conference, Hartford, CT*, 2008.

[52] Fiehler, D. and Oleson, S., "Radioisotope Electric Propulsion Missions Utilizing a Common Spacecraft Design," *International Astronautical Congress, Vancouver,Canada*, October 2004.

[53] Oleson, S. and Fiehler, D., "Mission Steering Profiles of Outer Planetary Orbiters Using Radioisotope Electric Propulsion," NASA/TM-2004-212877, September 2004.

[54] Alliance, U. L., "Delta II Payload Planners Guide," December 2006.

[55] Technologies, S. S. E., "Falcon 9 Launch Vehicle Data Sheet," http://www.spacex.com/Falcon9DataSheet.pdf.

[56] S. D. Ross, W. S. Koon, M. W. L. and Marsden, J. E., "Design of a multi-moon orbiter," *13th AAS/AIAA Space Flight Mechanics Meeting, Ponce, Puerto Rico*, Vol. 03-143, 2003.

[57] S. D. Ross, W. S. Koon, M. W. L. and Marsden, J. E., “Constructing a Low Energy Transfer Between Jovian Moons,” *Contemporary Mathematics*, Vol. 292, 2002, pp. 129–145.

[58] Topputo, F., *Low-Thrust Non-Keplerian Orbits: Analysis, Design and Control*, Ph.D. thesis, Politecnico di Milano, 2007.

[59] Seidelmann, P. K., *Explanatory Supplement fo the Astronomical Almanac*, University Science Books, 2006.

[60] Belbruno, E. and Miller, J., “Sun-Perturbed Earth-to-Moon Transfers with Ballistic Capture,” *Journal of Guidance, Control and Dynamics*, Vol. 16, No. 4, 1993, pp. 770–775.

[61] R. Killinger, H. B. and Miller, J., “Development of an High Petformance RF-Ion Thruster,” *AIAA-99-2445, 35th AIAA/ASME/SAE/ASEE Joint Propulsion Conference, Los Angeles, California*, June 1999.

[62] S. R. Oleson, L. Gefert, e. a., “Sub-Kilowatt Radioisotope Electric Propulsion for Outer Solar System Exploration,” *Forum on Innovative Approaches to Outer Planetary Exploration 20001 -2020, Lunar and Planetary Institute, Houston, Texas*, 2001.

[63] S. R. Oleson, S. Benson, e. a., “Radioisotope Electric Propulsion For New Frontiers Class Missions,” *IEPC-2001-0137, 28th International Electric Propulsion Conference, Toulouse, France*, 2003.

[64] Wertz, J. R. and Larson, W. J., *Space Mission Analysis and Design*, Kluwer Academic Publishers, 3rd ed.

[65] official web site, N. N. H., “http://pluto.jhuapl.edu/,” .

[66] Broucke, R. A. and Cefola, P. J., “On the Equinoctial Elements,” *Celestial Mechanics*, Vol. 5, 1972, pp. 303–310.

[67] P. K. Seidelmann, e. a., “Report of the IAU/IAG Working Group on Cartographic Coordinates and Rotational Elements of the Planets and Satellties: 2000,” *Celestial Mechanics and Dynamical Astronomy*, Vol. 82, 2002, pp. 83–91.

[68] P. Pergola, C. Casaregola, K. G. and M.Andrenucci, “Power Constrained Uranus Transfer and Moons Tour by Three Body Invariant Manifolds and Electric Propulsion,” *AAS-08196, 18th Space Flight Mechanics Meeting, Galveston, Texas*, January 2008.

[69] R. R. Bate, D. D. M. and White, J. E., *Fundamentals of Astrodynamics*, Dover Publications Inc., New York, 1971.

[70] Battin, R. H., *An Introduction to the Mathematics and Methods of Astrodynamics*, AIAA Inc., New York, 1st ed., 1987.

[71] Beutler, G., *Methods of Celestial Mechanics, Volume I*, Springer-Verlag, Berlin-Heidelberg, 2005.

[72] Brown, C. D., *Spacecraft Mission Design*, AIAA Inc., Washington DC, 1992.

[73] Chobotov, V. A., *Orbital Mechanics*, AIAA Inc., Reston, Virginia, 2nd ed., 1996.

[74] Einstein, A., *The Meaning of Relativity*, Princeton University Press, 1956.

[75] Geyling, F. T. and Westerman, R. H., *Introduction to Orbital Mechanics*, Addison-Wesley Publishing, Reading (MA), 1971.

[76] Kepler, J., *Harmonices Mundi Libri V*, 1619.

[77] Lambeck, K., *Geophysical Geodesy*, Oxford University Press, Oxford, UK, 1st ed., 1988.

[78] Long, A. C., *Goddard Trajectory Determination System Mathematical Theory*, NASA Goddard Spaceflight Center, 1989.

[79] Marsden, J. E. and Ratiu, T. S., *Introduction to Mechanics and Symmetry*, Springer-Verlag, 2nd ed., 1999.

[80] K. Riley, M. H. and Bence, S., *Mathematical Methods for Physics and Engineerings*, Cambridge University Press, Cambridge, UK, 2nd ed., 2003.

[81] Souchay, J., *Dynamics of Extended Celestial Bodies and Rigns*, Springer-Verlag, Berlin-Heidelberg, 1st ed., 2006.

[82] Vallado, D. A., *Fundamentals of Astrodynamics and Applications*, Microcosm, El Segundo, California, 2nd ed., 2004.

[83] Wiggins, S., *Introduction to Applied Nonlinear Dynamical Systems and Chaos*, Pringer-Verlag, Berlin, vol 2 of texts in applied mathematics science ed., 1990.

[84] Will, C. M., *Experimental Gravitation*, Academic Press, New York, 1974.

[85] Canalias E., Gomez G., M. M. and J.J, M., "Assessment of Mission Design Including Utilization of Libration Points and Weak Stability Boundaries," *Final Report, ESTEC Contract No. 18142/04/NL/MV*, 2004.

[86] Cefola, P. J., "Equinoctial Orbit Elements - Application to Artificial Satellite Orbits," *AIAA/AAS Astrodynamics Conference*, Palo Alto, California, 1972.

[87] McCarthy, D. D. and Petit, G., "IERS Technical Note N.32," *IERS Conventions (2003)*, Frankfurt am Main, 2003.

[88] Roncoli, R. B., "Lunar Constants and Models Document," Jet Propulsion Laboratory, September 2005.

[89] Kaplan, G. H., "The IAU Resolutions on Astronomical Reference Systems, Time Scales, and Earth Rotation Models," *Explanation and Implementation*, U.S. Naval Observatory, Washington DC, October 2005.

Publications

The studies and work discussed in this thesis have been the result of three years of research at the University of Pisa, faculty of aerospace engineering and at Alta S.p.A. in Pisa. Parts and applications of this work have been presented at various international conferences and are in the process of journal publication and inclusion in a book of Springer US. Hereby a detailed overview of these works:

Journals

1. P. Pergola, K. Geurts, C. Casaregola, M. Andrenucci: *Three-Body Invariant Manifold Transition with Electric Propulsion*, Springer Space Technology Library - Space Manifold Design, spring 2009.
2. P. Pergola, K. Geurts, C. Casaregola, M. Andrenucci: *Earth-Mars Halo to Halo Low Thrust Manifold Transfers*, Journal of Celestial Mechanics and Dynamical Astronomy, spring 2009.

Conferences

1. C. Casaregola, L. Biagioni, W. Pecorella: *Declining Power vs Constant Power: RTG-enabled Electric Propulsion Exploration of the Outer Planets*, AAAF Conference "Changes in Aeronautical and Space Systems - Challenges for on-board Energy", Avignone 26-28 Giugno 2006
2. C. Casaregola, K. Geurts, P. Pergola, L. Biagioni, M. Andrenucci: *Mission Analysis and Architecture Definition for a Small Electric Propulsion Transfer Module to the Moon*, 43rd Joint Propulsion Conference, 8-11 July 2007, Cincinnati OH.
3. C. Casaregola, K. Geurts, P. Pergola, M. Andrenucci: *Radioisotope Low-Power Electric Propulsion Missions to the Outer Planets*, 43rd Joint Propulsion Conference, 8-11 July 2007, Cincinnati OH.

4. C. Casaregola, K. Geurts, P. Pergola, L. Biagioni, M. Andrenucci: *A VEGA Dedicated Electric Propulsion Transfer Module to the Moon*, 30th International Electric Propulsion Conference, Florence, Italy, September 17-20, 2007.

5. K. Geurts, C. Casaregola, P. Pergola, M. Andrenucci: *Exploitation of Three-Body Dynamics by Electric Propulsion for Outer Planetary Missions*, 43rd Joint Propulsion Conference, 8-11 July 2007, Cincinnati OH.

6. P. Pergola, C. Casaregola, K. Geurts, M. Andrenucci: *Three Body Invariant manifold Transition with Electric Propulsion*, 30th International Electric Propulsion Conference, Florence, Italy, September 17-20, 2007.

7. K. Geurts, C. Casaregola, P. Pergola, M. Andrenucci: *Power Constrained Electric Propulsion Missions to the Outer Planets*, 30th International Electric Propulsion Conference, Florence, Italy, September 17-20, 2007.

8. P. Pergola, C. Casaregola, K. Geurts, M. Andrenucci: *Power Constrained Uranus Transfer and Moons Tour by Three Body Invariant Manifolds and Electric Propulsion*,18th Space Flight Mechanics Meeting, Galveston, Texas, January 2008 (AAS-08196).

9. P. Pergola, K. Geurts, C. Casaregola, M. Andrenucci: *Electric Propulsion in a Three Body Model for Interplanetary Transfers*, 5th Space Propulsion Conference, Heraklion, Crete, Greece, May 2008.

10. K. Geurts, C. Casaregola, P. Pergola, M. Andrenucci: *Trajectory Design Considerations and Computational Tools for Electric Propulsion Missions*, 44th Joint Propulsion Conference, Hartford, CT, July 2008.

11. C. Casaregola, K. Geurts, P. Pergola, M. Andrenucci: *Cost Effective Electric Propulsion Missions to the Outer Planets*, 44th Joint Propulsion Conference, Hartford, CT, July 2008.